Ph.D. Thesis

Micro/Nano fabrication of polymer-based devices

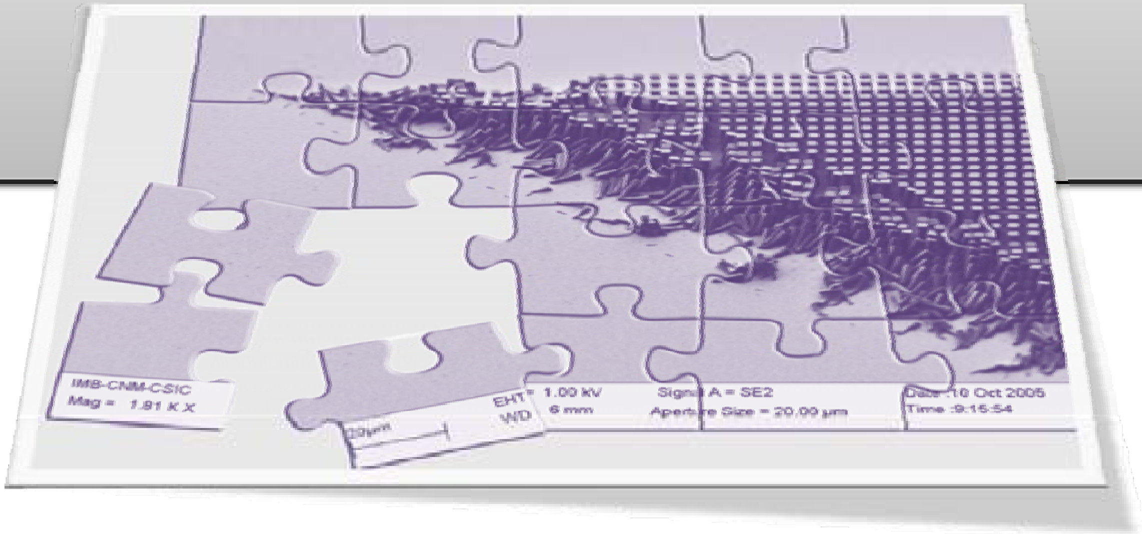

Cristina Martin

March 2008

Universitat Autònoma de Barcelona

CNM Centre Nacional de Microelectrònica CSIC

Micro/Nano fabrication of polymer-based devices

Memòria per optar al grau de Doctor en Enginyeria Electrònica

***Autora*:** Cristina Martín Olmos

***Directors*:** Francesc Pérez-Murano
Andreu Llobera Adan

***Tutor*:** David Jiménez Jiménez

En Dr. Francesc Pérez-Murano, Professor d'investigació del CSIC i en Dr. Andreu Llobera, Investigador "Ramón y Cajal" del CSIC, directors de la present Tesi Doctoral i en Dr. David Jiménez, Professor Agregat del Departament d'Enginyeria Electrònica de l'Escola Tècnica Superior d'Enginyeria de la Universitat Autònoma de Barcelona,

CERTIFIQUEN:

Que la memòria " *Micro/Nano fabrication of polymer based devices* " presentada per Cristina Martín Olmos, ha estat realitzada sota la seva direcció.

Bellaterra, Febrer de 2008.

Francesc Pérez-Murano Andreu Llobera David Jiménez

A la vida,
als meus pares per donar-me-la,
al meu germà per compartir-la,
i a en Guillermo per millorar-la

OVERVIEW

This document summarizes the research work performed in order to obtain the Ph.D. degree in Electronic Engineering at the *Universitat Autònoma de Barcelona* (UAB).

The work has been done at the National Centre for Microelectronics (*Centro Nacional de Microelectrónica* CNM), at the Institute of Microelectronics in Barcelona (IMB).

CNM-IMB activities are divided into 6 different research areas covering a wide range of microelectronic devices: microsystems and silicon technology, chemical transducers, power devices and systems, biomedical applications, electronic circuits design and nanotechnology. The present work has been performed in the latter area.

Most of the work has been performed in the frame of the FP6 European research project NOVOPOLY (*Novel functional polymer materials for MEMS and NEMS applications*) which aims to develop new functional materials for applications in the area of micro- and nano- systems technology (MEMS and NEMS). Also, a part of the thesis was performed within the frame of the FP6 European research project NaPa (*Emerging Nanopatterning Methods*) which aims the development of novel nanopatterning techniques as can be NIL, soft lithography, MEMS-based lithography, etc. Both projects have been source of funding, motivations and collaborators that have contributed notoriously to the development of this Thesis.

The first objective of the project was to establish the basis for polymer fabrication technology in the CNM Clean Room. CNM has always been working on silicon technology but, provided that polymer technology is showing itself as a low-cost alternative, it was interesting (at a local level) to optimize these processes.

On the other hand, there is a large interest in adding functionality to existing photostructurable polymers, like SU-8, and overcome the current limitations of these systems with respect to mechanical, electrical conductivity and high temperature stability properties. These novel polymers can represent in the near future a cornerstone in the development of polymer technology, with both academic and industrial applications. Taking profit of some collaborations

established in the projects mentioned above, the processing of some novel polymers is also presented in this Thesis for a few targeted applications.

Therefore, the Thesis is a compendium of different polymeric devices, each of them fabricated with a different process, because either the materials or the techniques were different; and the memory is divided in seven different chapters:

The introduction, aims to review the state of the art of polymer fabrication techniques. As this Thesis is focused in the use of photostructurable polymers for the fabrication of devices, the main process is the UV lithography although others methods have been developed in order to achieve higher resolution and better performance. Lithographic techniques usable for polymers are briefly described and the three kinds of polymers used are introduced in order to give the basic knowledge and main concepts used through all the work.

Chapter 2 presents the fabrication of usable polymeric AFM probes, demonstrating their field of application and low cost production and its feasibility to commercialization. This is the main activity that CNM had in Novopoly project.

Chapter 3 is an extension of the previous chapter but using a new composite material. The new material overcomes some of the drawbacks properties of the original epoxy based resist and also adds functional properties as it can be magnetic actuation.

In Chapter 4 another new composite is shown. In this case, optothermal actuation is demonstrated because this material has a higher thermal expansion coefficient than the undoped version. In addition, given the fact that the material is black, which means that optical actuation in the visible is possible, opening new possibilities compared with the standard polymer. A theoretical model and a fully study of the actuation behaviour is reported.

Chapter 5 describes polymer structures definition by ink-jet printing and soft-lithography. These two techniques were used to avoid the cross contamination between dispensing holes of a previously fabricated microfluidic chip. This chapter is itself an example of how flexible polymer technology is.

Scanning Probe Lithography (SPL), Electron-Beam Lithography (EBL) and UV lithography techniques have been combined to pattern thin layers of polymers as it is depicted in Chapter 6. This chapter includes details mechanism and operation of the local modification of polymers using an Atomic Force Microscope (AFM).

Finally, this Thesis ends with the conclusions that are summarized in Chapter 7. The main results of each fabrication process developed are commented.

Castellano

Este documento resume el trabajo de investigación realizado para la obtención del título de Doctora en Ingeniería Electrónica en la *Universitat Autònoma de Barcelona (UAB)*.

El trabajo ha sido elaborado en el Centro Nacional de Microelectrónica (CNM), en el Instituto de Microelectrónica de Barcelona (IMB).

Las actividades del CNM-IMB están divididas en 6 áreas de investigación diferentes, cubriendo un amplio rango de dispositivos microelectrónicos: microsistemas y tecnología de silicio, transductores químicos, dispositivos y sistemas de potencia, aplicaciones biomédicas, diseño de circuitos electrónicos y nanotecnología. Este trabajo se ha ejecutado dentro de esta última área.

La mayor parte del trabajo se ha elaborado en el marco del proyecto de investigación europeo FP6 NOVOPOLY (*Novel functional polymer materials for MEMS and NEMS applications*) que tiene como objetivos desarrollar nuevos materiales para aplicaciones en el área de la tecnología de los micro- y de los nano- sistemas (MEMS y NEMS). Otra parte de la Tesis se realizó en el marco del proyecto de investigación europeo FP6 NaPa (*Emerging Nanopatterning Methods*) cuya meta es el desarrollo de nuevas técnicas de estampación nanométrica como puede ser el NIL, soft lithography, la litografía basada en MEMS, etc. Ambos proyectos han sido fuentes de motivaciones, capital para recursos y colaboradores que han contribuido notoriamente en la formación de esta Tesis.

El primer objetivo de este trabajo fue el de establecer las bases de la tecnología de fabricación con polímeros en la Sala Blanca del CNM. El CNM siempre ha trabajado con tecnología de silicio pero, dado que los polímeros están demostrando ser una alternativa de bajo coste, era interesante (a nivel local) optimizar estos procesos.

Por otra parte, existe un gran interés en modificar los polímeros fotoestructurables existentes, como la SU-8, añadiéndoles diferentes funcionalidades y superar así las actuales limitaciones de estos materiales con respecto a sus propiedades mecánicas, a su conductividad eléctrica, a mejorar su estabilidad en altas temperaturas, etc. Estos nuevos polímeros pueden representar en un futuro próximo las bases del avance de la tecnología de polímeros, tanto para aplicaciones académicas como industriales. Gracias a las colaboraciones establecidas en los proyectos europeos antes mencionados, se ha podido presentar en esta Tesis el procesado de algunos nuevos polímeros para algunas aplicaciones concretas.

Por todos los motivos mencionados, esta Tesis es un compendio de diferentes dispositivos poliméricos, cada uno de ellos fabricado con procesos distintos, porque o bien los materiales o bien las técnicas no eran las mismas. Por esta razón, la Tesis se divide en 7 Capítulos:

La introducción pretende repasar el estado del arte de las técnicas de fabricación con polímeros. Como esta Tesis está enfocada en el uso de polímeros fotoestructurables para la fabricación de dispositivos, el principal proceso es la UV lithography aunque otros métodos han sido desarrollados para alcanzar mayor resolución y mejores resultados. Las técnicas litográficas que pueden ser usadas con polímeros están brevemente descritas y también se introducen tres tipos diferentes de polímeros para dar un conocimiento básico de los conceptos más usados a lo largo de esta memoria.

El Capítulo 2 presenta la fabricación de sondas de AFM poliméricas que pueden ser usadas en cualquier equipo de AFM comercial, demostrando así su campo de aplicación, su bajo coste de producción y su capacidad para ser comercializadas. Esta es la principal responsabilidad que el CNM tenía dentro del proyecto Novopoly.

El Capítulo 3 es una extensión del capítulo anterior pero usando un nuevo material compuesto por nanopartículas y polímero. El nuevo material mejora algunas de las propiedades del polímero original y también se añaden propiedades que antes no tenía como puede ser la actuación magnética.

En el Capítulo 4 se introduce otro nuevo polímero. En este caso, se demuestra que el material es capaz de proporcionar actuación optotérmica debido a que tiene un mayor coeficiente de expansión térmica que la versión no dopada. Además, dado que el material es negro, la actuación óptica en el visible es posible, lo que abre nuevas posibilidades comparado con el polímero estándar. Un modelo teórico y un estudio completo del comportamiento de esta actuación están detallados.

El Capítulo 5 describe cómo definir estructuras de polímero usando el ink-jet printing y la soft-lithography. Estas dos técnicas han sido usadas para evitar la contaminación cruzada entre los depósitos de un previamente fabricado chip de microfluídica. Este capítulo es un claro ejemplo de la flexibilidad que ofrece la tecnología de polímero.

Las técnicas de Scanning Probe Lithography (SPL), Litografía por Haz de Electrones (EBL) y la litografía UV se pueden combinar para imprimir en finas capas de polímeros tal y como se describe en el Capítulo 6. En este capítulo se incluyen los detalles del mecanismo de modificación local de polímeros usando en Microscopio de Fuerzas Atómicas (AFM).

Finalmente, esta Tesis termina con las conclusiones que están resumidas en el Capítulo 7. En él se comentan los principales resultados de cada uno de los procesos de fabricación desarrollados en esta memoria.

Català

Aquest document resumeix el treball d'investigació realitzat per l'obtenció del títol de Doctor en Enginyeria Electrònica a la *Universitat Autònoma de Barcelona (UAB)*.

El treball ha estat elaborat al Centre Nacional de Microelectrònica (CNM), a l'Institut de Microelectrònica de Barcelona (IMB).

Les activitats del CNM-IMB estan dividides en 6 àrees d'investigació diferents, cobrint un ampli rang de dispositius microelectrònics: microsistemes i tecnologia de silici, transductors químics, dispositius i sistemes de potència, aplicacions biomèdiques, diseny de circuits electrònics i nanotecnologia. Aquest treball s'ha dut a terme dins d'aquesta última àrea.

La major part de la feina s'ha emmarcat en el projecte d'investigació europeu FP6 NOVOPOLY (*Novel functional polymer materials for MEMS and NEMS applications*) que té com a objectius desenvolupar nous materials per aplicacions en l'àrea de la tecnologia dels micro- i dels nano-sistemes (MEMS i NEMS). Una altra part de la Tesi es va realitzar en el marc del projecte d'investigació europeu FP6 NaPa (*Emerging Nanopatterning Methods*) que pretén desenvolupar noves tècniques d'estampació nanomètrica com poden ser el NIL, soft lithography, la litografia basada en MEMS, etc. Ambdós projectes han estat fonts de motivacions, capital per recursos y col·laboradors que han contribuït notòriament en la formació d'aquesta Tesi.

El primer objectiu d'aquest treball va ser el de establir les bases de la tecnologia de fabricació amb polímers en la Sala Blanca del CNM. El CNM sempre ha treballat amb tecnologia de silici però, donat que el polímers estan demostrant ser una alternativa de baix cost, era interessant (a nivell local) optimitzar aquests processos.

Per altra banda, existeix un gran interès en modificar els polímers fotoestructurables existents, com la SU-8, afegint-los diferents funcionalitats i superant així les actuals limitacions d'aquests materials pel que fa a les seves propietats mecàniques, a la seva conductivitat elèctrica, a millorar la seva estabilitat a altes temperatures, etc. Aquests nous polímers poden representar en un futur pròxim les bases de l'avanç de la tecnologia de polímers, tant per aplicacions acadèmiques com industrials. Gràcies a les col·laboracions establertes en els projectes europeus abans mencionats, s'ha pogut presentar en aquesta Tesi el processat d'alguns nous polímers per algunes aplicacions concretes.

Per tots aquests motius esmentats, aquesta Tesi és un compendi de diferents dispositius polimèrics, cadascun d'ells fabricat amb processos diferents, perquè o bé els materials o bé les tècniques no eren les mateixes. Per aquesta raó, la Tesi es divideix en 7 Capítols:

La introducció pretén repassar l'estat de l'art de les tècniques de fabricació amb polímers. Com aquesta Tesi està enfocada en l'ús de polímers fotoestructurables per a la fabricació de dispositius, el principal procés és la UV lithography tot i que altres mètodes han estat desenvolupats per assolir millor resolució i millors resultats. Les tècniques litogràfiques que es poder utilitzar amb polímers estan breument descrites i també s'introdueixen tres tipus diferents de polímers per donar un coneixement bàsic dels conceptes més fets servir al llarg d'aquesta memòria.

El Capítol 2 presenta la fabricació de sondes d'AFM polimèriques que podes ser utilitzades en qualsevol equip d'AFM comercial, demostrant així el seu camp d'aplicació, el seu baix cost de producció i la seva capacitat per a ser comercialitzades. Aquesta és la principal responsabilitat de què el CNM tenia dins del projecte Novopoly.

El Capítol 3 és una extensió del capítol anterior però usant un nou material compost per nanopartícules i polímer. El nou material millora algunes de les propietats del polímer original i també s'afegeixen propietats que abans no tenia com pot ser l'actuació magnètica.

En el Capítol 4 s'introdueix un nou polímer. En aquest cas, es demostra que el material és capaç de proporcionar actuació optotèrmica degut a que té un coeficient d'expansió tèrmic més elevat que la versió no dopada. A més, donat que el material és negre, l'actuació òptica en el espectre del visible és possible, el que obre noves possibilitats comparat amb el polímer estàndard. Un model teòric i un estudi complert del comportament d'aquesta actuació estan detallats.

El Capítol 5 descriu com definir estructures de polímer utilitzant l'ink-jet printing i la soft-lithography. Aquestes dues tècniques han estat emprades per evitar la contaminació creuada entre els dipòsits d'un, prèviament fabricat, xip de microfluídica. Aquest capítol és un clar exemple de la flexibilitat que ofereix la tecnologia de polímer.

Les tècniques d'Scanning Probe Lithography (SPL), Litografia per Feix d'Electrons (EBL) i la litografia UV es poden combinar per imprimir en fines capes de polímers tal i com es descriu en el Capítol 6. En aquest capítol s'inclouen els detalls del mecanisme de modificació local del polímers fent servir el Microscopi de Forces Atòmiques (AFM).

Finalment, aquesta Tesi acaba amb les conclusions que estan resumides en el Capítol 7. En ell es comenten els principals resultats de cada un dels processos de fabricació desenvolupats en aquesta memòria.

ACKNOWLEDGEMENTS

During the period of time comprised in this Thesis, one person has mostly made everything possible and achievable. His nice character and nice personality, his availability, his great ideas and his capacity to find answers, have made the resolution of all the problems much easier. I feel very lucky to have been supervised by Dr. Francesc Pérez-Murano. Thank you for giving me the opportunity to explore the world of nanofabrication, polymers, and the experiences of living in Japan and in California. Thank you also for your advices, your comments and for helping me when I needed.

The fact of having been also supervised by Dr. Andreu Llobera brought me strong support. His invaluable help, his transfer of knowledge in many fields and his original solutions have been essential to this work. But what I appreciate most from him are his enthusiasm and confidence.

I also would like to thank my academic supervisor, Dr. David Jimenez for his friendship and comprehension.

In addition to this, I would like to acknowledge to all the people that collaborated with me during these years. Firstly to all the partners of Novopoly project, specially to Dr. Anja Voigt and Ms. Gabi Grützner for all the shipped polymer material and fruitful discussions; to Dr. M. Lucia Curry and Dr. Chiara Ingrosso for the nanoparticles incorporation and their kindly support; to Mr. Vahid Fakhfouri, Dr. Joo Yeon Kim and Mr. Kris Pataky for his help with the ink-jetting of polymers and to Professor Jürgen Brugger and Professor Anja Boisen for his interest and encouragement. I would like to add some partners of NaPa project, Dr. Liviu Nicu and Dr. Thierry Leichlé to make so easy and pleasant the work with them.

I would like also to recognize all the other collaborations indispensable in this Thesis. To Dr. Ismael Díez-Perez, Dr. Gerard Oncins and Sara Chamadoira, for their help with the AFM measurements and their interpretations. To Dr. Oriol Ossó for all the indentations performed in order to determine the Young's Modulus of the different materials. Thanks also to Dr. Gabriel Abadal, Dr Kirill Zinoviev, Dr. Montserrat Calleja, Dr. Javier Tamayo and Dr. María Arroyo for having given me the opportunity to measure with their measure system, which made possible

the optothermal characterization. To Dr. Javier del Campo, Dr. Olga Ordeig and Ms. Roser Mas for having shared with me their experience in electrodes fabrication and electrochemistry and for having performed the measurements.

Let me give my thanks to all the advices and contributions that Dr. Jaume Esteve, Dr. Joan Bausells, Dr. Josep Montserrat, Dr. Álvaro San Paulo, Dr. Gabriel Abadal, Dr. Xavier Borrisé, Dr María Villarroya and Ms. Ana Sanchez have made to work. I also would like to thank to Dr. Hiromi Kuramochi and Sensei Yokohama for having accepted me for an internship, giving me the opportunity to work with them.

No less important are all the people who made more enjoyable, entertaining, rapid and feasible many of the most boring and difficult processes like Marta Gerbolés, Llibertad Solé, Iñigo Martin, Carles Mateu, Jordi Llobet, Julien Arcamone and Víctor Cadarso. Thank you for having always made me feel welcome.

All the work performed in this thesis required of a clean room facility. Daily work of many people contributed to make possible many processes and fabrications described in this Thesis. Many thanks to all the CNM-IMB-CSIC clean room staff, particularly to Zenón Navarro. In addition, I would like not to forget all the people that watch for the correct operation of the center and the help received from José Rus and Roger Llopis.

Very special thanks go to Raquel Palencia and Dr. Mª Angeles Benítez, for making possible so many processes, for always change an “impossible to do” for a “we can try…”. I appreciate a lot your dedication.

Personal relationships have helped me in many occasions to overcome and forgive the bad moments. In this sense I would like to deeply thank to Ana Tarrega, Monica Sarrión, María Sánchez, Riccardo Rurali, Sergio Díez, Juan Pablo Esquivel, Fredy Segura and Jorge Barreto in addition to the most of the people mentioned previously. I would like to dedicate these few lines to thank Gemma Rius, for her help in the experiments, her advices in many fields, her concern and friendship that have been indispensable for me during these years and to Sergio Sanchez who also helped me in many occasions with informatics issues as well as in everyday life matters.

Good friends are also always required to keep your mind out of work during free time and make you feel happy and stable. Most of the work has been done by my lovely Carol, my adventurer Marta, my understanding Estel and my sweet Roser.

Special thanks go to my brother, for his unconditional assistance everywhere, every time since he was two years old. All my love to my parents, even though they will not understand a word

of all the work here described, they have always valued me, helped me, and felt proud of me as anybody else, and that was one of the reasons for me to fight everyday. Also, my tightest hug for my grandma, that survived a civil war; overcame a death father, a death sister and a death husband; that saved her four children and that has suffered more than eighty summers without air conditioning.

Last but not least, I would like to emphasize the huge help received from Guillermo Villanueva. Since our beginnings in the CNM-IMB, his interest in all the scientific lines, his capacity to understand and explain, his constructive criticism, his incredible intelligence and his braveness and honesty have been teaching me through all these years. My warmest thanks. I just only can hope that you always be my best friend, my best confident and my best partner. You are essential to me.

Finally and considering that during these five years at the CNM-IMB-CSIC, I have interacted with many people, I wouldn't like to miss anybody. If something makes characteristic this place is the kindness of all the workers. Many thanks to all the IMB staff.

INDEX

Chapter 1. Polymers for lithography 1

1.1 Introduction 3
1.2 Micro/Nano lithography 5
1.2.1 Photolithography 5
1.2.2 Electron Beam Lithography (EBL) 7
1.2.3 Ion Beam Lithography (IBL) 9
1.2.4 Nano Imprint Lithography (NIL) 9
1.2.5 Soft lithography 10
1.2.6 Ink-jet printing 12
1.2.7 Scanning Probe Microscope (SPM) Lithography 13
1.3 Specific polymers 15
1.3.1 Poly-(Methyl Methacrylate) (PMMA) 15
1.3.2 Poly(dimethyl siloxane) (PDMS) 16
1.3.3 SU-8 and epoxy-based photoresist 17
1.4 Summary 25
1.5 References 27

Chapter 2. Epoxy based resist AFM probes 33

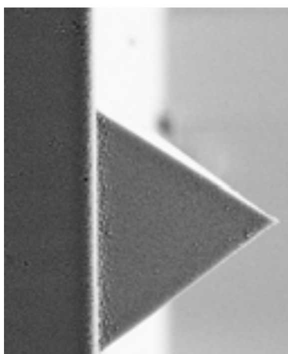

2.1 Introduction 35
2.1.1 AFM 35
2.1.1.1 Contact Operation Mode 37
2.1.1.2 Dynamic Operation Mode 38
2.1.2 AFM Probes 39
2.2 Fabrication process of epoxy based resist AFM probes 41
2.2.1 Mould preparation 41
2.2.2 Probes fabrication 43
2.3 Design 45
2.4 Fabrication process optimization 51
2.4.1 Tip aspect ratio 51
2.4.2 Cantilever deflection 54

INDEX

2.4.2.1 Description of processes 56
2.4.2.2 Comparison of results 60
2.5 Structural/functional characterization 65
2.5.1 Contact mode in air 65
2.5.2 Dynamic mode in air 68
2.5.3 Dynamic mode in liquid 71
2.6 Aging study 75
2.6.1 Study in clean room environment 75
2.6.2 Study in non controlled environment 78
2.6.3 Study after delivery 80
2.7 Conclusions 83
2.8 References 85

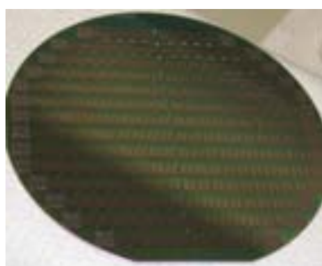

Chapter 3. Nanoparticles doped epoxy based resist AFM probes 89

3.1 Introduction 91
3.1.1 Incorporation of Nanoparticles to polymers 94
3.1.2 Composite assembly 95
3.1.2.1 Iron oxide composite (γ-Fe_2O_3) 95
3.1.2.2 Titanium Oxide composite (TiO2) 99
3.2 Process flow 101
3.2.1 Single layer cantilever 101
3.2.2 Double layer cantilever 103
3.3 Structural/functional characterization 107
3.3.1 Preliminary characterization of NCs 108
3.3.2 Dynamic mode in air 110
3.3.2.1 Single layer cantilever 110
3.3.2.2 Double layer cantilever 113
3.3.3 Dynamic mode in liquid 115
3.3.4 Magnetic Actuated Drive mode in air 118
3.3.5 Magnetic Force Mode in air 119
3.4 Conclusions 121
3.5 References 123

Chapter 4. Optothermal actuators 127

4.1 Introduction 129
4.1.1 Actuation techniques 129
4.1.2 Actuating materials 131

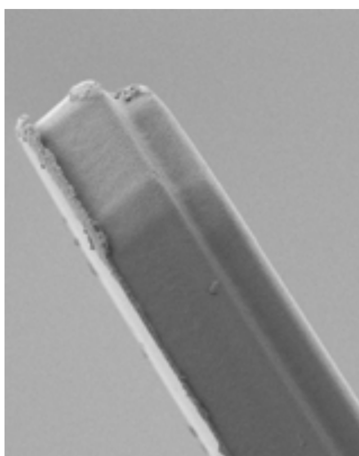

4.1.3 Polyaniline doped epoxy based resist 132
4.2 Theoretical study 135
4.2.1 Basic mechanics for a multi-layered structure 135
4.2.1.1 Thin metal layer 138
4.2.1.2 Bi-layered structure 138
4.2.2 Deflection due to thermal expansion 139
4.2.2.1 Constant temperature 140
4.2.2.2 Rectangular distribution of the temperature 140
4.2.2.3 Rectangular distribution of the incident power 142
4.2.3 Optothermal actuation 147
4.2.4 Design rules 148
4.3 Fabrication 149
4.3.1 Process flow 149
4.3.2 Preliminary characterization of the composite 152
4.3.3 Fabrication results 152
4.4 Characterization 155
4.4.1 Constant temperature 155
4.4.2 Optothermal actuation – Experimental setup 1 157
4.4.3 Optothermal actuation – Experimental setup 2 161
4.4.4 Discussion of results 163
4.5 Conclusions 165
4.6 References 167

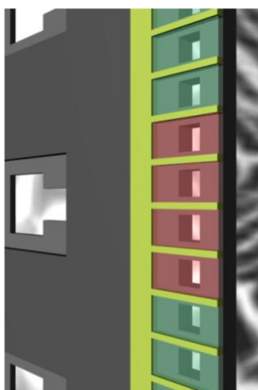

Chapter 5. Polymeric Hydrophobic Barriers 171

5.1 Introduction 173
5.2 Bioplume system 177
5.3 Fabrication of microfluidic chip 181
5.4 Hydrophobic barriers 185
5.4.1 Ink-jet printing 186
5.4.2 Soft-lithography 189
5.5 Validation test 193
5.6 Conclusions 195
5.7 References 197

INDEX

Chapter 6. AFM based fabrication **201**

6.1 Introduction 203
6.1.1 Force-assisted AFM nanolithography 203
6.1.1.1 Mechanical indentation 204
6.1.1.2 Thermomechanical writing 205
6.1.1.3 Manipulation 206
6.1.2 Bias-assisted AFM nanolithography 207
6.1.2.1 Anodic oxidation 207
6.1.2.2 Electrochemical deposition 212
6.1.2.3 Electrochemical modification 212
6.1.3 Force-distance curves 213
6.1.4 Experimental conditions 218
6.2 Local modification of thin PMMA layers 221
6.2.1 Additional/Specific experimental details 221
6.2.2 Results 222
6.2.3 Discussion 227
6.3 Local modification of thin epoxy based resist layers (non exposed) 231
6.3.1 Additional/Specific experimental details 231
6.3.2 Results on Si surfaces 233
6.3.3 Results on Au surfaces 237
6.3.4 Discussion 239
6.4 Local modification of thin epoxy based resist layers 241
6.4.1 Additional/Specific experimental details 241
6.4.2 Results on silicon surfaces 241
6.4.3 Results on Au surfaces 246
6.5 Applications 249
6.6 Conclusions 253
6.7 References 255

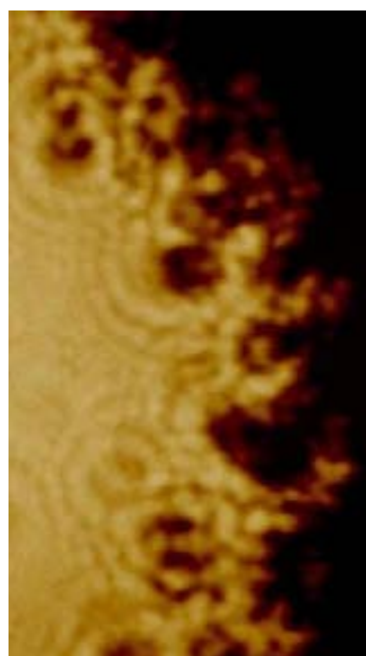

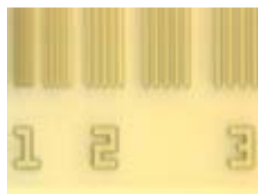

Chapter 7. Conclusions **261**

List of Publications 265

Chapter 1. POLYMERS FOR LITHOGRAPHY

Technologically, polymers are interesting because they offer a fast and cheap way of producing Microsystems, as can be sensors, actuators, chips for microfluidics, etc. Substituting silicon as a structural material for polymers, building polymer based micro/nano systems, will allow a drastic reduction of the production cost, together with a huge increase of the technological flexibility. Scientifically, polymers are also interesting since they can be doped with organic or inorganic materials, which can give the polymer new functionalities and properties. The main process step in the fabrication of polymeric devices is the lithography. Many lithographic techniques can be used to pattern polymers so a review of the different techniques is presented.

1.1 INTRODUCTION

During the last decades, the development of microelectronics and microfabrication technologies [1] has implied a revolution in our society, mainly by reducing the size of the transistors and electronic circuits, but also by the fabrication of Micro Electro Mechanical Systems (MEMS) [2, 3], as for example sensors or small mechanical components for larger macroscopic devices.

Reducing the size of the transistors brought more powerful and cheap microprocessors, and hence computers, allowing their domestic use. This represents one of the main targets of microfabrication: the reduction in size of the components, what currently is moving deep into the sub-micron dimensions. Furthermore, the development of MEMS permitted the production of cheaper and more sensitive sensors, which can currently be found in most of the security and health care devices, e.g. airbag systems, fire and poisonous gases detectors, glucose measurement, etc; and also the precise fabrication of mechanical components for, e.g., watches. These mechanical components must have micrometric precision in shape but must be thick enough to withstand friction and weariness, which represents then the second main target for microfabrication technologies, i.e. obtaining high aspect ratio structures.

Microfabrication technologies can be divided into three different groups, i.e. silicon technology, polymer technology and LIGA. Wafers are processed using basically three kinds of steps: a step in which the material at/on the surface is modified or deposited (e.g. oxidation, deposition of dielectric layers, deposition of metallic layers, ionic implantation); another step in which that material is structured or patterned (e.g. wet etching, dry etching, lift-off process); and a third kind of step in which the parts of the surface that are removed, patterned or modified are locally selected according to a pre-existing custom pattern (lithography process).

The main differential characteristic of silicon technology is that all the constitutive materials are solid-state (inorganic). Polymers are used and are of great importance, but just as a part of the lithographic process, in order to pattern the underlying material. On the contrary, polymers fabrication technology includes polymers as structural materials. Finally, LIGA is a very specific fabrication technique developed at the beginning of the 80s [4] for the fabrication of high aspect ratio structures. It consists in the machining, with the use of X-rays, of a thick layer of poly (methyl-methacrylate) and then using it as a mould for the electrodeposition (ED) of a metal layer.

As it has been commented, the fabrication of high aspect ratio structures has been one of the main targets of microfabrication. LIGA technology solved this issue but, as it is necessary the use of X-rays, the access to a synchrotron radiation is needed, what makes the process quite

expensive. As an economic alternative, silicon technology with the use of Deep Reactive Ion Etching (DRIE) [5]; and polymer technology with the use of a high aspect ratio resist, i.e. SU-8 [6], can be used, representing an inflection point for, e.g., watch industry.

On the other hand, the need for reducing the dimension of transistors has induced the development of new techniques for fabrication, especially for lithography that is one of the pillars of the whole process of micro/nano fabrication, given that no device can be built without the use of lithography.

1.2 MICRO/NANO LITHOGRAPHY

Lithography comes from the Greek words “lithos” (stone) and “graphos” (write) and it refers to the process invented by Alois Senefelder in Bohemia in 1796. Such process consisted in the use of a smooth piece of limestone which had an oil-based image put on its surface. On the rest of the surface, Gum Arabic was applied sealing it. Finally, the printing could be done with oily or watery ink, transferring to the substrate either the oily-based image or its negative respectively.

At present, a number of different lithography processes can be found, e.g. standard UV lithography, Electron Beam Lithography (EBL), nanoimprint lithography, soft lithography, stencil lithography, etc. The parameters used to measure the quality of the lithographic process are the resolution, the alignment precision and the throughput (as the number of wafers or samples that can be processed in one hour).

1.2.1 Photolithography

Currently, photolithography is the most widely used form of lithography. It is used by the integrated circuits (IC) industry, e.g. in the processing of CMOS wafers, in order to produce the required circuitry. During the photolithographic process the pattern is transferred from a glass mask with chromium onto photosensitive polymer which then is used as a mask for the etching that finally replicates the pattern in the underlying layer.

The basic photolithographic sequence could be summarized in the following steps:

Coating

First of all, all moisture is removed from the wafer surface by increasing its temperature. The wafer is cooled before the photoresist is dispensed at the centre of the wafer and spun over the entire surface. The thickness of the resist is a solution of the combination of three factors: resist viscosity, spinning speed and contact angle between the resist and the substrate. Subsequently, a soft-bake removes solvent out of resist.

Align/Exposure

Once the photosensitive resist is on top of the wafer, it is illuminated by a UV radiation. This illumination is performed locally by placing a glass mask with a metal absorber pattern on top. Each mask must be defined carefully upon insertion to the system, and then each wafer must be held in the correct position and indexed across the exposure location to allow the pattern for each layer on the wafer to be accurately transferred over previous exposures (alignment).

Development

After exposition, a post-exposure bake (PEB) is optionally performed in order to enhance the exposure and prepare the wafers for the subsequent dip in a developer, that is an etchant solution that selectively etches the exposed resist (for positive resists) or the non-exposed areas (for negative resists). Afterwards, another bake (sometimes also known as hard bake, HB) is performed, in order to evaporate solvents and harden the resist.

Using projection optics, the resolution is limited by diffraction effects created by the chromium patterns in the photomask, which lead to blurring of those patterns when transferred to the resist. The resolution varies as:

$$Resolution = \frac{k \cdot \lambda}{NA}$$

where k is a constant that depends on the resist (material and thickness) and process technology; λ is the wavelength of the light used to expose the resist and NA is the numerical aperture of the systems, which is proportional to the refraction index (n) of the medium where the system is immersed and the angle (θ) of the maximum cone of light during the exposure.

Hence, due to the diffraction limit, it is generally not possible to use photolithography to define sub-wavelength structures. However, changes in the numerical aperture or in the constant k can improve the resolution. Those changes can be made, e.g. using top surface imaging, silylation of resists, sophisticated mask technology (including phase-shift masks and optical proximity corrections), etc. Currently, optical lithography might be used to achieve features down to 35 nm (Table 1.1) [7, 8]. Unfortunately, this implies more and more complex masks and processes, which implies an increase of costs.

In Table 1.1, photolithography methods are enumerated. As it can be seen, reducing the wavelength implies a reduction in the minimum achievable dimensions. Most of the Clean Rooms, at least at research level, are equipped with photolithography equipments working with UV lithography (using G- or I-line of a Hg lamp), which implies a limit of around 300 nm if projection lithography is used (stepper) or around 1-2 microns if contact or proximity lithography are used.

It is possible to mention several advantages of optical lithography, e.g. full wafer processing; exposition times in the range of several seconds (what implies a fast process) and, maybe the

most important of all, the joint expertise acquired by all the different laboratories and/or companies after many years working with this technique.

<table>
<tr><th colspan="2">Light Source</th><th>Wavelength</th><th colspan="2">Resolution</th></tr>
<tr><td rowspan="2">Hg lamp (UV)</td><td>G line</td><td>436 nm</td><td colspan="2">400 nm</td></tr>
<tr><td>I line</td><td>365 nm</td><td colspan="2">300 nm</td></tr>
<tr><td rowspan="3">Deep UV (Laser excimer)</td><td>KrF</td><td>248 nm</td><td colspan="2">180 nm</td></tr>
<tr><td>ArF</td><td>193 nm</td><td colspan="2">100 nm</td></tr>
<tr><td>F_2</td><td>157 nm</td><td colspan="2">70 nm</td></tr>
<tr><td>Deep UV (Immersion lithography)</td><td>ArF</td><td>193 nm</td><td colspan="2">35 nm</td></tr>
<tr><td colspan="2">X Ray</td><td>1-10 nm</td><td colspan="2">50 nm</td></tr>
<tr><td colspan="2" rowspan="3">Extreme UV</td><td rowspan="3">14 nm</td><td>k = 0.75</td><td>100 nm</td></tr>
<tr><td>k = 0.60</td><td>80 nm</td></tr>
<tr><td>k = 0.37</td><td>50 nm</td></tr>
</table>

Table 1.1: Decreasing the wavelength. New methods have been developed to achieve better resolution [7].

On the other hand, the main drawbacks for this technique are the limited resolution that the standard technique (UV lithography) presents, around 1 micron; the impossibility of working with pre-existing topography and the processing cost of more advanced techniques (DUV, X-rays, etc.), just available for a few Clean Rooms in the world.

Therefore, when nanometric dimensions are needed, photolithography is not the most common option and usually alternative techniques are chosen.

1.2.2 Electron Beam Lithography (EBL)

Electron beam lithography (EBL) is currently the most used nanostructure fabrication method. The basic concept is similar to that of photolithography, i.e. an electron beam exposes an electron sensitive resist and, during the subsequent development, either the exposed areas or the non exposed are removed, depending if the resist is positive or negative respectively. The main difference is that diffraction effects for electrons are much smaller because the wavelength is much lower than that of photons with the same energy and therefore this is not the limiting factor for the resolution. The second difference is that EBL is mostly used as a serial process, which means that a Gaussian beam is created and it exposes "pixel-by-pixel" the full

pattern. The beam is deflected and modulated with the use of electrostatic and/or magnetic fields in order to produce an image. The size of the beam is limited by aberrations and quantum effects (Heisenberg's principle); which with modern optics for electrons implies a limit of around 1 nm for the diameter of the beam, as opposed to 500 nm for light.

However, electrons scatter quickly in solid materials, which makes that the effective exposed area is larger than the beam size. This leads also to the so-called "proximity effect" meaning that the distance between patterns matters when optimizing the dose and the size of the beam. In order to minimize the proximity effect and the scattering in the resist material, high energy electron beams (100-200 keV) or very low energy electron beams (below 5 keV) are used. Also, as electrons are charged particles, vacuum operation is needed, which increases the cost of the system. Moreover, as it is a serial process, the processing time is relatively high, which also increases processing cost. As a result of these two last points, EBL has been mainly limited to mask making for photolithography. As an alternative, many research laboratories have adapted their Scanning Electron Microscopes to use them as EBL systems.

Considering the resists, several commercial options are available in the market. Although almost any material could be used as a resist for EBL (meaning that electrons affect any material), it is necessary to consider sensitivity, tone, resolution and etching resistance.

PMMA is one of the first resists that was ever used with EBL and it is still in use, mainly for lift-off processes. On the other hand, to act as a mask for subsequent etch, it is more convenient to use ZEP, given that the etching resistance is better. Both positive resists have shown patterns down to tens of nm. On the other hand, a negative resist called HSQ is dedicated for ultra-high resolution EBL. 12 nm features with 12 nm gap have been achieved with this resist [9] that also shows a high resistance as a mask.

As it has been commented, this technique is mostly used as a serial technique, which is one of the drawbacks, as it slows the processing. The throughput can be increased using a matrix of parallel e-beams (sometimes called Projection Maskless Lithography, or PML). This increases the complexity of the system and puts high requirements for the individual beams in terms of brightness, energy spread and beam opening, as well as on the optics of the lenses.

One of the options for a parallel processing, inside PML, is known as "scattering with angular limitation projection electron-beam lithography" (SCALPEL) [10]. This approach combines the high resolution and wide process latitude inherent in EBL with the throughput of a parallel projection system. In the SCALPEL system, a mask consisting of a low atomic number membrane and a high atomic number pattern layer is uniformly illuminated with high energy electrons (100 keV). The entire mask structure is essentially transparent to the electron beam, so very little of

the beam energy is deposited in it. The portions of the beam passing through the high atomic number pattern layer are scattered through angles of a few milliradians. Afterwards, a lens system focuses the electron beams in the plane of the substrate. An aperture in the back focal plane of the lenses stops the scattered electrons and produces a high contrast image in the wafer [10, 11].

However, all the parallel processing techniques for EBL are still under development given the fact that with photolithography the resolution has been pushed down to some tens of nanometers. As throughput is mainly sought by the IC manufacturing companies and they use photolithography, EBL is mostly used as a serial technique for prototyping (research level) or mask manufacturing for photolithography.

1.2.3 Ion Beam Lithography (IBL)

Using a very similar approach than EBL, there exists also the possibility to expose and/or pattern using ion beams instead of electron beams. In this case, given the fact that the ions suffer less scattering than electrons because they are heavier, the proximity effect is reduced and the resolution increased. It has to be considered that ions of adequate energy (50-100 keV) deposit their energy completely in the resist layer while electrons of 100 keV penetrate deeply into the substrate. This leads to quite different resist sensitivities (equal dose to clear large areas in $\mu C/cm^2$) [12].

Alternatively, ions can also be used for resistless processes, meaning that they can directly machine the surface of a substrate [13].

1.2.4 Nano Imprint Lithography (NIL)

Nano Imprint Lithography (NIL) [14] is an emerging patterning method that combines nanometer-scale resolution and high throughput. The working principle is completely different to the two lithography techniques already presented. In this case, the resist is locally displaced by mechanical pressure exerted by a stamp on the substrate.

The first step for NIL is the fabrication of a stamp. This is basically a rigid chip or wafer with some reliefs in the surface. Those reliefs correspond to the features that will be transferred to the resist afterwards. A basic step in the preparation of the stamp previously to the imprinting is the deposition of an anti-sticking layer (normally a Self Assembled Monolayer, SAM) on top of the pre-patterned face of the stamp. Once the stamp is ready, there exist basically two different ways to proceed and transfer the pattern into the resist: thermal NIL or UV-NIL.

In the first case [15], the substrate or stamp temperature is increased above the glass transition temperature (T_g) of the resist, reducing its viscosity. Then, a pressure is applied and the resist flows from the places where stamp protrusions are located, causing an eventual decrease in thickness in those areas. The temperature of the sample is decreased and subsequently the pressure released.

In the second case, UV-NIL, the resist is initially not solid because T_g is lower than room temperature, so the pressure is applied without heating. Once the resist has flowed to conform to the stamp, a UV exposure is performed, causing a reaction in the resist that increases T_g, making the resist solid.

In both cases, the stamp is finally separated from the substrate and the replication is complete after the thin residual layer has been removed (thin resist layer remaining in the places where the protrusions of the stamp were present).

Patterns with nano- to micrometer scale features can be replicated in a parallel process, and the stamp may be reused many times. Therefore, the throughput is very high (enabling even the fabrication of large numbers of nanostructures over a large area), with a low process cost and a high resolution (below 10 nm [16]).

The fundamental limit for the resolution using this technique is given by the radius of gyration of the resist polymer used. Historically the most used resist has been PMMA, a known polymer from other applications (EBL, X-rays, LIGA, etc.) that works very well with thermal NIL. More recently, new generations of polymers have been developed specifically for NIL (e.g. mr-l 70XX and mr-l 80XX families from Microresist technology [17]), increasing resolution, improving etching resistance and tuning T_g.

Great advances have been performed in NIL in the last few years, most of them in the reliability of the technique for its use in an eventual commercial application, i.e. fabrication of IC, CMOS, etc [14]. However, this technique is still in its first stage of development and further improvements are necessary before the inclusion of NIL in circuit fabrication.

1.2.5 Soft lithography

Soft lithography provides an alternative set of techniques for microfabrication. It does not have the limitations of using materials that are photosensitive, and it can be applied to non-planar surfaces, in contrast to the previously exposed methods.

Soft lithography includes a suite of techniques that use physical contact between a topological patterned stamp and a substrate [18, 19]. It can seem somehow similar to NIL but there is a

main and basic difference: the stamp is made of a soft material, hence it is not rigid. The most used materials are the elastomer poly(dimethyl siloxane) (PDMS) and silicon rubbers.

The fabrication of the stamp is done by pouring a prepolymer of the elastomer onto a master having relief structure on its surface. The prepolymer is then cured and subsequently peeled off.

Figure 1.1

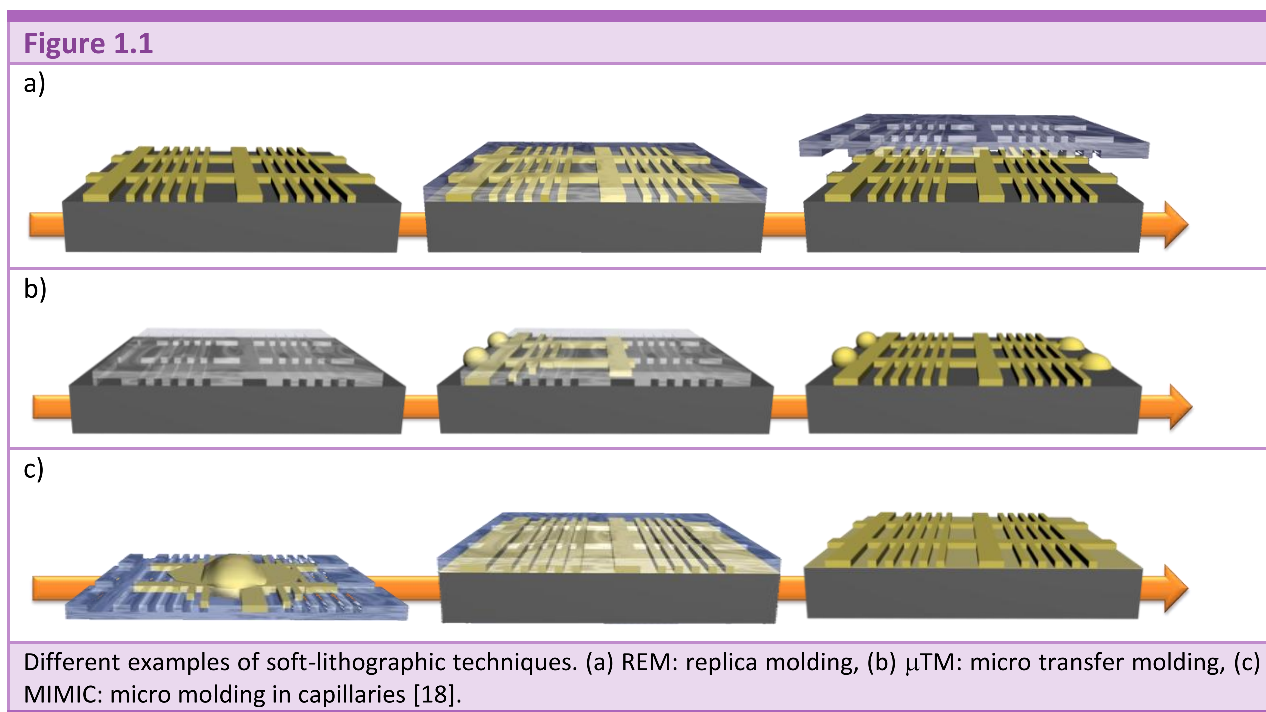

Different examples of soft-lithographic techniques. (a) REM: replica molding, (b) μTM: micro transfer molding, (c) MIMIC: micro molding in capillaries [18].

Once the mould has been made, it can be used, for example, to create patterned self assembled monolayers SAMs on a substrate (μCP) and then used them as a mask to pattern the substrate [20, 21], to generate gradients of hydrophobicity [22], etc.

Another possibility is to use the stamp to replicate its relief structures in a polymeric material (Figure 1.1). This can be made by pouring the polymer onto it to generate a replica (REM, technique similar to the initial preparation of the mould); or transfer the reliefs onto a substrate after removing the excess of polymer (μTM); or replicating the reliefs on a substrate by means of capillary action (MIMIC). All these techniques are then based on the use of the stamp as a mould, transferring the shape into a polymer or prepolymer that becomes solid and stiff after curing, exposing to UV-light, etc.

Soft lithography techniques have five characteristics that are useful for the microfabrication of functional devices [23, 24]:

- They are fast. It often takes less than 24 hours to go from a concept to a prototype device.
- They are inexpensive: they do not require the use of expensive equipment or infrastructure.
- They allow the patterning of a range of functional materials (metals, polymers, molecules, and biological organisms) directly onto surfaces.
- They can be used to pattern non-planar surfaces.
- They are simple to use, and do not require specialized training.

On the other hand, reproducibility and number of defects are two of the main drawbacks that this technique is presenting.

1.2.6 Ink-jet printing

Ink-jet printing is a technique that allows drop-on-demand dispensing of microscale droplets (tens of microns in diameter) by means of an actuated nozzle [25, 26].

Originally, this technique was developed in order to produce printers for computers. Currently, it is possible to find ink-jet printers for domestic users that allow the deposition of ink droplets with a size below 100 μm in radius [27], though an specialized ink is necessary. At a research level, ink-jet systems have been used in order to fabricate structures with materials that are difficult to machine by other methods [28].

Figure 1.2

a)

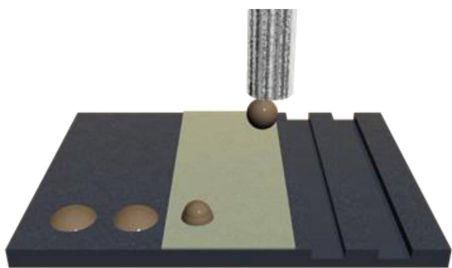

b)

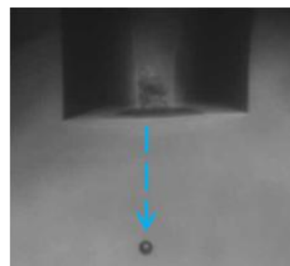

(a) Schematic of an ink-jet printing experimental setup and (b) optical picture of the extreme of a nozzle with a released droplet. The core of the dispensing head consists of a glass capillary which is surrounded by a tubular actuator (thermal, piezoelectric or both). At one end the capillary is formed to a nozzle (diameter 30 to 100 μm). The actuator creates a pressure wave which propagates through the glass into the liquid. In the nozzle region the pressure wave accelerates the liquid. A small liquid column leaves the nozzle. If the kinetic energy is enough, the column breaks off and forms a droplet which flies freely through the air. Depending on the nozzle sizes (30 to 100 μm) volumes of 25 up to 500 pl are generated.

A standard ink-jet system [29] consists of (Figure 1.2.a) a glass capillary with a narrow end (nozzle) in the tens of microns range in diameter, integrated with an actuator. These two parts together form any commercial printing head. In addition, it is necessary to have a moving xy-system to allow locally selective deposition of material onto the substrate. This can be attained by moving the nozzle or the substrate by means of a xy-moving stage. The basic principle of ink-jet starts with the generation of a pressure wave inside the glass capillary (that is full of the fluid material to be printed) by means of the actuator. This pressure wave implies that, in the orifice of the nozzle, the fluid surface will be deformed. If the energy of the wave is enough, the fluid close to the surface will have enough kinetic energy to generate a droplet and detach from the nozzle (Figure 1.2.b).

Depending on the actuation method that is used, three different technologies can be distinguished: thermal, piezoelectric or combined ink-jet. In thermal ink-jet, small resistors are located all around the nozzle and rise temporarily and locally the temperature. This gradient of temperature is translated rapidly into a movement in the inner fluid. Piezoelectric ink-jet is based on the application of a mechanical pressure to a part of the nozzle. Again, this gradient converts into a movement of the fluid. The most complete ink-jet systems are formed by both types of actuations, what increases the possibilities to obtain a better control of the droplets generation. Thermal actuation is much cheaper so it is used in the majority of the commercial ink-jet devices, even though it presents some issues, as the fact that the ink is exposed to temperatures in the range of 200°C, which is really high for polymers and resists, implying the necessity of optimization of the solvents and add-ins to the materials to be ink-jetted. For research, piezoelectric actuation is preferred because then it is possible to avoid such high temperatures for the polymers. In addition, it is possible to better control the size of the droplets. However, it is always necessary an optimization of the solvent(s) of the materials to be printed, in order to improve the volatility, solubility, wettability, viscosity and surface tension.

1.2.7 Scanning Probe Microscope (SPM) Lithography

Scanning Probe Lithography (SPL) encompasses techniques that use small (<50 nm) tips scanned near the surface of a sample in the configuration of scanning tunneling microscopes (STMs) [30], atomic force microscopes (AFMs) [31], scanning electrochemical microscopes (SECM) [32] or scanning near-field optical microscopes (SNOMs) [33]. Although scanning probes were originally designed to provide high-resolution images of surfaces, their lithographic capability was demonstrated in a set of experiments with an STM, just five years after the first STM images were recorded [34]. In that work, a large electrical bias applied between a tungsten tip and a germanium surface caused transfer of a single atom from the tip to the surface. Since then,

STMs, AFMs, SCEMs and NSOMs have been used in many different ways to perform sophisticated lithography.

Advantages of SPL methods include high resolution that, for AFM and STM methods, approaches the atomic level (5-15 nm); the ability to generate features with nearly arbitrary geometries; and its precise positioning. These methods are serial techniques, however, and have writing times that are typically limited by the mechanical resonances of the tips and the piezoelectric elements that maintain constant separation between the tips and the samples. Research is looking for a method to increase the speed of these techniques by incorporating integrated arrays of the tips that can write in parallel [35] and by incorporating piezoelectric elements that have higher resonance frequencies [36]. Unless these approaches yield a huge increase in speed, it is likely that SPL methods will be better suited for research labs and for masters fabrication for NIL or SL [37].

1.3 SPECIFIC POLYMERS

Up to now, several lithographic techniques that are used to pattern polymers have been described. In this section, it is aimed to give a brief introduction to the polymeric materials that will appear in following chapters, i.e. PMMA, PDMS and SU-8.

1.3.1 Poly-(Methyl Methacrylate) (PMMA)

Poly-(Methyl Methacrylate) (PMMA) is a versatile positive resist that is well suited for many microelectronic applications. It is most commonly used as a high resolution, high contrast resist for EBL, deep UV (190-250 nm) and X-rays lithographic processes and also for thermal NIL (given that its T_g is around 105ºC).

Positive resists are generally macromolecules containing functional groups that strongly influence the solubility characteristics of the molecule. Upon illumination these functional groups are removed or replaced by others, thus rendering the molecule soluble in different kinds of solvents. For example, a photochemical reaction can be induced to replace certain functional groups with carboxyl groups, thus making the exposed resist soluble and developable in aqueous alkali solutions. This approach works well in the case of exposure by light because the light is absorbed by the functional groups only, and the subsequent photochemical reaction is limited to, or to the neighbourhood of, the absorbing chromophores.

A higher resolution approach is to change the solubility characteristics by using electron beam exposure to alter the size of macromolecules. The chemical effect of ionizing radiation of polymers is twofold: cross-linking of neighbouring chains and random scission of the chains take place simultaneously [38].

Exposure dose for a good contrast with PMMA resist ranges between 50 and 500 $\mu C/cm^2$, depending on substrates, thickness of the PMMA layer, beam energy, equipment used, etc. The range of suitable beam energies is really broad, from below 5 keV to 200 keV. Overexposure of the resist one order of magnitude beyond these charge densities causes the reactions leading to cross-linking to dominate, turning the resist behaviour into negative [39]. Hence, the resist in such overexposed areas cannot be removed with acetone or ethyl acetate. Photosensitivity is low for any wavelength, maximizing for DUV (220 nm). When using pure PMMA the required dose is around 500 mJ/cm^2 for λ = 250 nm. For X-rays (λ = 0.83 nm), dose must be 1-2 J/cm^2. This resist is insensitive to white or ultraviolet light exposure.

Standard commercial PMMA products for EBL have 495k and 950k as molecular weights (MW) and can be found formulated in chlorobenzene or in anisole (more environmental friendly). With the standard products, a wide range of thicknesses is covered, from 100 nm to 5 μm, depending on the spin speed and the concentration of solvent in the resist. An example of spin curve, extracted from [40], can be found in Figure 1.3.

As for the mechanical characteristics, PMMA has a low elastic modulus (1.8-3.1 GPa) compared to that of silicon and a high coefficient of thermal expansion (CTE), $76 \cdot 10^{-6}$ K^{-1}.

Figure 1.3

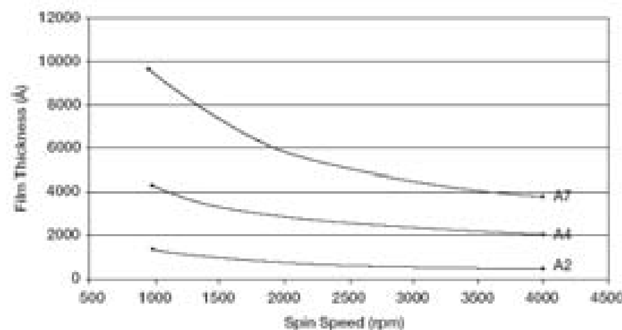

Spin curve for PMMA with a MW of 950k in an anisole solution with a concentration of around 5% [40].

1.3.2 Poly(dimethyl siloxane) (PDMS)

Poly(dimethyl siloxane) (PDMS) is a commercially available clean room compatible type of silicone rubber with a wide range of applications, as can be sensors [41], microvalves [24], microfluidics [23], etc.

PDMS has some unique properties, as for example an extremely low T_g of around −125ºC, which yields a ultra low elastic modulus, ranging from 100 kPa and 5 MPa. As it is an uncompressible fluid, its Poisson's ratio is 0.5, which implies a huge amount of possible applications. Its coefficient of thermal expansion (CTE) is very high ($200 \cdot 10^{-6}$ K^{-1}), as well as its biocompatibility and its chemical inertness. For fluidic devices results very interesting given the fact that, although in principle is hydrophobic, it is possible to oxidize its surface, generating a hydrophilic material and also allowing two pieces of material to bond between them.

One of the main drawbacks of this material, at least for microfluidics applications, is its gas permeability, which means that it is not possible to drive gases through PDMS channels. On the other hand, that permeability can be used to fabricate gas sensors out of or containing some PDMS.

In order to obtain PDMS, it is possible to acquire directly solid films already prepared or to prepare the elastomer by mixing a PDMS prepolymer, e.g. SYLGARD® 184 (Dow Corning) with its curing agent in a given proportion, for example 10:1 in volume, although it can be different. After the mixing, some bubbles will be present in the viscous fluid, so a vacuum procedure is usually performed in order to get rid of them. By placing the mixing at a relatively low pressure, e.g. 0.1 mbar, the gas in the bubbles is extracted. Once the material is free of bubbles, it is poured on the substrate to be replicated and it is cured at high temperature during some time. The temperature and time depend one on the other, i.e. the higher the temperature the shorter the required time. Some standard values are 80ºC and 20 minutes. After curing, PDMS is ready to be used.

1.3.3 SU-8 and epoxy-based photoresist

SU-8 is a chemically amplified epoxy based negative resist [6]. Negative photoresists are materials that become insoluble in developing solutions when exposed to optical radiation. Negative resists were the first materials used to pattern semiconductor devices, and still comprise the largest segment of the photoresist industry because they are widely used to define the circuitry in printed circuit boards (PCB). However, the current use of negative resists in the semiconductor industry is reduced because of the difficulties in achieving high-resolution patterns. Recent advances in the chemistry of negative-resist systems, however, have provided materials with wide processing latitude and high resolution that are used to manufacture advanced CMOS devices and to achieve high-aspect-ratio patterns for micromachining applications [42] (Figure 1.4).

Figure 1.4

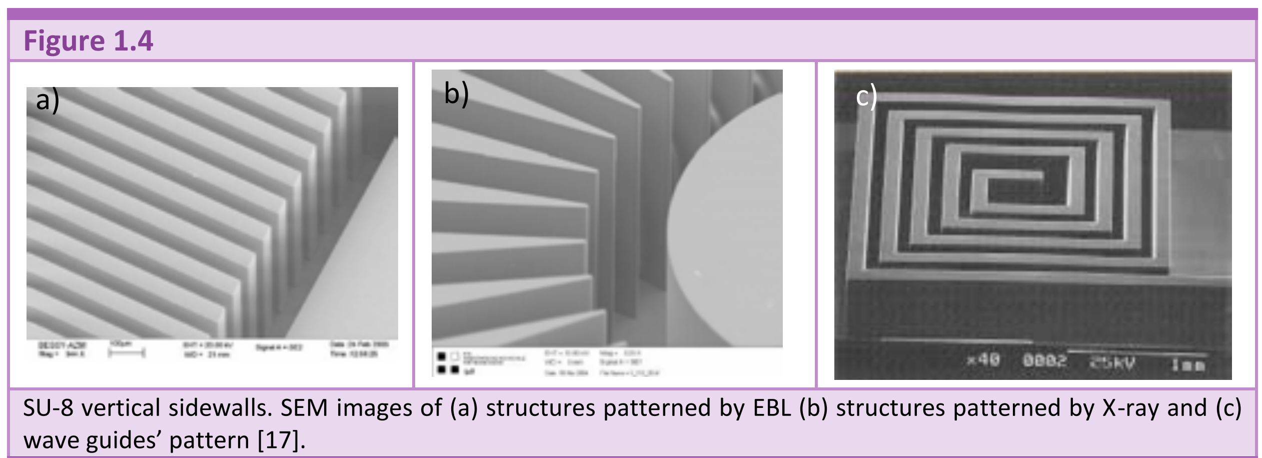

SU-8 vertical sidewalls. SEM images of (a) structures patterned by EBL (b) structures patterned by X-ray and (c) wave guides' pattern [17].

SU-8 is a negative-tone photoresist based on EPON SU-8 resin and is photosensitized by the addition of a triaryl sulfonium salt, e.g. Cyracure UVI from Union Carbide, which is also called

Photo Acid Generator (PAG). The resist has two important properties suited for ultrathick applications. First, its low molecular weight; which implies that it can be dissolved in a variety of organic solvents to form very high concentrations mixtures (72%–85% solids by weight). Second, the layer has very low optical absorption in the near-UV spectrum. At 365 nm, UV transmission through a 100 μm thick layer is 46%, as shown in Figure 1.5. This low optical absorption implies that the light is able to reach the bottom part of the resist layer. Additionally, during exposure, the refractive index increases, creating a waveguide effect and hence achieving the vertical walls (Figure 1.4).

Figure 1.5

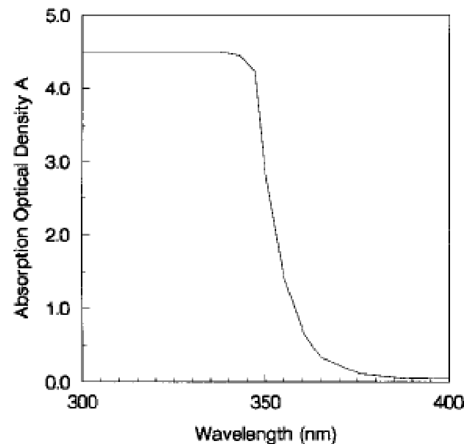

UV absorption spectrum for a 100 μm thick SU-8 film (figure extracted from [6]). The transmission coefficient (T) is defined as: $T = 10^{-A}$. This implies that at λ = 365 nm, T is 46%.

As it has been commented, the low MW of the epoxy allows the preparation of a wide range of solutions with different amounts of solvents. The concentration in weight of the epoxy molecules in the solvent affects directly to the viscosity of the resist, and therefore to the spin curve, i.e. to the thickness of the layer as a function of the spin speed. As an example, Figure 1.6 presents the spin curves for 4 different solutions of the epoxy in solvent, with their dynamic viscosities.

It is very important then to choose the appropriate resist for the application that is aimed. Then, a product with a higher or lower concentration of solvent will be used. For example, to deposit a layer of 200 μm, the appropriate amount of the SU-8 resin is dissolved in cyclopentanone in a weight ratio of 75:25 (other solvents used to prepare epoxy based resists are γ-butyrolactone, GBL, and anisole). To this solution is added 5% in weight of a triaryl sulfonium salt and then the resist is ready. When spinning at 1500 rpm, a layer of around 200 μm is obtained (in this case the viscosity would be 55.5 Pa·s, for comparison with the data in Figure 1.6). Once the

appropriate resist solution has been chosen, the processing can start. This processing of SU-8 or other epoxy based resists is crucial for the development of this Thesis, therefore it is presented here in detail.

Figure 1.6

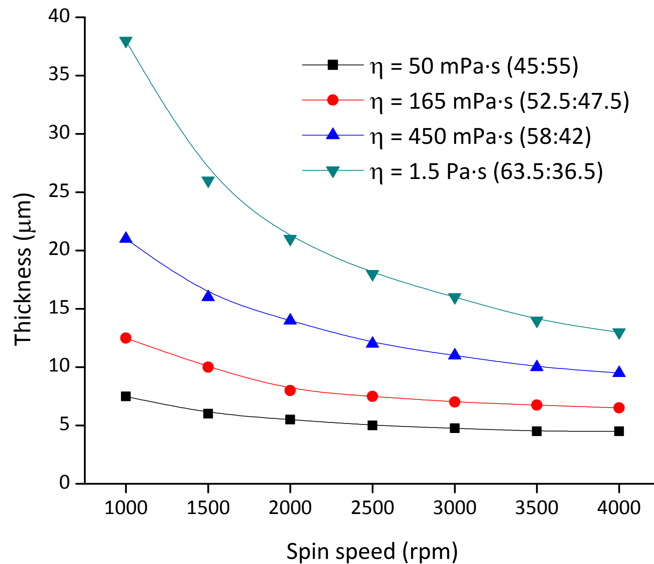

Spin curves for 4 different commercially available products [40] with different concentrations of solvent and viscosities.

It is important to introduce that SU-8 is mainly a commercial name. IBM developed resist royalties were bought by few companies which have the rights to call it in this famous name. In fact, as it has been explained, SU-8 is an epoxy based resist that can be dissolved in different solvents (cyyclopentanone and GBL for MicroChem formulations). Changing the solvent a very similar resist is obtained but not exactly SU-8. This is the particular case of the Novopoly project where micro resist technology company is involved. Micro resist technology company developed special formulations of epoxy based resist using anisole to keep the exact resist for all the partners to use in all our processes. Of course the viscosity, the solvents concentrations and the PAG is changed for each application, but Novopoly project has an extensive material library with the properties and characteristics of the used materials. For that reason in this Thesis it is always write that the polymeric resist used is an "epoxy based resist" and in the cases that the resist is commercially available, the products names from micro resist technology are referenced.

The full set of fabrication steps can present some variations depending on the resist. For example, MicroChem [40] and Gersteltec Sarl [43] provide slightly different runcards for the processing. However, the basic steps are present in both processes:

Preparation of the substrate

To obtain maximum process reliability, it is better to clean and dry the wafers prior to applying the SU-8 resist. Wafers can be cleaned by dipping them in acetone with a subsequent rinsing in isopropyl alcohol (IPA) and de-ionized (DI) water. Another option is to clean them in piranha solution (sulphuric acid and hydrogen peroxide solution), followed by DI water rinsing. Subsequently, during 30 minutes the wafers are dehydrated using a hotplate or a convection oven at high temperature (typically 200ºC). Alternatively, oxygen plasma can be used (e.g. 10 minutes @ 500 W and 400 sccm) to clean the wafers, which also dehydrates the surface; therefore it is not necessary to heat the wafer. Usually adhesion promoters are not needed but, if necessary, hexamethyldisilazane (HMDS) can be used.

Spin coating

After the substrate has cooled down, SU-8 layer is deposited by spin coating. A certain amount of resist (from 1 to 10 ml depending on the viscosity of the resist and the diameter of the substrate) is dispensed on the wafer. As it has been commented, the thickness of the deposited layer depends of the spin speed and the viscosity of the resist (Figure 1.6). In order to select the proper spin speed, the data from the vendor must be consulted.

Relax

After the sinning an optional relaxation time of around 10 minutes can be used. Wafers remain in levered position to level and blend the resist layer. In addition, if there are some bubbles just after spin-coating they can be burst using a clean and thin tip.

Soft bake

This step is performed in order to partially evaporate the solvent and hence increasing the density of the film. Although it is possible to bake the wafers in a convection oven, is preferred to use the hot plate because the solvent evaporation rate is influenced by the rate of heat transfer and ventilation. It is also important to take into account that lower initial bake temperatures allow the solvent to evaporate out of the film at a more controlled rate, which results in better coating fidelity, reduced edge bead and better resist-to-substrate adhesion. Standard procedure for soft baking involves a two steps

process, first rising the temperature up to 65ºC, keeping the substrate 5-10 minutes, and then up to 95 ºC, keeping the substrate 5-30 minutes. The ramping speed is 2-4 ºC/min.

Exposure

The exposure dose will depend on the thickness of the layer. Standard SU-8 is sensitive to near UV (λ = 350 – 400 nm) exposure (Figure 1.5). It is highly recommended to use i-line exposure tools, because the characteristics for that wavelength (λ = 365 nm) are the most widely studied. Though it is always necessary to perform some exposure test using the same tool and resist thickness that will be used in the final process, data from vendors can (and must) be consulted as a first approximation to the optimal exposure dose/time. For example, Gersteltec Sarl [43] provides with a very complete data for a 40:60 resist, as it is shown in Figure 1.7.

Figure 1.7

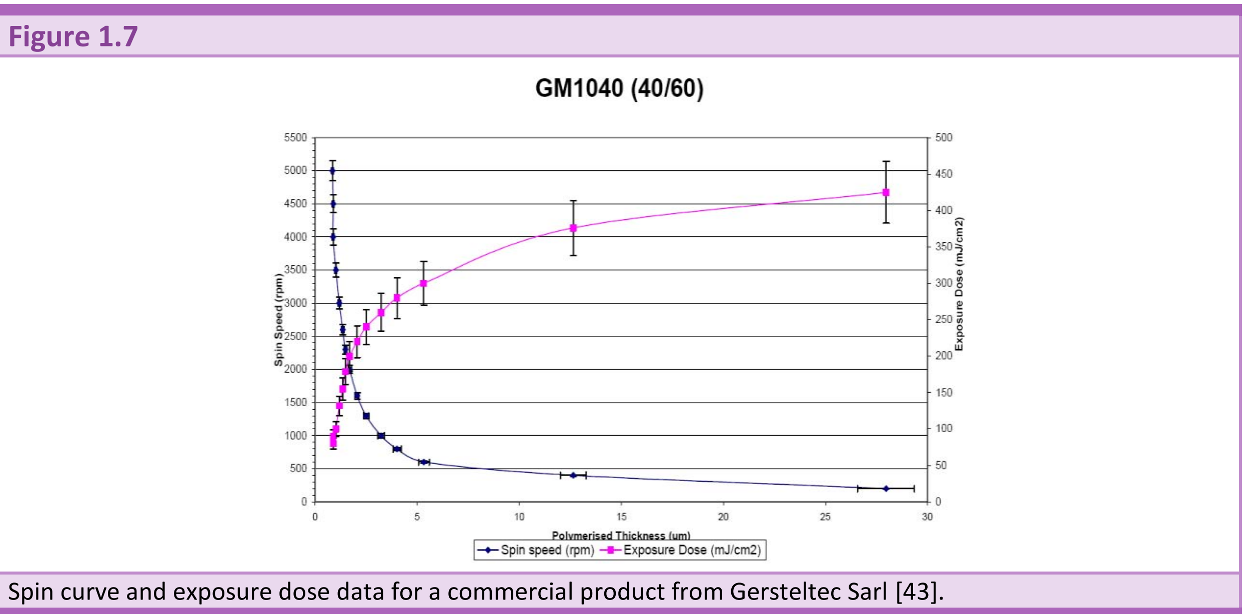

Spin curve and exposure dose data for a commercial product from Gersteltec Sarl [43].

Post Exposure Bake (PEB)

Following exposure, a post exposure bake must be performed to accelerate the cross-linking of the exposed areas of the film, making them insoluble to developer. Optimum cross-linking is obtained through careful adjustments of the exposure and PEB process conditions. Standard parameters for PEB are similar to those for the soft bake, i.e. from 65ºC to 95ºC.

Relax

After PEB, cross-linked SU-8 is a highly stressed material. Development under these conditions may lead to wafer bowing, lack of adhesion to the substrate, fractures or even resist cracking. To minimize this effect, a stress stabilization step, which consist on a delay of 24 hours between PEB and develop, can be done.

Development

For the developing process, the wafers are immersed in SU-8 Developer (Propylen Glycol Methyl Ether Acetate, PGMEA). During the immersion the wafer must be agitated for faster development, even more if high aspect ratio structures are present. Develop time has determined not to be very critical, but it also depends on film thickness (thicker films requires longer times) and processes parameters. It is recommended to change the developer solution after some time, given that it can saturate and therefore the development stops.

Following development in PGMEA, the wafers are rinsed briefly with IPA and then dried with a gentle stream of air or nitrogen.

Hard bake (HB)

Optionally, a hard bake process can be performed to the sample. It can reduce the cracks that the polymeric structures present, further remove solvents, harden the resist, improve etch resistance, reduce internal stresses, etc. HB conditions can be different and it is up to the application and previous processing that will be selected. It can be performed either in an oven or on a hot plate and involves temperatures that are always higher than the ones reached during soft bake or PEB.

As well as the lithography technique to pattern SU-8 and epoxy based resist, other techniques have been also successfully used, they are the EBL [44, 45] and a combination of the UV lithography and EBL [46].

SU-8 and epoxy based resists have high functionality, high optical transparency and are sensitive to UV radiation. Their most remarkable attributes are the high aspect ratio imaging with near vertical sidewalls (aspect ratios up to 100:1 have been reported), the incredibly high resistance to solvents, acids and bases after being cured; its suitability for prolonged plasma etching or metal plating; and its excellent thermal and chemical stability, making it well suited for applications in which cured structures are a permanent part of the device [47-54]. One of the most significant drawbacks is the high coefficient of thermal expansion (CTE), of $52 \cdot 10^{-6}$ K^{-1},

which limits their application in those devices suitable to be heated. However, as it will be explained in Chapter 4, this CTE can be used as the working principle of some devices [55].

Material	Young's Modulus	CTE	Photosensitive
PMMA	1.8 - 3.1 GPa	$76 \cdot 10^{-6}$ K^{-1}	X-Rays
PDMS	100 kPa - 10 MPa	$150 \cdot 10^{-6}$ K^{-1}	Non photosensitive
SU-8	4.5 GPa	$52 \cdot 10^{-6}$ K^{-1}	UV light

Table 1.2: Table compiling the material properties for all three polymers described in Chapter 1.

1.4 SUMMARY

Photolithography is one of the most important fabrication steps in microfabrication. Moreover, it acquires in this work an even larger relevance because most of the devices are made out of photostructurable materials. As a matter of fact, devices described in chapter 2, 3 and 4 are completely defined using this technique. In addition, in chapter 5 and 6 photolithography is also used, either as a step in silicon technology, to fabricate a mould or as a necessary step to improve the throughput of a technique with a better resolution.

Even though photolithography is the main technique used in this Thesis, other lithographic techniques have been used, as for example EBL, Soft Lithography, Ink-Jet lithography or SPM lithography. The first one plays a small role in chapter 6 to increase the throughput of SPM lithography, which is the leading technique in that chapter, presenting alternative ways of nanostructure thin layers of polymers.

Micro molding using capillaries (a soft lithography technique) and Ink-jet printing are used in chapter 5 as non standard techniques in order to complement the fabrication of a microfluidic chip, building polymeric barriers in between adjacent holes and hence avoiding cross contamination.

Regarding the different materials, PDMS and PMMA are used in chapter 5 and 6 respectively. The first one, as a key component of any soft lithographic technique, is needed to fabricate a stamp that later is used to pattern transfer some polymeric structures. The second one is used in chapter 6 to demonstrate the feasibility of a novel patterning technique using AFM-based lithography.

As for the rest of the Thesis, the materials used there are SU-8 or another epoxy based resist, with the same kind of behavior. In chapter 2, standard epoxy based resist is used in order to fabricate AFM probes. In chapter 3, a version of the previous resist doped with inorganic nanoparticles is used to fabricate improved and even functional AFM probes. In chapter 4, another version of the standard epoxy based resist, this time mixed with another organic component is presented and used to fabricate opto-thermal actuators. Finally, in chapter 6 a standard epoxy based resist with a lowest viscosity is used in order to obtain thin layers of resist.

1.5 REFERENCES

1. M.J. Madou
"Fundamentals of microfabrication : the science of miniaturization".
Ed. *CRC Press*, 2002, ISBN: 0849308267.

2. S.D. Senturia
"Microsystem design".
Ed. *Kluwer Academic Publishers*, 2001, ISBN: 0792372468.

3. M. Gad-el-Hak
"The MEMS handbook".
Ed. *CRC Press*, 2002, ISBN: 0849300770.

4. E.W. Becker, W. Ehrfeld, D. Munchmeyer, H. Betz, A. Heuberger, S. Pongratz, W. Glashauser, H.J. Michel, and R. Vonsiemens
"Production of Separation-Nozzle Systems for Uranium Enrichment by a Combination of X-Ray-Lithography and Galvanoplastics".
Naturwissenschaften, 1982, **69**(11), 520-523.

5. F. Laermer and A. Schilp
"Anisotropic etching of silicon substrates - using a polymerisation process in between etching stages to protect lateral edges of the etched shape".
Licensed by *Robert Bosch Gmbh (Bosch)*, 1994, Patent number: WO9414187-A, EP625285-A, US5501893-A.

6. K.Y. Lee, N. LaBianca, S.A. Rishton, S. Zolgharnain, J.D. Gelorme, J. Shaw, and T.H.P. Chang
"Micromachining applications of a high resolution ultrathick photoresist".
Journal of Vacuum Science & Technology B, 1995, **13**(6), 3012-3016.

7. T. Ito and S. Okazaki
"Pushing the limits of lithography".
Nature, 2000, **406**(6799), 1027-1031.

8. P.J. Yoo, K.Y. Suh, Y.S. Kim, J. Brugger, and G.J. Leggett
"Nanolithography and patterning techniques in microelectronics".
Ed. 2005, ISBN: 1-85573-931-3.

9. K.A. Lister, B.G. Casey, P.S. Dobson, S. Thoms, D.S. Macintyre, C.D.W. Wilkinson, and J.M.R. Weaver
"Pattern transfer of a 23 nm-period grating and sub-15 nm dots into CVD diamond".
Microelectronic Engineering, 2004, **73-74**, 319-322.

10. J.A. Liddle, S.D. Berger, C.J. Biddick, M.I. Blakey, K.J. Bolan, S.W. Bowler, K. Brady, R.M. Camarda, W.F. Connelly, A. Crorken, J. Custy, R.C. Farrow, J.A. Felker, L.A. Fetter, B. Freeman, L.R. Harriott, L. Hopkins, H.A. Huggins, C.S. Knurek, J.S. Kraus, D.A. Mixon, M.M. Mkrtchyan, A.E. Novembre, M.L. Peabody, W.M. Simpson, R.G. Tarascon, H.H. Wade, W.K. Waskiewicz, G.P. Watson, J.K. Williams, and D.L. Windt
"The SCattering with angular limitation in projection electron-beam lithography (SCALPEL) system".
Japanese Journal of Applied Physics Part 1-Regular Papers Short Notes & Review Papers, 1995, **34**(12B), 6663-6671.

11. M.M. Mkrtchyan, J.A. Liddle, A.E. Novembre, W.K. Waskiewicz, G.P. Watson, L.R. Harriott, and D.A. Muller
"Electron scattering and transmission through SCALPEL masks".
Journal of Vacuum Science & Technology B, 1998, **16**(6), 3385-3391.

12. W.L. Brown, T. Venkatesan, and A. Wagner
"Ion-Beam Lithography".
Nuclear Instruments & Methods in Physics Research, 1981, **191**(1-3), 157-168.

13. R.E. Lee
"Microfabrication by Ion-Beam Etching".
Journal of Vacuum Science & Technology, 1979, **16**(2), 164-170.

14. B. Bhushan
"Springer handbook of nanotechnology".
Ed. *Springer-Verlag*, 2003, ISBN: 3540012184.

15. S.Y. Chou, P.R. Krauss, and P.J. Renstrom
"Imprint lithography with 25-nanometer resolution".
Science, 1996, **272**(5258), 85-87.

16. S.Y. Chou and P.R. Krauss
"Imprint lithography with sub-10 nm feature size and high throughput".
Microelectronic Engineering, 1997, **35**(1-4), 237-240.

17. Microresist
"Micro Resist Technology GmbH Webpage".
http://www.microresist.de, 2008.

18. Y.N. Xia and G.M. Whitesides
"Soft lithography".
Annual Review of Materials Science, 1998, **28**, 153-184.

19. X.M. Zhao, Y.N. Xia, and G.M. Whitesides
"Soft lithographic methods for nano-fabrication".
Journal of Materials Chemistry, 1997, **7**(7), 1069-1074.

20. A. Kumar and G.M. Whitesides
"Features of Gold Having Micrometer to Centimeter Dimensions Can Be Formed through a Combination of Stamping with an Elastomeric Stamp and an Alkanethiol Ink Followed by Chemical Etching".
Applied Physics Letters, 1993, **63**(14), 2002-2004.

21. G.P. Lopez, H.A. Biebuyck, R. Harter, A. Kumar, and G.M. Whitesides
"Fabrication and Imaging of 2-Dimensional Patterns of Proteins Adsorbed on Self-Assembled Monolayers by Scanning Electron-Microscopy".
Journal of the American Chemical Society, 1993, **115**(23), 10774-10781.

22. J. Drelich, J.D. Miller, A. Kumar, and G.M. Whitesides
"Wetting Characteristics of Liquid-Drops at Heterogeneous Surfaces".
Colloids and Surfaces A-Physicochemical and Engineering Aspects, 1994, **93**, 1-13.

23. T. Thorsen, S.J. Maerkl, and S.R. Quake
"Microfluidic large-scale integration".
Science, 2002, **298**(5593), 580-584.

24. M.A. Unger, H.P. Chou, T. Thorsen, A. Scherer, and S.R. Quake
"Monolithic microfabricated valves and pumps by multilayer soft lithography".
Science, 2000, **288**(5463), 113-116.

25. F. Kamphoef
"Ink Jet Printing".
Ieee Transactions on Electron Devices, 1972, **Ed19**(4), 584.

26. T.W. Shield, D.B. Bogy, and F.E. Talke
"Drop Formation by Dod Ink-Jet Nozzles - a Comparison of Experiment and Numerical-Simulation".
Ibm Journal of Research and Development, 1987, **31**(1), 96-110.

27. EPSON
"EPSON Webpage".
http://www.epson.com, 2008.

28. M. Mott, J.H. Song, and J.R.G. Evans
"Microengineering of ceramics by direct ink-Jet printing".
Journal of the American Ceramic Society, 1999, **82**(7), 1653-1658.

29. T. Okamoto, T. Suzuki, and N. Yamamoto
"Microarray fabrication with covalent attachment of DNA using Bubble Jet technology".
Nature Biotechnology, 2000, **18**(4), 438-441.

30. N. Kramer, H. Birk, J. Jorritsma, and C. Schonenberger
"Fabrication of metallic nanowires with a scanning tunneling microscope".
Applied Physics Letters, 1995, **66**(11), 1325-1327.

31. J.A. Dagata
"Device fabrication by scanned probe oxidation".
Science, 1995, **270**(5242), 1625-1626.

32. A.J. Bard, G. Denuault, C. Lee, D. Mandler, and D.O. Wipf
"Scanning electrochemical microscopy - A new technique for the characterization and modification of surfaces".
Accounts of Chemical Research, 1990, **23**(11), 357-363.

33. E. Betzig and J.K. Trautman
"Near-Field-Optics - Microscopy, spectroscopy and surface modification beyond the diffraction limit".
Science, 1992, **257**(5067), 189-195.

34. R.S. Becker, J.A. Golovchenko, and B.S. Swartzentruber
"Atomic-scale surface modifications using a tunneling microscope".
Nature, 1987, **325**(6103), 419-421.

35. S.C. Minne, S.R. Manalis, A. Atalar, and C.F. Quate
"Independent parallel lithography using the atomic force microscope".
Journal of Vacuum Science & Technology B, 1996, **14**(4), 2456-2461.

36. S.C. Minne, S.R. Manalis, and C.F. Quate
"Parallel atomic force microscopy using cantilevers with integrated piezoresistive sensors and integrated piezoelectric actuators".
Applied Physics Letters, 1995, **67**(26), 3918-3920.

37. Y.N. Xia, J.A. Rogers, K.E. Paul, and G.M. Whitesides
"Unconventional methods for fabricating and patterning nanostructures".
Chemical Reviews, 1999, **99**(7), 1823-1848.

38. I. Haller, M. Hatzakis, and Srinivas.R
"High-Resolution Positive Resists for Electron-Beam Exposure".
Ibm Journal of Research and Development, 1968, **12**(3), 251-&.

39. A.N. Broers, J.M.E. Harper, and W.W. Molzen
"250-a Linewidths with Pmma Electron Resist".
Applied Physics Letters, 1978, **33**(5), 392-394.

40. MicroChem
"MicroChem Corporation Webpage".
http://www.microchem.com, 2008.

41. J.C. Lotters, W. Olthuis, P.H. Veltink, and P. Bergveld
"The mechanical properties of the rubber elastic polymer polydimethylsiloxane for sensor applications".
Journal of Micromechanics and Microengineering, 1997, **7**(3), 145-147.

42. J.M. Shaw, J.D. Gelorme, N.C. LaBianca, W.E. Conley, and S.J. Holmes
"Negative photoresists for optical lithography".
Ibm Journal of Research and Development, 1997, **41**(1-2), 81-94.

43. Gersteltec
"Gersteltec Sarl Webpage".
http://www.gersteltec.ch, 2008.

44. C. Martin, G. Rius, A. Llobera, A. Voigt, G. Gruetzner, and F. Perez-Murano
"Electron beam lithography at 10 keV using an epoxy based high resolution negative resist".
Microelectronic Engineering, 2007, **84**(5-8), 1096-1099.

45. B. Bilenberg, S. Jacobsen, M.S. Schmidt, L.H.D. Skjolding, P. Shi, P. Boggild, J.O. Tegenfeldt, and A. Kristensen
"High resolution 100 kV electron beam lithography in SU-8".
Microelectronic Engineering, 2006, **83**(4-9), 1609-1612.

46. M. Gersborg-Hansen, L.H. Thamdrup, A. Mironov, and A. Kristensen
"Combined electron beam and UV lithography in SU-8".
Microelectronic Engineering, 2007, **84**(5-8), 1058-1061.

47. H. Lorenz, M. Despont, N. Fahrni, N. LaBianca, P. Renaud, and P. Vettiger
"SU-8: a low-cost negative resist for MEMS".
Journal of Micromechanics and Microengineering, 1997, **7**(3), 121-124.

48. H. Lorenz, M. Despont, N. Fahrni, J. Brugger, P. Vettiger, and P. Renaud
"High-aspect-ratio, ultrathick, negative-tone near-UV photoresist and its applications for MEMS".
Sensors and Actuators a-Physical, 1998, **64**(1), 33-39.

49. J. Zhang, K.L. Tan, G.D. Hong, L.J. Yang, and H.Q. Gong
"Polymerization optimization of SU-8 photoresist and its applications in microfluidic systems and MEMS".
Journal of Micromechanics and Microengineering, 2001, **11**(1), 20-26.

50. J. Zhang, K.L. Tan, and H.Q. Gong
"Characterization of the polymerization of SU-8 photoresist and its applications in micro-electro-mechanical systems (MEMS)".
Polymer Testing, 2001, **20**(6), 693-701.

51. V. Seidemann, J. Rabe, M. Feldmann, and S. Buttgenbach
"SU8-micromechanical structures with in situ fabricated movable parts".
Microsystem Technologies, 2002, **8**(4-5), 348-350.

52. V. Seidemann, S. Butefisch, and S. Buttgenbach
"Fabrication and investigation of in-plane compliant SU8 structures for MEMS and their application to micro valves and micro grippers".
Sensors and Actuators A-Physical, 2002, **97-8**, 457-461.

53. V. Seidemann and S. Buttgenbach
"Closely coupled micro coils with integrated flux guidance: Fabrication technology and application to proximity and magnetoelastic force sensors".
IEEE Sensors Journal, 2003, **3**(5), 615-621.

54. A. Llobera, V. Seidemann, J.A. Plaza, V.J. Cadarso, and S. Buttgenbach
"SU-8 optical accelerometers".
Journal of Microelectromechanical Systems, 2007, **16**(1), 111-121.

55. A. Llobera, G. Villanueva, V.J. Cadarso, S. Buttgenbach, and J.A. Plaza
"Polymeric MOEMS variable optical attenuator".
IEEE Photonics Technology Letters, 2006, **18**(21-24), 2425-2427.

Chapter 2 EPOXY BASED RESIST AFM PROBES

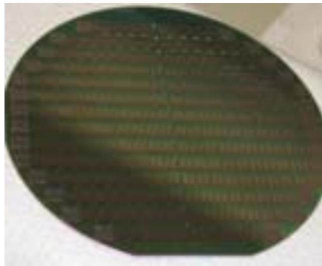

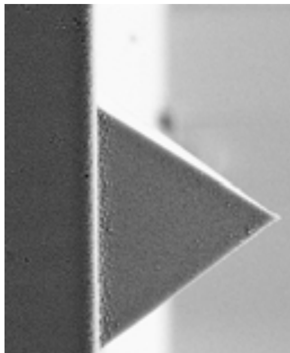

Epoxy based resists, like SU-8, have been widely used to build MEMS. In order to prove how stable polymer MEMS technology is at CNM, the fabrication and characterization of epoxy based resist atomic force microscope (AFM) probes was targeted.

These devices, already developed and fabricated by other authors [1, 2], represent a low-cost approach for the fabrication of probes and could potentially have an impact in the market. Therefore, a complete study of the probes from an eventual commercialization point of view has been done, including fabrication parameter optimization, operation in different modes and environments, and a complete aging study to check the actual feasibility of these probes as a commercial product.

In addition to the fabrication costs, epoxy based resist is a soft material, its Young's Modulus is around 4 GPa, which makes it suitable for non-destructive AFM analysis on fragile samples such biological materials [3]. Moreover, it can be modified by chemical treatments for surface functionalization.

2.1 Introduction

2.1.2 AFM

Since its development in 1986 [4], the atomic force microscope (AFM) has become a revolutionary tool for surface analysis. Binning, Quate and Gerber describe the atomic force microscope as a combination of the principles of the scanning tunneling microscope and the stylus profilometer. In an AFM, a very sharp tip located at the end of a cantilever is scanned over the sample surface, sensing the variations of the sample and generating three dimensional images. The tip-sample interaction is converted by the cantilever into a displacement, which is measured by a deflection sensor. This interaction, or force, between the sharp tip and the sample is kept small and at a constant level by means of a feedback mechanism. Therefore, when the tip is moved sideways, it will follow the surface topography, if the interaction is given by the substrate material; or it will give information about other properties (e.g. magnetic, electric, etc.) of the substrate, which actually exerts a force on the tip.

Figure 2.1

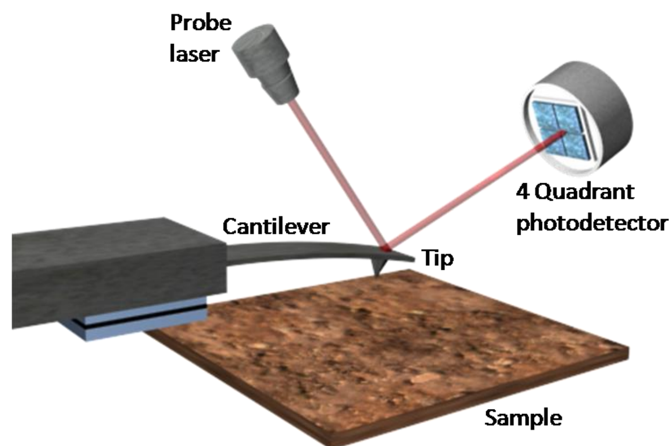

Schematic draw of a working AFM system by optical readout. The tip is mounted in the cantilever which reflects the laser beam on to the 4 quadrant photodetector. This mechanism allows reporting the cantilever movement which is reproducing the surface topography. A computer is in charge of convert the data in a 3D image of the scanned surface. [Courtesy of Ramsés Martínez]

To detect the cantilever motion, different readouts methods can be used (Figure 2.2), e.g. optical [5], capacitive [6], piezoresistive [7], etc, although the first one is still the most widely used.

Optical detection (Figure 2.1) is based on the detection of a laser beam reflected by the free end of the cantilever. The reflection of the laser is recorded by a photodectector (photodiode) and, processing the position of the laser, it is possible to map the surface. Some drawbacks of this technique are that the measurements is not very robust, given that the laser beam has to be continuously aligned; and that, given the impossibility of a whole integrated sensor, their size is not as small as it could be. On the other hand, noise is lower than in any other method, what implies that, in general, resolution is higher.

Figure 2.2

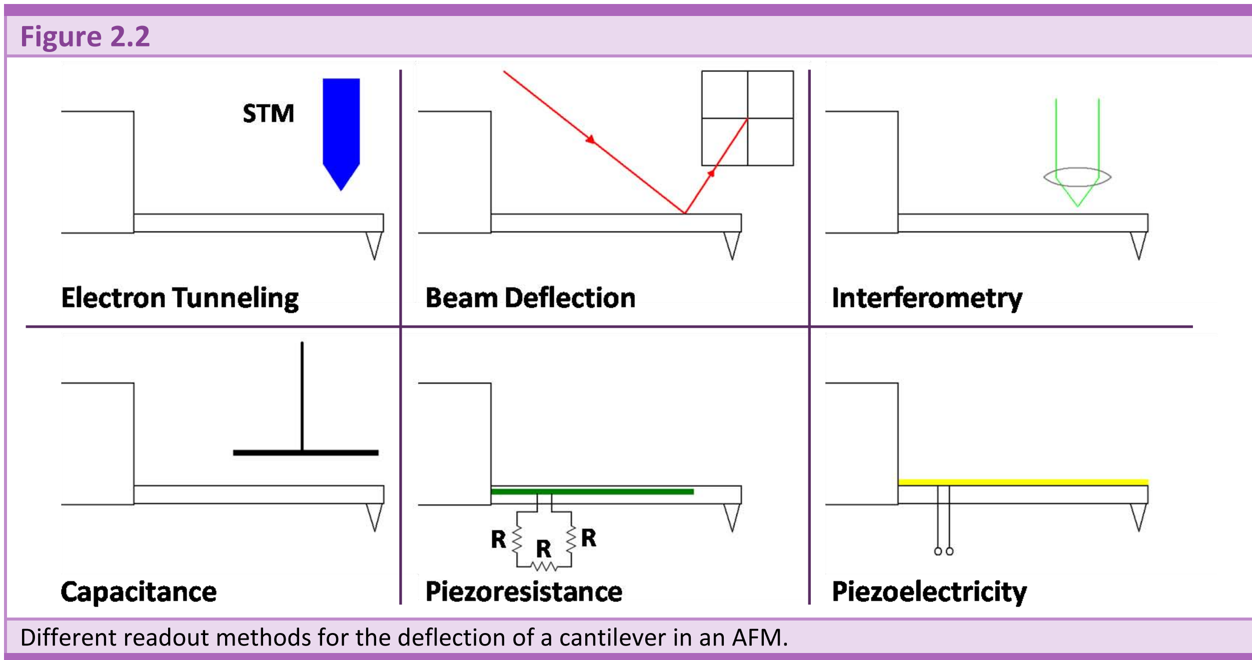

Different readout methods for the deflection of a cantilever in an AFM.

AFM is one of the so called Scanning Probes Microscopes (SPM), a family of microscopes dedicated to scan surfaces by means of tip-sample interactions. AFM is the most versatile of the whole SPM family given the fact that it can be operated in different environments, normal conditions (room temperature, atmospheric conditions), ultra high vacuum (UHV), liquid environment, low temperature, etc… It also can be used for different materials, in contrast to Scanning Tunneling Microscope (STM) that can only characterize conductive samples. Even more, a lot of applications have been developed during the last years that allow measuring a wide range of magnitudes. The most common application of the AFM is the topographic imaging of surfaces, but other extended techniques include the Magnetic Force Microscopy (MFM) that allow to measure magnetic properties, Electrostatic Force Microscopy (EFM), that allow measure the conductivity and Scanning Capacitance Force Microscopy (SCFM), to measure the capacitance, for example.

There are two basic modes in which an AFM can be operated, the dynamic (or non-contact) mode and the contact mode. This distinction relies in the working distance between the tip and the surface. The different force regimes between the tip and sample are described in a force-distance curve like the one shown schematically in Figure 2.3. Selection of the mode depends on the kind of sample to be imaged.

Figure 2.3

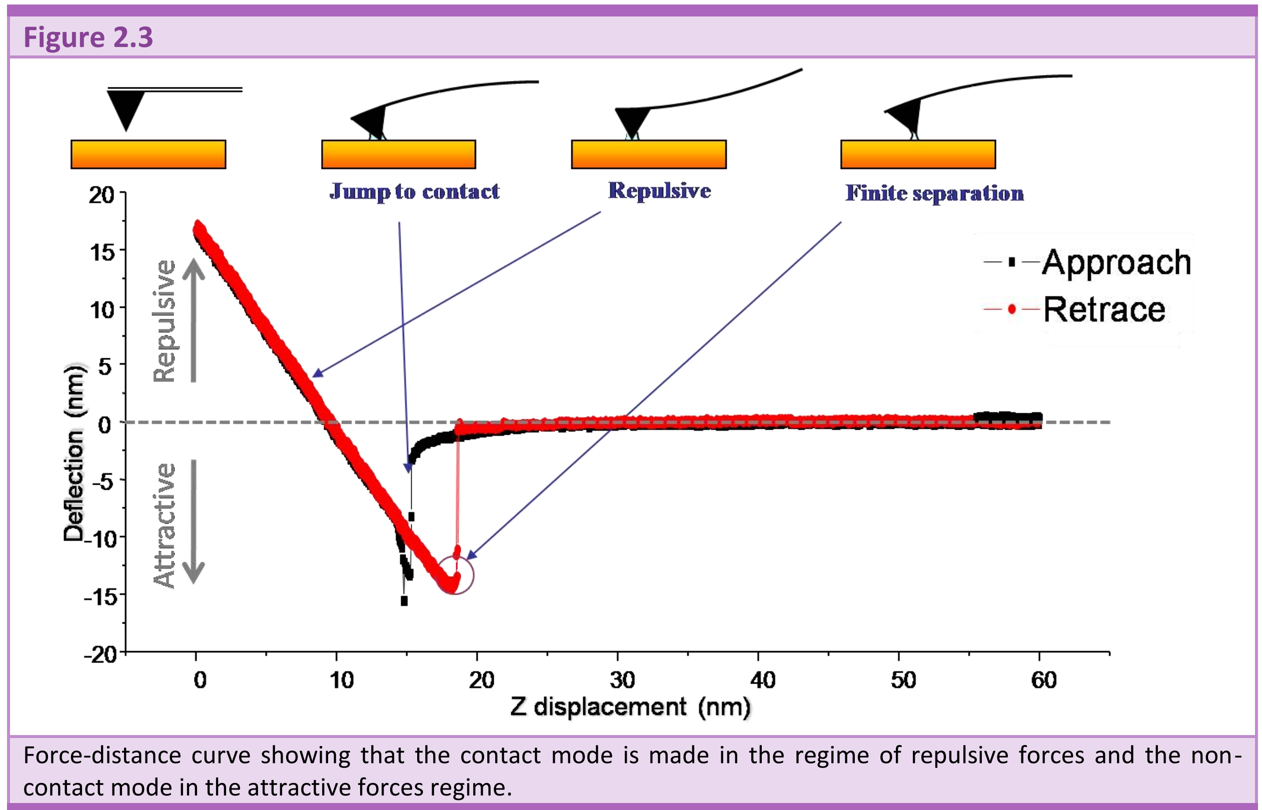

Force-distance curve showing that the contact mode is made in the regime of repulsive forces and the non-contact mode in the attractive forces regime.

2.1.2.1 Contact Operation Mode

In contact mode, repulsive forces dominate the tip sample interaction. The force applied on the tip is sensed directly by the deflection induced on the cantilever. If the measured deflection is different from the desired value (set point), the voltage of the piezo positioning element increases or decreases to correct the distance between the sample and the cantilever in order to restore the desired value of deflection. The voltage that the feedback amplifier applies to the piezo is a measure of the height of features (topography) on the sample surface. Although operation in UHV is possible, usually it is operated in ambient atmosphere or in liquids.

Problems with contact mode are caused by excessive forces applied by the probe to the sample. The effects can be reduced by minimizing the applied force, but there are practical limits to the magnitude of the force that can be controlled by the user during standard operation conditions

(room temperature, atmospheric pressure, etc.). Under such conditions, sample surfaces are covered by a layer of adsorbed gases consisting primarily of water vapor and nitrogen which is 10-30 monolayers thick. When the probe touches this contaminant layer, a meniscus forms and the cantilever is pulled by surface tension towards the sample surface, this capillary force typically is in the range of few nanometers. In addition, a large class of samples, including semiconductors and insulators, can trap electrostatic charges. These charges will generate substantial attractive forces between the probe and sample. The combination of all the previously mentioned forces defines the minimum normal force that can be controllably applied by the probe to the sample. This normal force creates a substantial frictional force as the probe scans over the sample; and these frictional forces are by far more destructive than the normal force and can damage both sample, making undesirable scratches; and the tip, causing a distortion in the resulting data.

However, it is possible to reduce the weariness of the tip by using probes with optimized cantilever dimensions, meaning that spring constants ranging from 0.01 N/m to 1 N/m are desired for contact mode operation.

Net forces acting between the tip and the sample are repulsive and are typically in the range of hundreds of nN (10^{-6}-10^{-7} N).

Using contact mode, atomic resolution was achieved [8] at the early stage of development of the technique, showing its potential as a high resolution scanning tool.

2.1.2.2 Dynamic Operation Mode

In dynamic mode [9] the tip is kept at a short distance from the sample, usually around 5-15 nm. Attractive Van der Waals forces acting between the tip and the sample are detected, and topographic images are constructed by scanning the tip above the surface. The attractive forces from the sample are substantially weaker than the forces used by contact mode. Therefore a small oscillation is applied to the tip, vibrating near its natural resonant frequency, so AC detection methods can be used to detect the small forces between the tip and the sample by measuring the change in amplitude, phase, or frequency of the oscillating cantilever in response to force gradients from the sample. In addition, the oscillation change in amplitude, phase and resonance frequency provide information about the sample's characteristics.

Schemes for dynamic mode operation include frequency modulation and the more common amplitude modulation. In frequency modulation [10], changes in the oscillation frequency provide information about tip-sample interactions.

In amplitude modulation, changes in the oscillation amplitude or phase supply the feedback signal for imaging. These changes provide information, as it has been already commented, about the tip-sample interaction. This interaction can be due to the topography of the substrate, to the different materials, etc.

In the same ways as for the static counterpart, in dynamic mode under ambient conditions, most samples develop a liquid meniscus layer. This is a larger issue in this case than in the previously presented "contact mode" because it is necessary to keep the tip close enough to the sample for short-range forces to become detectable while preventing the tip from sticking to the surface. On the other hand, the total force between the tip and the sample is very low, generally in the pN range (10^{-12} N) what is very advantageous for studying soft or fragile samples.

The probes that are used for the operation in dynamic mode are stiffer (k = 5 - 50 N/m) than for contact mode, given the fact that they do not enter in contact with the sample and that a high resonant frequency (typically in the hundreds of kHz) together with a high mechanical quality factor (Q) are desired.

2.1.3 AFM Probes

An AFM probe comprises the cantilever and the tip at its free end. These simple devices are a key component of the atomic force microscope. AFM equipments require to change probes very often to keep good resolution, that is to say probe lifetime is very short. Probes are the most important fungible on the characterization. Therefore, although the AFM equipment is further more expensive that probes, for the whole cost it has to be taken into in account probe cost, quality, lifetime, and resolution.

Probe characteristics determine for the resolution of an AFM. The tip has to be sharp enough to record the investigated sample with high lateral resolution. The cantilever must also have appropriate mechanical characteristics, according to the type of operation selected. There is no universal probe to perform any purpose measurement. The probes have to be designed and chosen according with the experiment that we want to study, but with some degrees of flexibility.

Initially, AFM probes were cantilevers made manually by cutting thin metal foils or were formed from fine wires [8]. Nowadays several different micromachining processes have been used for

the fabrication of the AFM probes. Their smaller dimensions allow higher resolution and better performance. The two most commonly used cantilever materials are silicon and silicon nitride.

Silicon AFM cantilevers are always fabricated using bulk micromachining [11] except in some special cases as, for example, in the Millipede project [12-14]. The cantilevers can be fabricated basically in two different ways, namely direct and indirect. The latter uses deposited thin films onto a silicon substrate. The cantilever is then defined by lithography and etched into the layer by wet or dry etching, followed by a release step, by removing either the silicon underneath the cantilever or a sacrificial layer.

Silicon oxide or silicon nitride cantilevers with add-on or integrated tips are fabricated using this method [15]. Cantilevers are made free-standing by etching a window through the silicon substrate from the backside of the wafer or by bonding the cantilever to a glass substrate. To fabricate integrated tips on cantilevers a combination of anisotropic and isotropic plasma and wet etching of Si is used to form either a sharp conical Si protrusion or a pyramidal depression on the surface of the wafer. The Si tip is incorporated in a thermally grown SiO_2 film, and the cantilever is formed from this film.

All parts of the sensor (AFM probe) are machined out of a silicon wafer. The cantilever (and tip) are defined and patterned by lithography on the front side and consecutively etched into the silicon. Then the wafer is thinned through a window from the backside below the cantilever until the etching front meets with a masking layer in order to protect the front side during the backside thinning. To define the tip a circular or square mask is photographically patterned and the silicon is etched away in the surroundings of the mask. Simultaneously the mask is undercut until it is completely under etched. When the mask is released and the etching is stopped, a silicon cone or pyramid remains with a sharp tip. This fabrication is interesting because the batch fabrication yields replicable sensors at moderate costs and tip, cantilever and holder are made out of one piece of material (they are monolithic). This avoids any strain due to thermal mismatch of bonded parts or stress associated with deposited thin films.

Using this fabrication method, all parts are single crystalline which yields exceptional mechanical properties, they do not have mechanical fatigue and they have a very high Q factor. In addition, the etch processes leave a flat, smooth and opaque surface at the backside of the cantilever suitable for optical detection of cantilever deflections.

In the next sections, the fabrication, characterization and testing of a completely photoplastic material AFM probes are presented. The chosen material(s) to constitute these probes is (are) negative epoxy based resists like SU-8.

2.2 FABRICATION PROCESS OF EPOXY BASED RESIST AFM PROBES

Micromachining technologies have enabled the batch fabrication of AFM probes made of silicon, silicon nitride, or silicon oxide. Such conventional probe fabrication, however, demands expensive tools that increase probes cost. While exploring cheaper alternatives, there is also some interest trying to achieve certain mechanical properties that are difficult to get with classical silicon technology. As a general and basic point, the standard requirements for a probe are: low stiffness, high resonance frequency and a high Q factor, together with a sharp tip. A fabrication process flow based on polymer technology will not only lower the cost of production but also the Young's modulus of the material, meaning that the cantilevers will be softer. Unfortunately, they will also have a smaller resonant frequency and it can be expected to find lower Q factors.

The fabrication process of epoxy based resist probes is based on the multiple spin-coating, exposure and development of epoxy based resist on a silicon wafer, which is acting as a mould for the tip. A 525 µm thickness double sided polished wafer (P-type silicon and 100 mm diameter) is used to fabricate the mould (Figure 2.4.a). Double sided polished wafers were chosen in order to allow a proper double side alignment, which is used when aligning a very thick layer of epoxy based resist. However, the alignment of such a thick layer is not critical, given that it is used to define structures with large lateral dimensions; therefore, it would be possible to use a single side polished and then, either do the double side alignment or an standard single side alignment, with the only consequence of a loss in alignment resolution of a few microns.

2.2.1 Mould preparation

First a 400 nm thermal oxide is grown at 1100°C in wet oxidation conditions (Figure 2.4.b). After that, the backside of the wafer is coated with standard positive resist (HIPR-6512) and alignment marks for double side alignment are transferred, first into the positive resist and, after development, into the silicon oxide by means of a dry etching in Alcatel GIR-160 (50 sccm CHF_3, 500 W, 0.5 Pa), using the resist as a mask. Afterwards, the resist is removed by oxygen plasma, what leaves the backside with the alignment marks to be used during the whole fabrication process. This initial step on the backside of the wafer is necessary in order to properly align all mask levels. Then, following exactly the same process (even with the same

mask), the front side is processed and the holes for the tip formation are performed in the silicon dioxide (Figure 2.4.c).

The patterned silicon dioxide is used as a mask to etch the silicon, defining inverted pyramids by using anisotropic wet etching (Figure 2.4.d). TMAH (Tetra-Methyl-Ammonium Hydroxide, $(CH_3)_4NaOH$) aqueous solution at 25% in volume is used as an anisotropic etchant of silicon [16]. The silicon is etched during 30’ at 80°C just after a short dip in hydrofluoric acid (HF) in order to remove the native oxide that can mask the whole etching. The etch rate for the (100) plane of Si using these conditions is about 26 μm/hour. As the square holes in the oxide are 10 μm in side, the silicon is overetched in order to assure that the inverted pyramids are formed.

Figure 2.4

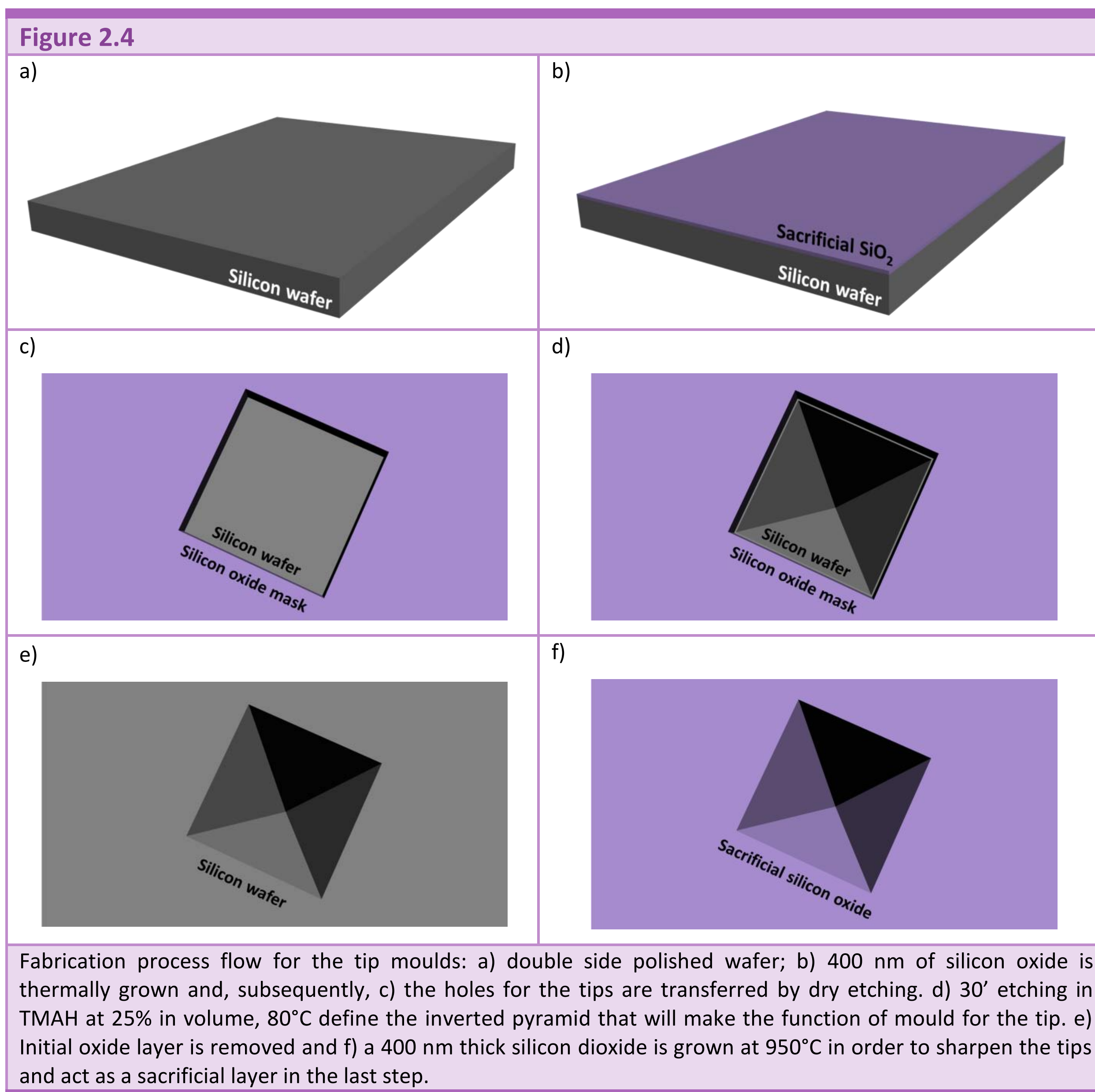

Fabrication process flow for the tip moulds: a) double side polished wafer; b) 400 nm of silicon oxide is thermally grown and, subsequently, c) the holes for the tips are transferred by dry etching. d) 30’ etching in TMAH at 25% in volume, 80°C define the inverted pyramid that will make the function of mould for the tip. e) Initial oxide layer is removed and f) a 400 nm thick silicon dioxide is grown at 950°C in order to sharpen the tips and act as a sacrificial layer in the last step.

After this etching step, the silicon oxide layer is completely removed from the wafer (Figure 2.4.e) and a new layer is grown (Figure 2.4.f) with a double objective: as a sacrificial layer that will allow us to release the devices at the final stage and recover the mould; and, in addition, to obtain sharpened tips. In order to achieve this second goal, the oxide is grown at 950°C and the selected thickness is 400 nm, given the fact that these are the optimum conditions regarding tip sharpening [17].

2.2.2 Probes fabrication

Once the mould is ready, it is possible to start with the successive epoxy based resist depositions. A detailed list of the steps required for the processing of an epoxy based resist layer can be found in the previous chapter. The first deposition is used to define the cantilever of the probe, and also the tip, which will be formed by filling the small holes of the inverted pyramids located at the very end of each cantilever. The thickness of this layer can be tuned to obtain the desired cantilever mechanical properties, i.e. elastic constant and resonant frequency. A typical thickness is 20 μm of mr-L 5025, which is spun at 3000 rpm during 45 seconds with an acceleration of 400 rpm/s (Figure 2.5.a). A soft bake is made just after the spinning and previous to the exposition and subsequent post exposure bake (PEB) (Figure 2.5.b). At this point, a second layer of SU-8 is deposited. As this layer must constitute the body of the probe, a thick body, e.g. 300 μm, is required (Figure 2.5.c). To achieve this thickness mr-L 5025 is spun at 400 rpm during 45 seconds with a final short step at 800 rpm (1-5 seconds) to get rid of the resist close to the border of the wafer (manual edge bid removal).

Once the second layer is fully processed (soft baked, exposed and PEB) (Figure 2.5.d); both layers are developed at the same time in PGMEA (Propylen Glycol Methyl Ether Acetate). During the immersion in PGMEA the wafer is gently agitated for faster development. Thicker films require longer times. In this case, at least 20 minutes are needed to fully develop the resist. In addition, it is convenient to change the PGMEA for a clean one after some minutes (around 10 minutes) for better results (Figure 2.5.e).

Here, it is interesting to mention that the reason why all the alignments are performed within the backside is the fact that after the spin coating of a 300 μm thick resist layer it is difficult to align with some markers located below the layer with a high precision. Therefore, it is more convenient to perform double side alignment.

After development, optionally a hard bake is performed to the wafer. Typical conditions are 120°C during 120 minutes in a N_2 atmosphere. Finally, they are released from the wafer (Figure 2.5.f). Releasing consists in etching the sacrificial silicon dioxide layer using HF or a buffered HF solution (SiOetch, commercially available, 6% HF + 16% NH_4F).

Figure 2.5

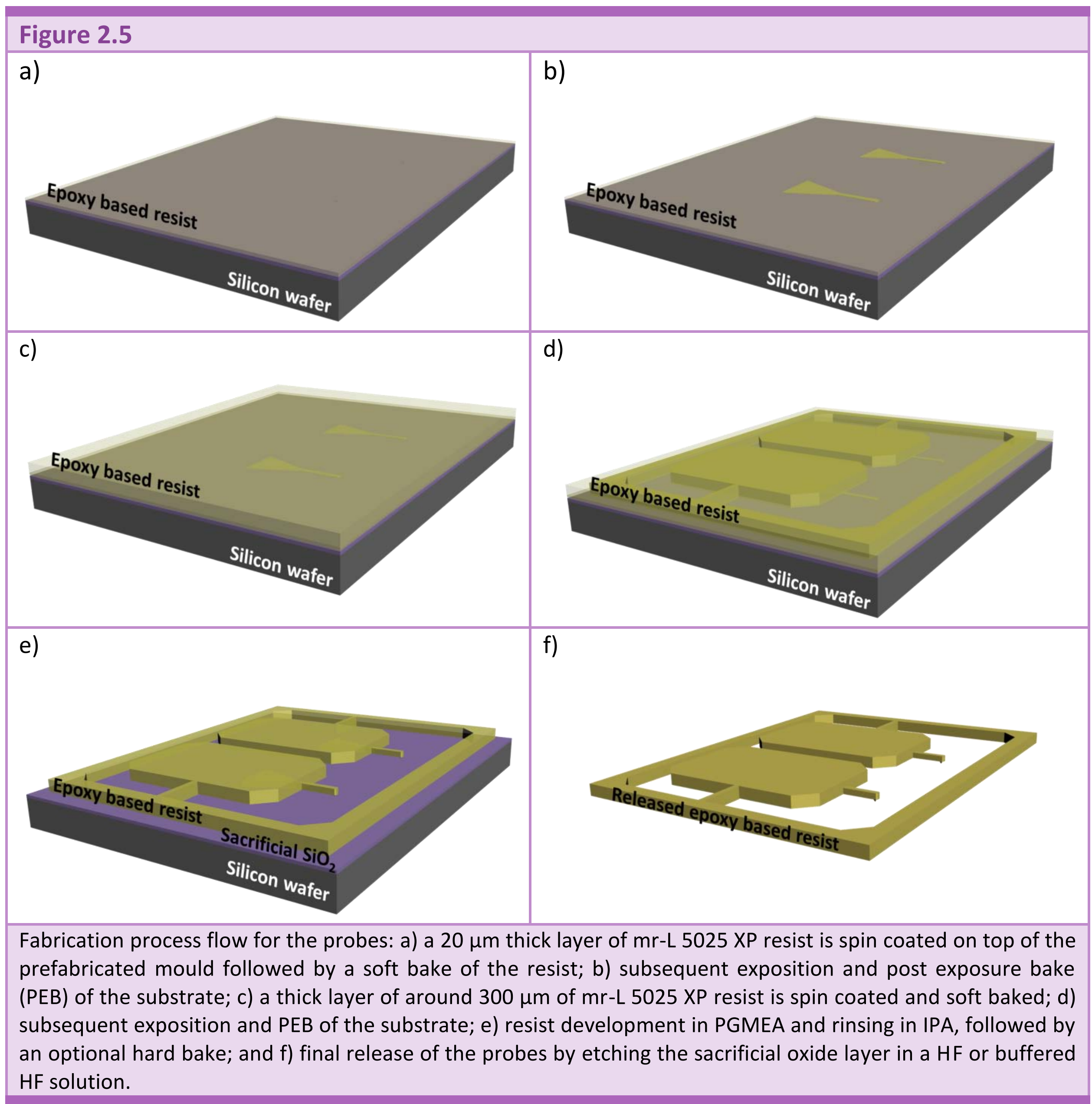

Fabrication process flow for the probes: a) a 20 µm thick layer of mr-L 5025 XP resist is spin coated on top of the prefabricated mould followed by a soft bake of the resist; b) subsequent exposition and post exposure bake (PEB) of the substrate; c) a thick layer of around 300 µm of mr-L 5025 XP resist is spin coated and soft baked; d) subsequent exposition and PEB of the substrate; e) resist development in PGMEA and rinsing in IPA, followed by an optional hard bake; and f) final release of the probes by etching the sacrificial oxide layer in a HF or buffered HF solution.

The presented steps correspond to the most standard process. In order to have a high yield and to make the fabrication reliable, different optimizations were done (which are explained in section 2.4), studying the effect of several parameters in the final result.

2.3 Design

As it has been commented while describing the process flow, three different mask layers are needed in order to fabricate photoplastic AFM probes: the body, the cantilever and the tip.

The body is a large anchor piece that supports the cantilever for handling purposes. It has to be thick enough to ease handling (this can be tuned by changing the spinning speed) and its lateral dimensions are given by the fact that it has to fit within the AFM microscope probe holder. For that reason lateral dimensions of commercial bodies have been taken, i.e. 1.6 mm in width and 3.4 mm in length. All the corners are smoothed (not 90°) to avoid epoxy based resist cracks. The thickness of the body can have also an important effect due to the fact that if it is too large, the body could be shadowing the laser from the cantilever. With a thickness of 300 μm, no shadowing effect should be seen.

Figure 2.6

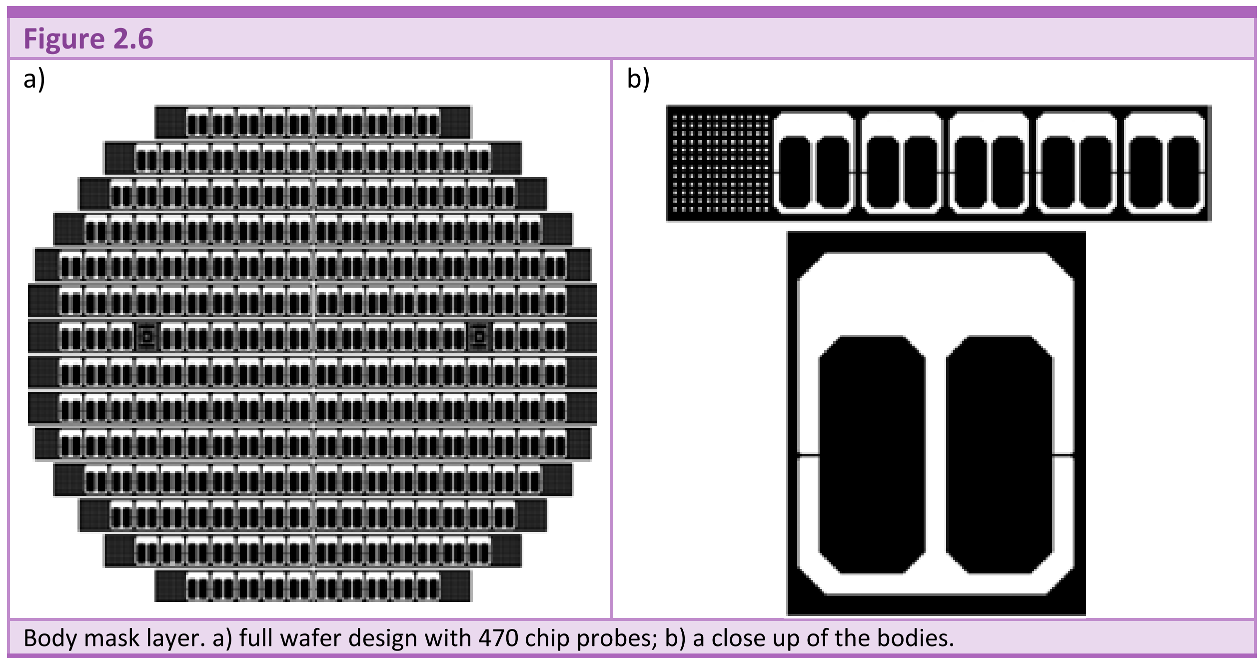

Body mask layer. a) full wafer design with 470 chip probes; b) a close up of the bodies.

In Figure 2.6, schematics of the designs for the body can be seen. Here, it has to be said that there exists the possibility of including some holes perforating the body in order to have a faster releasing step [18]. Although from the processing time point of view it would have been interesting, it was not known how that would affect the performances of the levers, so it was decided to keep solid bodies.

The second mask layer is used to define the cantilever. From the two different shapes of AFM probes that can be found commercially available (the V-shaped or triangular and the

rectangular) just the latter one was included in the designs (Figure 2.7). In Figure 2.7, it is observed that the rectangular cantilevers have a triangular part which is located below the body of the chip (Figure 2.7.c and Figure 2.7.d) and that has the function of improve the adhesion between the first and the second layer of deposited resist.

Figure 2.7

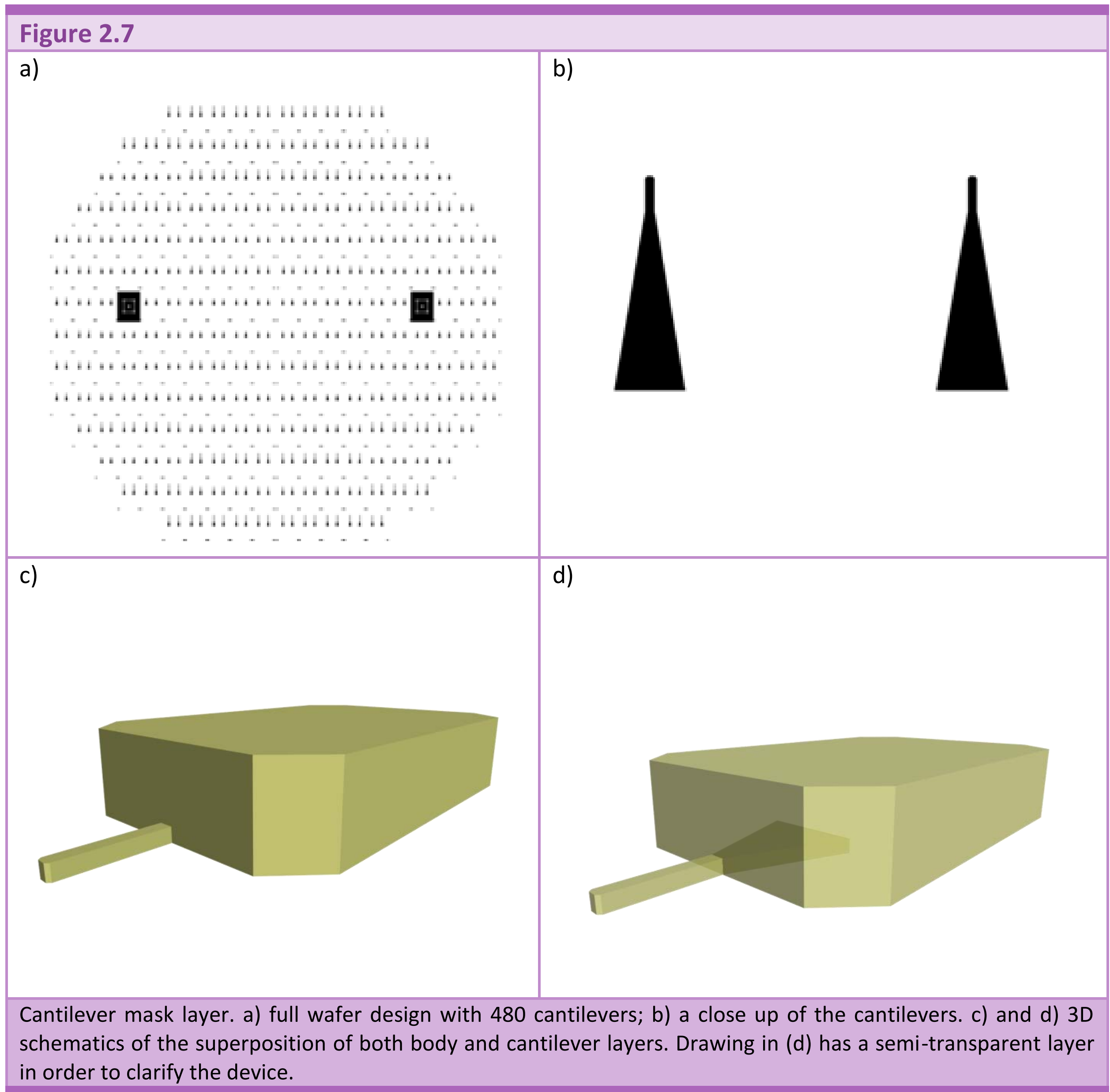

Cantilever mask layer. a) full wafer design with 480 cantilevers; b) a close up of the cantilevers. c) and d) 3D schematics of the superposition of both body and cantilever layers. Drawing in (d) has a semi-transparent layer in order to clarify the device.

A certain width of the cantilever is necessary to allow the laser reflection and a simple alignment of the laser beam. Standard silicon nitride and silicon cantilevers have a width around 30-50 µm. The designed cantilevers were taken all of them of the same width, i.e. 50 µm. The length of the cantilever is the parameter with highest influence on the resonance frequency and

the spring constant. Given a fixed width and designing different lengths a complete range of resonance frequencies and spring constants can be covered.

Figure 2.8

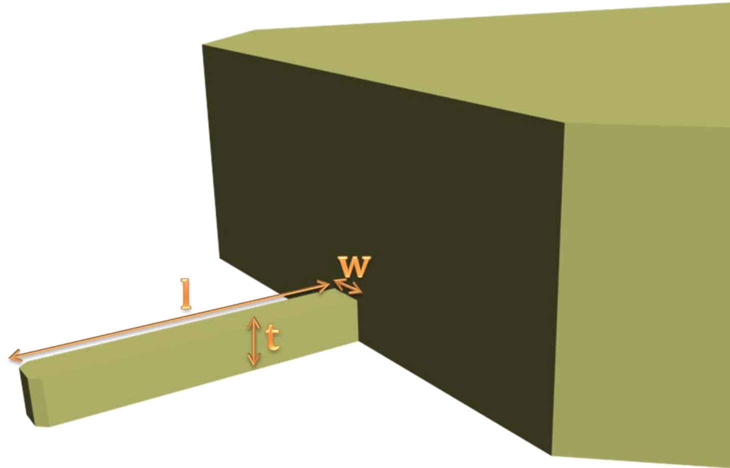

Schematics of a rectangular cantilever with its three characteristic dimensions: length (l), width (w) and thickness (t).

The spring constant (for normal bending) of a rectangular cantilever (Figure 2.8) is given by the following equation:

$$k_N = \frac{Ewt^3}{4l^3}$$

where w is the width, l the length, t the thickness of the cantilever and E the Young's Modulus of the material. On the other hand, the resonance frequency can be determined by

$$f_{RES} = 0.1615\sqrt{\frac{E}{\rho}} \cdot \frac{t}{l^2}$$

where ρ is the mass density. Typical value of the Young Modulus for processed SU-8 is 4.6 GPa (measured by indentation) and the density is around 1.21 kg/m^3. The same values have been taken for the epoxy based resist.

The thickness of the cantilever was initially chosen to be around 20 µm, what implies that the values for the elastic constant and the resonant frequency of the different designed cantilevers (15 in total) can be calculated. They are shown in Table 2.1.

Probe number	Length (l)	Spring Constant (k)	Frequency (f)
01	100 µm	460 N/m	620 kHz
02	175 µm	86 N/m	203 kHz
03	200 µm	58 N/m	155 kHz
04	225 µm	40 N/m	123 kHz
05	250 µm	29 N/m	99 kHz
06	350 µm	11 N/m	51 kHz
07	400 µm	7 N/m	39 kHz
08	425 µm	6 N/m	34 kHz
09	450 µm	5 N/m	31 kHz
10	500 µm	4 N/m	25 kHz
11	525 µm	3 N/m	23 kHz
12	800 µm	0.9 N/m	10 kHz
13	850 µm	0.7 N/m	8 kHz
14	1000 µm	0.5 N/m	6 kHz
15	1050 µm	0.4 N/m	5 kHz

Table 2.1: Summary of cantilever sizes and corresponding theoretical spring constant and resonance frequency, assuming 20 µm as the thickness of the cantilever.

Figure 2.9

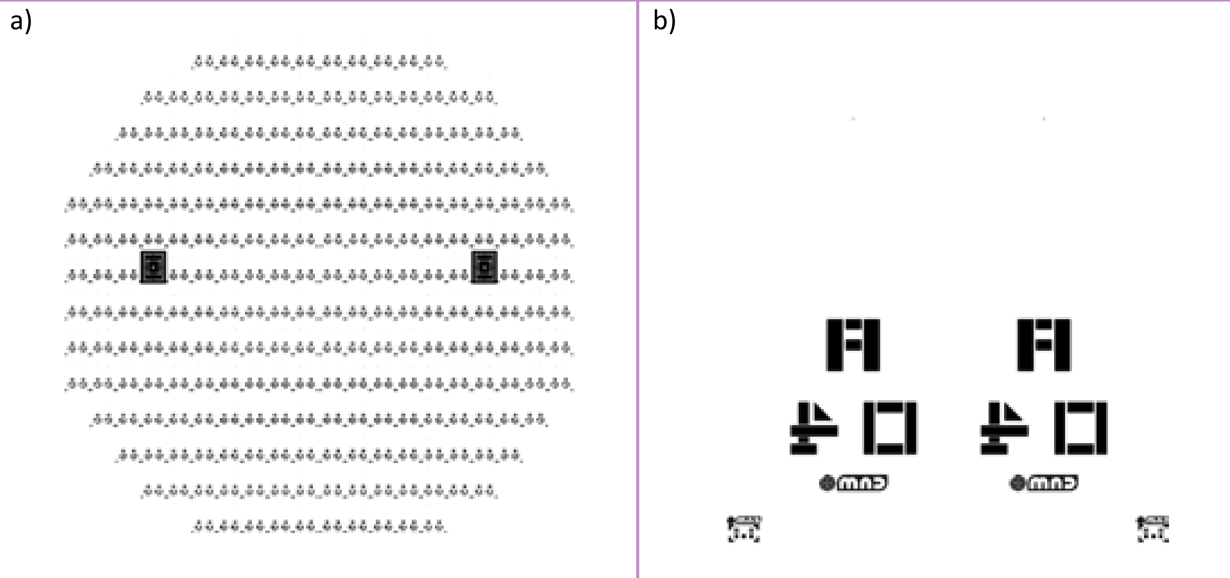

Tip mask layer. a) full wafer design with 480 tips; b) a close up of two of the chips with some marks to easily spot the length of the cantilever in that particular chip.

Finally, the third mask layer defines the tip. The design of the tip is not as flexible as the previous pieces of the probe. As mentioned above, the tip is fabricated by filling a silicon mould. The etch process to define the inverted pyramid is what fixes most of the characteristics of the

tip. Squares of 10 µm side are defined in order to have tips of around 10 µm in the basis and 7 microns high. In this level, some marks for each chip are also patterned in order to distinguish the type of cantilever (length). It is important to take into account that even this mask will be used on a positive resist (HIPR-6512), as the tips are etched in the silicon wafer, the dark field is the same that in the masks introduced before.

2.4 FABRICATION PROCESS OPTIMIZATION

To improve the quality of the probes, two characteristics have been targeted to be optimized: increasing the tip sharpness and decreasing the deflection angle of the cantilever.

2.4.1 Tip aspect ratio

One of the most important characteristics of an AFM probe relies on the tip sharpness and the tip aspect ratio; except for a few special cases in which the tip does not need to be sharp, like indentations [19, 20]. The objective of this part of the project was the development of SU-8 AFM probes for standard AFM measurements. Therefore, a key point was to develop proper tips for imaging, i.e. sharp tips.

As it has been described in the previous section, the mould for the tip is fabricated by anisotropic wet etching of silicon and subsequent oxidation (Figure 2.4). A cross-sectional view of the whole process flow can be seen in Figure 2.10.

Figure 2.10

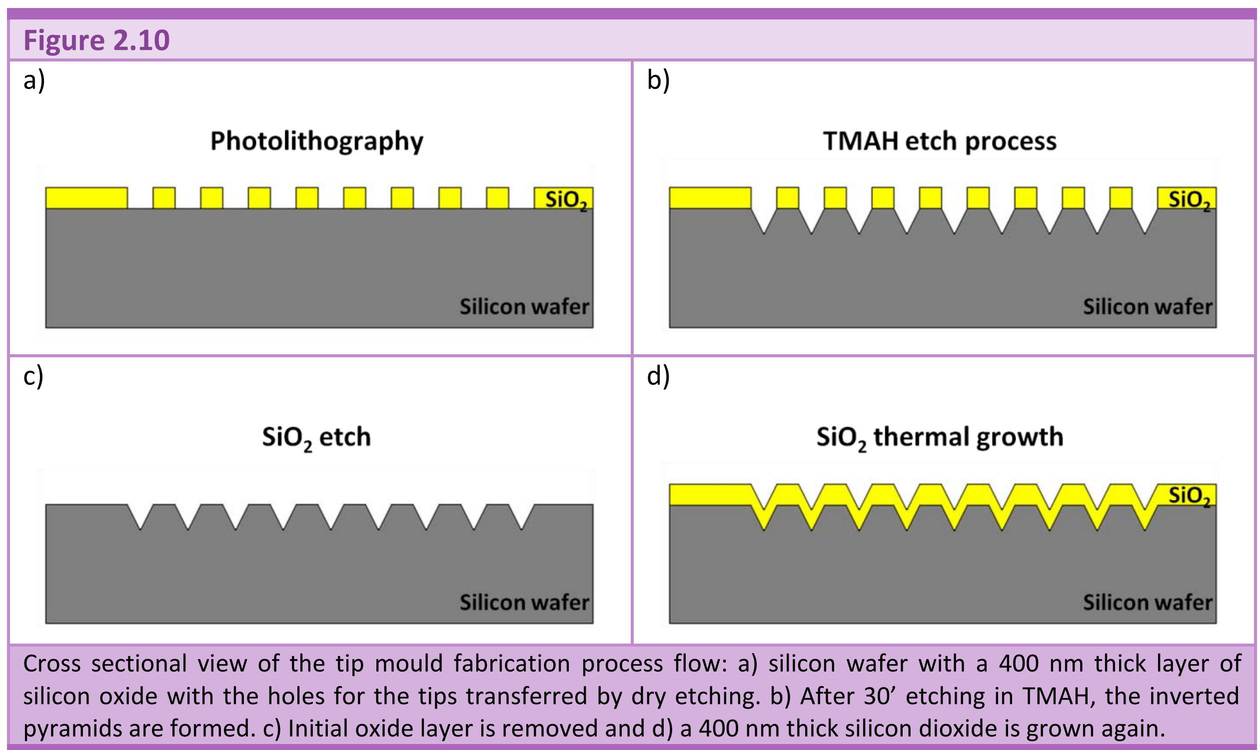

Cross sectional view of the tip mould fabrication process flow: a) silicon wafer with a 400 nm thick layer of silicon oxide with the holes for the tips transferred by dry etching. b) After 30' etching in TMAH, the inverted pyramids are formed. c) Initial oxide layer is removed and d) a 400 nm thick silicon dioxide is grown again.

In the process described in Figure 2.10, wet anisotropic etching was chosen because its behavior is widely known and the results could be foreseen, i.e. inverted pyramids formed by (111) planes in a standard <100> p-type silicon wafer. The use of TMAH instead of other anisotropic

etchant, like KOH, was motivated by the fact that TMAH does not contaminate the wafers, e.g. with potassium ions. In addition, selectivity to oxide is much higher for TMAH. However, the fact that the pyramids are always formed by (111) planes means also that the shape of the pyramids, and hence the tips, will always be the same. This implies that the walls of the pyramids form 54.7° with the horizontal plane. In Figure 2.11, four micrographs of the inverted pyramids, two of them made by TMAH and the other two by KOH.

Figure 2.11

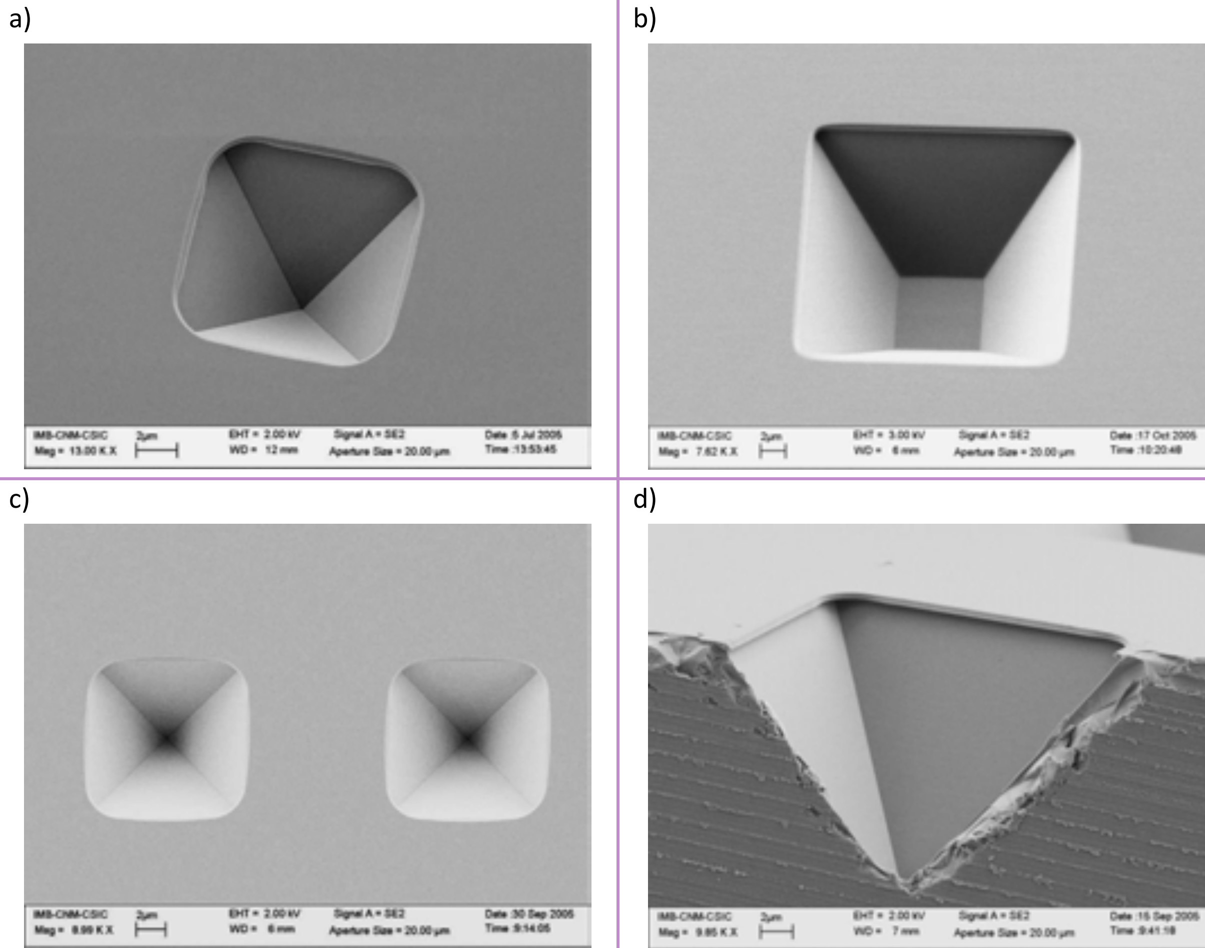

SEM micrographs of inverted pyramids etched in the silicon. a) and b) made by TMAH; c) and d) made by KOH. No difference in shape can be established.

In order to improve the aspect ratio of the tips, the slope of the lateral walls of the pyramids has to be increased. The intended approach was to machine the moulds for the tips using dry etching, as it has already been demonstrated [21]. As it has been reported in the literature, variation of the reactive ion etching conditions can modify the tapered profile of the vertical walls [22, 23], allowing the control of the anisotropy of the moulds. Several trials were made,

testing different conditions, but no difference was observed, hence this approach was abandoned. Figure 2.12 shows different cross sections of the etched moulds, and it can be seen that in all the cases the slope of the walls is 90°. Therefore, the definition of the moulds was fixed to be done by TMAH etching.

Figure 2.12

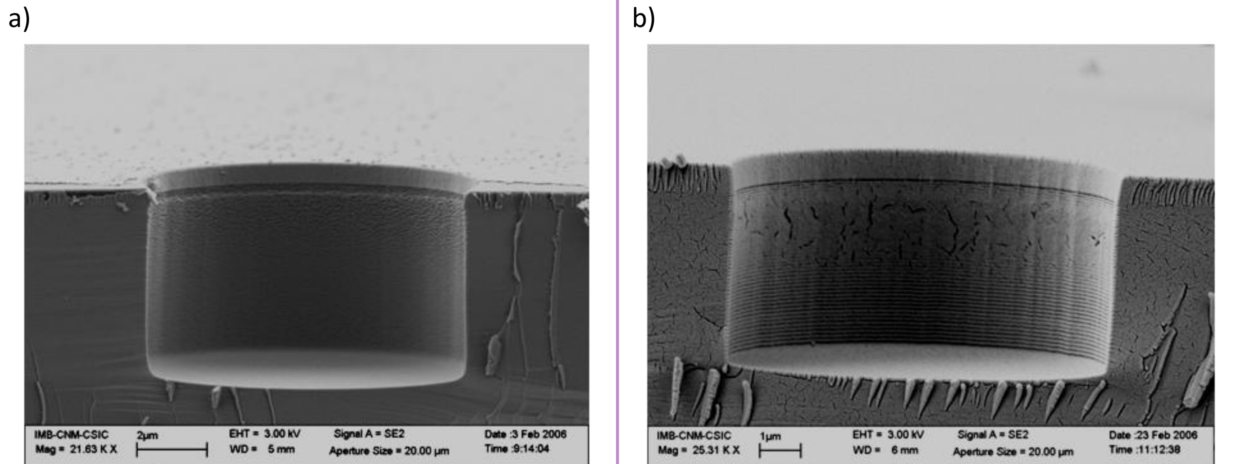

SEM micrographs of different conditions to obtain anisotropic reactive ion etch where just a small variation in the aspect of the vertical side walls can be observed.

Although the slopes of the lateral walls in that case are fixed, there is something that can be done in order to improve the sharpness and the aspect ratio of the top part of the tip, and this is making an oxidation of the mould. This oxidation is needed as a sacrificial layer for the release of the structures. In addition, it is known [24] that a low-temperature thermal wet oxidation helps to sharpen the bottom of the pyramidal holes. Non uniform oxide growth in the bottoms of pits and other highly non-planar regions occurs because there is less surface area available for oxidizing species to be incorporated, allowing fewer of them to reach the oxide/silicon interface to react with the available silicon atoms (Figure 2.13.b). Thus, the local oxidation rate is depressed in comparison to rates in flat areas. At high oxidation temperature (1100°-1200°C) (Figure 2.13.a), this geometric effect is less significant since viscous flow of the oxide film tends to increase the radius of curvature of the non-planar regions such that the surface area of the oxide film is more comparable to the area at the oxide/silicon interface [17]. In addition to the reduction of the oxidation rate due to the non-planarity, the oxide for the (111) planes of the pyramidal hole grows slower than the one for the (100) planes due to a dependence of the oxidation kinetics on the crystallographic orientation [25].

Consequently, all the fabricated moulds incorporated a thermal oxide layer, not only as a sacrificial layer but also in order to sharpen the tip. Just for test purposes, a batch of moulds was

fabricated performing the oxidation with a standard process of CNM clean room at 1100°C. The rest of the batches were oxidized at 950 °C. In all the cases, the thickness of the oxide was 400 nm. In Figure 2.13, two examples of tips fabricated by both methods can be observed, and the difference between them established. Both tips shown in Figure 2.13.c and Figure 2.13.d have a thin (20 nm) aluminum layer on top to reduce the charging effect while performing SEM. Therefore, the actual and exact measurement of the tip radius is difficult to realize this way. Instead, AFM images were acquired using both kinds of tips, evidencing the difference between both processes, as it will be described in section 2.5.1.

Figure 2.13

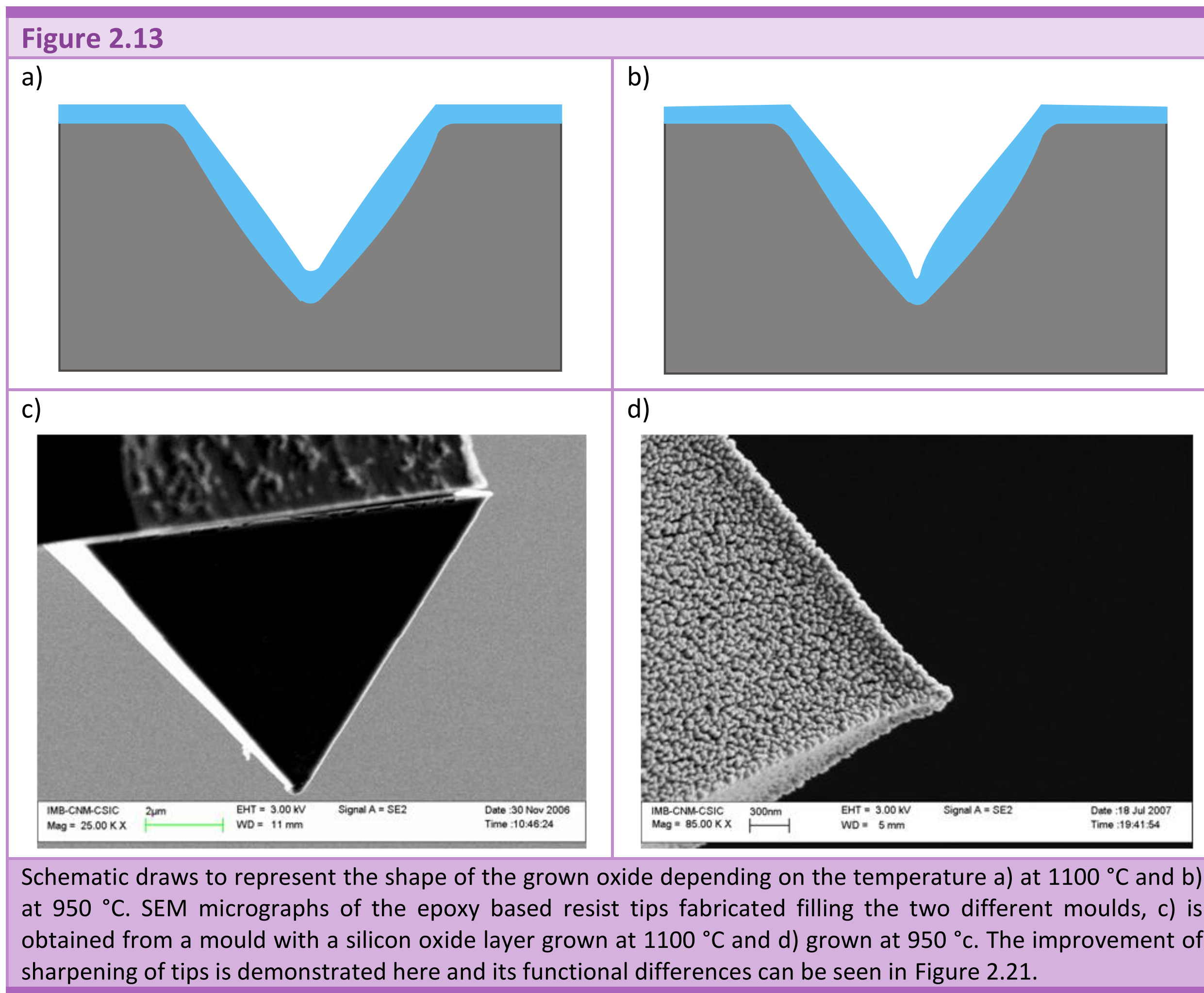

Schematic draws to represent the shape of the grown oxide depending on the temperature a) at 1100 °C and b) at 950 °C. SEM micrographs of the epoxy based resist tips fabricated filling the two different moulds, c) is obtained from a mould with a silicon oxide layer grown at 1100 °C and d) grown at 950 °c. The improvement of sharpening of tips is demonstrated here and its functional differences can be seen in Figure 2.21.

2.4.2 Cantilever deflection

In order to fabricate AFM tips that can be used in the most of the AFM equipments available in the market, it is necessary to restrict the cantilever bending to be below 1° angle deflection at the tip. Hence, it is ensured that the reflection of the laser will be collected by the photodiode

(provided an optical beam deflection is used to measure the cantilever's motion, as it is in the majority of the AFM equipments).

In any MEMS, mechanical properties such as elasticity constants, internal stresses, fracture limits, etc. of the materials constituting the device are very important for the design, fabrication and use. This is because device mechanical properties depend not only on the material of the structure but also on the size and the shape of the microelement as well as the processes by which it was manufactured and how the loads are applied. In the case of AFM cantilevers, geometry and dimensions of the devices are fixed by the application to which they are oriented. Therefore, having the geometries fixed, it is just possible to change either the material or the processing parameters in order to obtain the final required characteristics. During this chapter, as the material used is an epoxy based resist, it is only possible to play with the processing parameters. However, chapter 3 will show the possibility to obtain better mechanical properties of the material just by its chemical modification.

MEMS [26] have been preferentially fabricated using silicon given that it is a crystalline material and, therefore, its mechanical properties are widely known and measured. When using another material (polycrystalline silicon, silicon nitride, silicon dioxide, etc.), it is necessary to study and measure the mechanical characteristics for each individual way of processing [27-29].

When epoxy based resist is used, the necessity of an optimization in the processing conditions is even higher given that the Young's modulus of the material is at least 20 times smaller than that of any of the materials previously mentioned, i.e. deformations will be at least 20 times larger in a epoxy based resist structure under the same boundary conditions.

In the case of the initial deflection of cantilevers, it is due to internal (residual) stresses or, more precisely, stress gradients. Usually, stresses can have two different origins: thermal stresses and intrinsic microstructural stresses. Thermal stresses are caused by thermal mismatch between two layers with different thermal expansion coefficients. Intrinsic stresses, on the other hand, have a complex physical and chemical origin [30].

First, on many suitable surfaces for spinning resist, e.g. SU-8, such as Si or glass, the thermal expansion coefficient (CTE) mismatch between the resist and the substrate is large (SU-8 has a thermal expansion coefficient of $50 \cdot 10^{-6}$ K^{-1} compared to silicon which has a coefficient of $3 \cdot 10^{-6}$ K^{-1}). Another contribution to the stresses is the dynamics of the chemical reaction that causes the cross-linking during curing. Both effects are more pronounced in thick polymeric structures (like typical structures made out of SU-8 or other epoxy based resist), causing the photoresist to be easily delaminated; even more when poor adhesion is obtained during processing.

It has been observed that the material properties of SU-8 strongly vary with slight variations of the process parameters [31]. Therefore, the fabrication process has been studied and modified in order to obtain less stressed epoxy based resist layers to conform the cantilevers. The differences consist basically in the hard bake step and in the release method. All the different processes are summarized in Table 2.2 and Table 2.3.

Method	Description
49% HF releasing method	The wafer is dipped in a 49% HF solution until the AFM probes are released.
SiOetch releasing method	The wafer is dipped in a buffered HF solution (SiOetch) until the AFM probes are released. The time to release the chips by SiOetch is longer than for HF.
Teflon layer	A C_4F_8 layer is deposited on the silicon mould by using an DRIE equipment to ease the release step.

Table 2.2: Description of the different release processes tested in order to obtain low deflection in SU-8 cantilevers.

Method	Description
O_2 Plasma	The wafer is etched 4 min by O_2 plasma. The devices have been released after this process.
CF_4 – O_2 Plasma	A CF_4 dry etch is performed. The devices have been released after by subsequent SiOetch release method.
HardBake#1 (120°,1h)	The wafer is hard baked during one hour at 120°C. The atmosphere is saturated in Nitrogen. The devices have been released after by following the SiOetch releasing method.
HardBake#2 (150°,1h)	The wafer is hard baked during one hour at 150°C. The atmosphere is saturated in Nitrogen. The devices have been released after by following the SiOetch releasing method.
HardBake#3 (120°,2h)	The wafer is hard baked during two hours at 120°C. The atmosphere is saturated in Nitrogen. The devices have been released after by following the SiOetch releasing method.

Table 2.3: Description of the different treatment processes tested in order to obtain low deflection in epoxy based resist cantilevers.

2.4.2.1 Description of processes

As a general remark for all the releasing processes, it has been observed that the probes are released before the expected time has finished. This can be due to internal stresses in the epoxy

based resist holder, which is much thicker than the cantilever and could eventually pull up the cantilever and the tip.

The removal of SiO_2 films with aqueous HF is one of the most common processes in standard microtechnology fabrication techniques. The etching rates are well studied and determined. 49% HF solution is etching 1 µm of thermal SiO_2 per minute. As the oxide layer to be removed is partially covered by the structured epoxy based resist, the under etching process time will depend on the widest epoxy based resist structure (in this case is around 2 mm) [32]. Considering the same etch rate for vertical than for lateral etching, theoretically the release process should take 30-35 hours (more if we consider that lateral etching is always slower due to poor renewal of reactants), but in all the cases the experiments yielded a release time below 4 hours.

The SiOetch removal solution as it has been commented before is an HF buffered solution which consists in 6% of HF and 16% of NH_4F. Its etch rate for thermal SiO_2 is ten times slower than HF solution, i.e. 0,098 µm/min. The expected time to completely release the AFM probes should be around 350 hours (15 days) approximately. Nevertheless, the AFM probes where released in a maximum time of 50 hours.

As it has been reported [33], it is possible to use a fluorocarbon film to ease the release of the polymeric structures. The fluorocarbon film is deposited using a dry etching equipment. Passivation plasma, C_4F_8, is used to create such an anti-sticking layer. Even though the composition and origin of this material is not yet clear, the film has a very low free energy surface causing the adhesion reduction. Micromachined epoxy based resist devices can be removed from the handling substrate by lifting them off using mechanical tweezers. The optimal conditions for the deposition of this layer are included in Table 2.4. The process time was 60 seconds.

Equipment	Gas Flow	Substrate temperature	Source Power (W)	Platen power (W)
Alcatel 601-E	C_4F_8 – 300 sccm	20°C	600	20

Table 2.4: Conditions for the deposition of an antisticking polymeric Teflon-like layer.

In this case, silicon moulds are fabricated in the standard way, even though the SiO_2 layer is not needed for the removal step is grown to sharp the tip. The plasma-deposited film has approximately 50 nm thick and the poor adhesion is enough to deposit the mr-L 5025 XP resist by spinning (surfaces with lower free energy were tested resulting in the impossibility of spin coat resist on top).

The method described in the literature consists in the use of mechanical tweezers to lift the cantilevers off the wafer, but that it was not possible for the AFM probes because the tip is abruptly pull out, resulting seriously damaged (Figure 2.16.f) or remains inside the mould. As an alternative, successive heating and cooling processes were performed, causing a spontaneous releasing of the probes as can be seen in Figure 2.14.

Figure 2.14

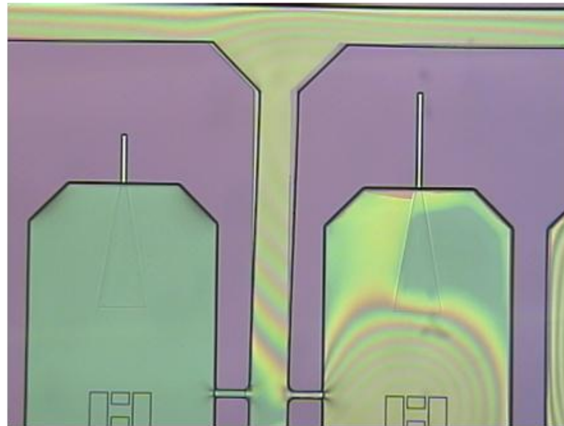

Optical image of fabricated AFM probes after the heating and cooling processes. It can be seen that some parts of the structure is already released but others are still stocked. That provokes friction between the tip and the mould damaging the most of them.

This technique avoids the inconvenient use of wet etchings, which lasts several hours and has a high risk of the etchant damaging the polymer. Nevertheless, the main drawback of this technique is the preservation of the tip. Due to the friction with the mould it is very difficult to obtain probes with sharp tips.

Apart from the different release methods, additional processes have been tried in order to optimize the final flatness of the levers. First of all, an oxygen plasma etching was tried. It has been demonstrated that plasma processes can be used for resist stripping or activation of polymer surfaces. The effect of O_2 plasma treatment on SU-8 in terms of surface energy, topography and surface chemistry has been investigated in several works [34, 35]. For example, it has been observed that the surface free energy can be increased significantly depending on the plasma conditions and, directly after plasma treatment, surfaces are completely wetted by water with a contact angle below 5°, whereas SU-8 surface is hydrophobic and has a low surface energy. This is due to both a chemical change in the surface (what is called activation) together with an increment in the surface roughness (Figure 2.15). Although SU-8, and other epoxy based resists, are quite resistant to oxygen plasma, when this is mixed with additional fluorinated gases, it is possible to efficiently strip and remove the polymer [36].

Figure 2.15

a) b)

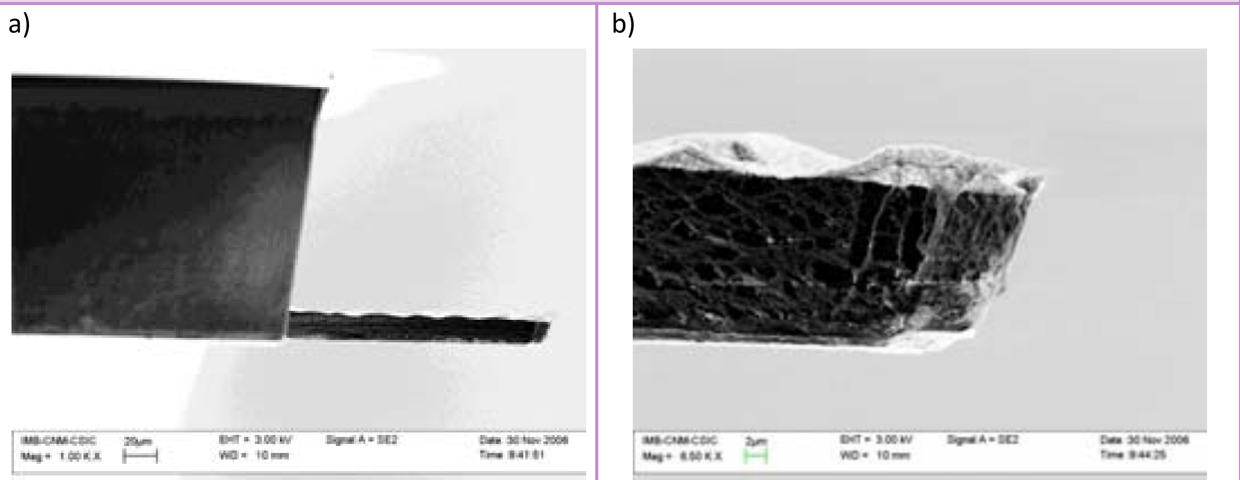

SEM micrographs of the released AFM probes with the O_2 plasma treatment. a) This treatment demonstrates its capacity to reduce the stress gradient of the cantilevers but b) roughness increases in the epoxy based resist, preventing a good laser reflection which made this process not to be further considered.

Using the O_2 plasma conditions (Table 2.5), although it was not expected, the AFM probes were abruptly released. Most of them resulted broken in the clamping edge (Figure 2.15). Only a 10% of the sample kept the cantilever but none of them presented the tip, i.e. in all the cases the tip rested in the mould.

Equipment	Gas Flow	Pressure	Source Power (W)	Platen power (W)
Tepla	O_2 – 50 sccm	80 Pa	500	0

Table 2.5: Oxygen plasma conditions applied as a release method.

With the same objective, CF_4 etching process has also been performed after development step. Alcatel GIR-160 dry etching equipment has been used. O_2/CF_4 etchings on PDMS has previously been reported [37], hence the same conditions (Table 2.6) were used for epoxy based resist. After this treatment the AFM probes where released using the SiOetch method. Most of them preserve the cantilever and the tip. The main drawback of this process relies in the low reproducibility of these results.

Equipment	Gas Flow	Pressure	Source Power (W)	Platen power (W)
GIR-160	O_2 – 80 sccm CF_4 – 20 sccm	7 Pa	100	0

Table 2.6: CF_4 with O_2 plasma conditions applied as a release method.

Finally, 3 different hard bake processes have been tested. As it has been explained before, a hard bake step is interesting in order to further cross link the material and minimize stresses and cracks. Hard bake optimal conditions (time and temperature) have to be found depending on the film thickness, resist and even exposure time. All three different hard bake processes were performed on a hot plate, from 21°C to the set temperature and in a saturated N_2 environment. These processes do not present any drawback, being a very cheap and reproducible solution.

2.4.2.2 Comparison of results

In order to compare the effect of the different processing techniques on the cantilever curvature, levers with similar spring constants (k) must be considered. As a first step, contact mode cantilevers (k<1 N/m) were compared. These geometries are the softest, which implies that the deflection angle will be larger in this type of structures than in others.

Method	K (N/m)	F (kHz)	Angle (°)	Variation	n
HF (49%)	0.6	8	6	± 1.2	8
SiOetch®	0.5	7	3.7	± 0.4	4
HB#1 (120°C - 1h)	0.6	8	4.5	± 0.2	6
HB#2 (150°C - 1h)	0.3	5	3.7	± 0.3	2
HB#3 (120°C - 2h)	0.6	8	1.9	± 0.5	2

Table 2.7: Deflection angle at the free edge of soft SU-8 cantilevers for contact mode

In Table 2.7, the results for the measurement in at least 5 cantilevers of each type are included. In that table, none of the processes involving any step with dry etching processes are included. This is due to the fact that none of them was susceptible of being considered as a possibility for the process. Teflon-like layer for the releasing process and oxygen plasma etching did not yield any sample to measure with. On the other hand, CF_4-O_2 plasma, gave an extremely good results (extremely flat cantilevers) during the first trial but those results were not reproducible.

It is possible to see from Table 2.7 that the best process is the HB#3, that is to say, performing a hard bake at 120°C during 120 minutes and then the etching of the sacrificial oxide layer using buffered HF solution (SiOetch®).

In Figure 2.16 and Figure 2.17, SEM micrographs of some examples of bent cantilevers due to internal stress gradient are shown.

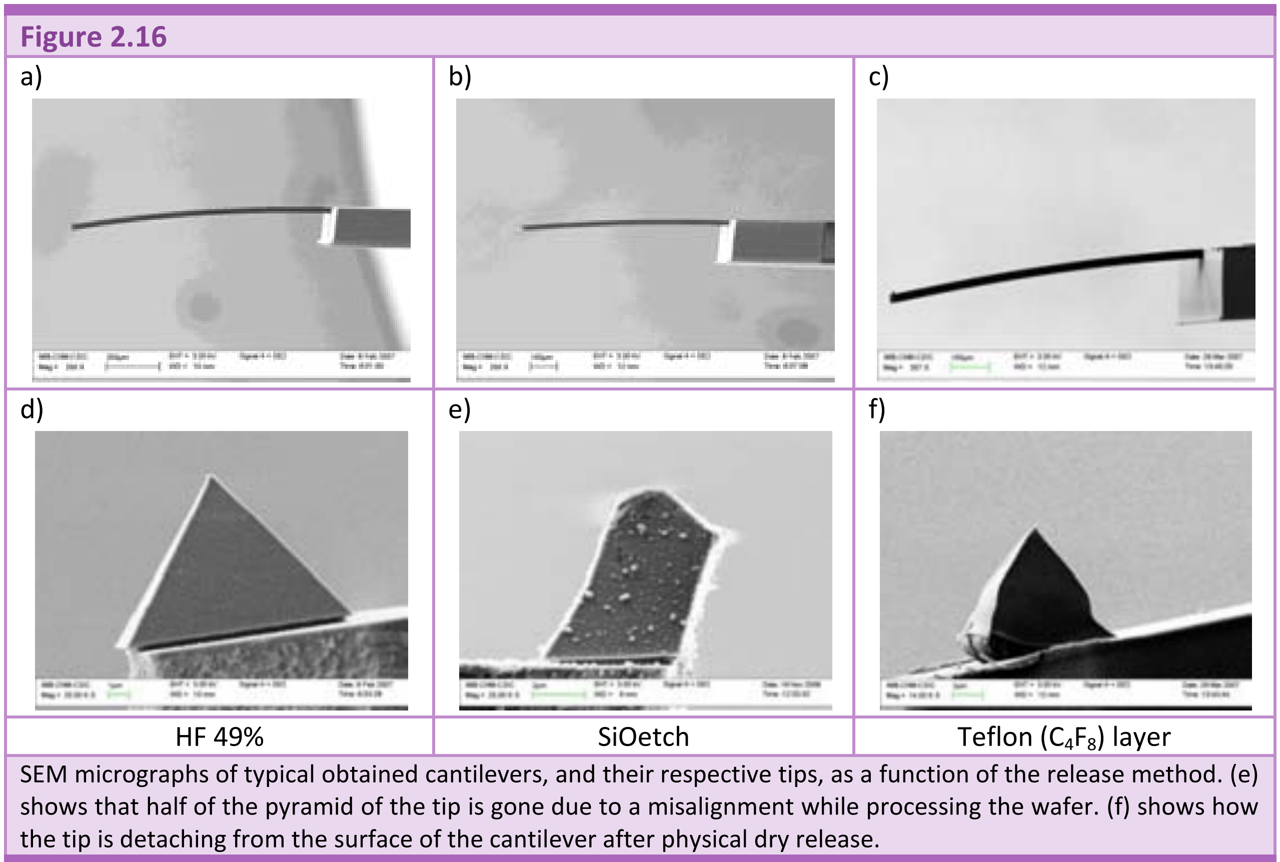

Figure 2.16

SEM micrographs of typical obtained cantilevers, and their respective tips, as a function of the release method. (e) shows that half of the pyramid of the tip is gone due to a misalignment while processing the wafer. (f) shows how the tip is detaching from the surface of the cantilever after physical dry release.

Although contact mode cantilevers were taken initially to test the deflection angle at the free end, the constraint that forces that angle to be smaller than 1° is not applicable to those cantilevers. When using contact mode, the response of the probe is much larger than for non-contact, which implies that the laser does not have to be located at the very end of the structure in order to have enough resolution as to scan the surface. Therefore, even if the lever is too deflected, in most of the cases it is possible to measure by locating the laser at a middle point.

Cantilevers dedicated to non-contact mode operation are stiffer than its contact counterpart; hence the angles will be smaller in this case. As a consequence, cantilevers for non-contact mode were measured and the results are gathered in Table 2.8, where the same method as for the contact mode is the one that offers the best results.

Figure 2.17

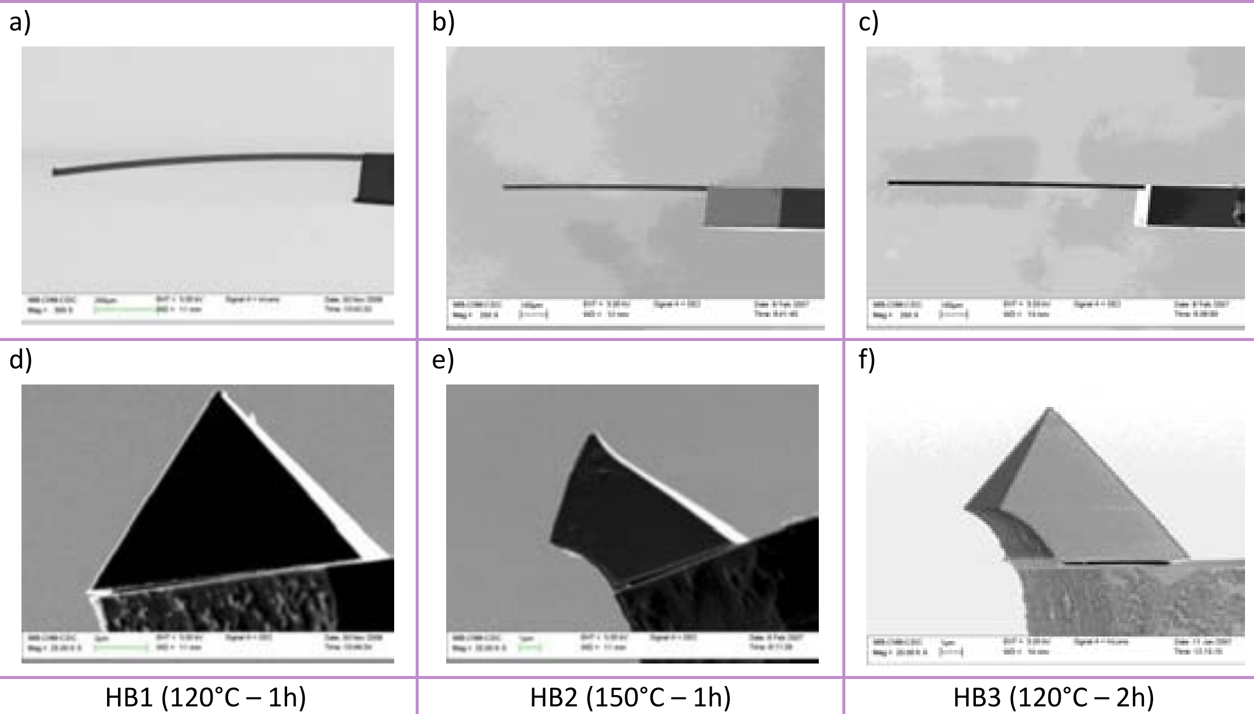

HB1 (120°C – 1h)	HB2 (150°C – 1h)	HB3 (120°C – 2h)

SEM micrographs of typical obtained cantilevers, and their respective tips, as a function of the processing technique before releasing. All three types of levers were released using SiOetch method. (e) and (f) show that half of the pyramid of the tip is gone due to a misalignment while processing the wafer.

Method	k (N/m)	F (kHz)	Angle (°)	Variation	n
HF (49%)	5-40	30-150	6	± 2	5
SiOetch®	5-40	30-150	4	± 1.5	6
HB#1 (120° - 1h)	5-40	30-150	2	± 0.5	8
HB#2 (150° - 1h)	5-40	30-150	1.5	± 0.3	8
HB#3 (120° - 2h)	5-40	30-150	0.4	± 0.15	8

Table 2.8: Deflection angle at the free edge of stiff SU-8 cantilevers for non-contact mode

An additional process that also can have some effect on the deflection of the lever is the metallization of the backside of the lever. As it is well known, SU-8 has a very low coefficient of reflection; usually it is transparent for the laser wavelength and just in some cases; like HF releasing or high temperature hard bakes, the reflectivity is changed and it turns a little bit yellow. For that reason the epoxy based resist AFM probes must be coated with a thin layer of metal in order to allow the laser signal being reflected to the photodiode. The metals used for

the coating process are gold and aluminum. The reflection of both is very good but the deposition method and the internal stress is very critical.

Usually, gold metallization results in more bent cantilevers than when aluminum is used. This is due mainly to the fact that gold has a higher internal stress than Al, but also to the fact that the temperature during the Au deposition is much higher than during the Al one. Almost all the coatings have been done by means of sputtering of any of both metals, but also evaporation has been tested, resulting in a bending not as large as for the sputtering counterpart. This is due to the fact that the evaporations were performed keeping the chamber at room temperature.

As it has been commented before, the deflection angle is always larger for softer cantilevers. Figure 2.18 shows this strong dependence of the deflection angle of the cantilever and the spring constant. It also shows the difference between the three hard bake methods that have been used.

Figure 2.18

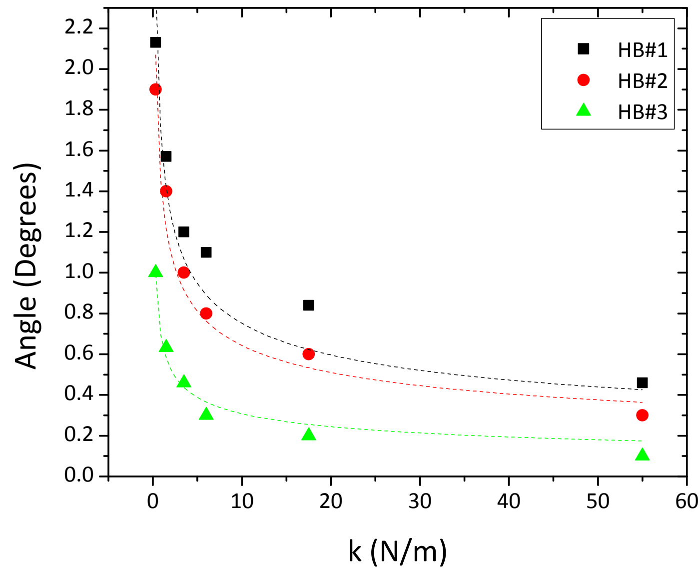

Deflection angle dependence with the spring constant. Each group of data corresponds to a different hard bake. In all cases the release was performed by a buffered HF solution. The dashed lines correspond to the fitted curves of the kind: $y = a \cdot x^b$, where b values are close to -0.3 in all three cases, while the theoretical value should be $-\frac{1}{3}$.

It can be seen from the above graphs that for larger spring constant the deflection angle is reduced, what was expected due to the fact that the cantilevers that corresponds to the smaller spring constants are the longer ones. Analytically, it can be shown that the angle is inversely

proportional to the length of the cantilever, so it is inversely proportional to the cubic root of the elastic constant.

The flattest cantilevers have been coated and tested by using two different AFM equipments and different methods of operation and conditions. The characterization is detailed in the next section.

2.5 STRUCTURAL/FUNCTIONAL CHARACTERIZATION

Once the devices fabrication was completed, it was essential to know their performance in an AFM system. In addition, epoxy based resist AFM probes have to demonstrate their validity for imaging different surfaces and for working in different operation modes and different AFM equipments.

Several probes have been tested in four different equipments. A *Dimension 3100* AFM system with a *NanoScope IV* controller from *Veeco* [38] and a *Cervantes* AFM system with *Dulcinea* controller from *Nanotec* [39] were used to test probes in both contact and dynamic mode in air. Two *MultiMode* AFM systems, one with a *NanoScope IIIa* controller and the other with a *NanoScope IVa* controller allowed us to measure in liquid. These both equipments are also from *Veeco*.

Each one of the mentioned equipments has differences in terms of holder, operation conditions, etc. that have to be overcome by the AFM probes. *Dimension 3100* AFM microscope is the most sophisticated system, presenting also the largest number of restrictions. For example, the photodiode has a range of movements really low, hence if the cantilevers have a deflection angle larger than 1° they cannot be used, unless you are working in contact mode and the laser can be placed in a middle point of the cantilever.

This section is divided regarding the different measurements performed, i.e. contact mode in air, dynamic mode in air and dynamic mode in liquid.

2.5.1 Contact mode in air

As it has been explained before, when operating in contact mode, the tip is in actual physical contact with the sample and the total forces acting between the tip and the sample range between 10^{-7} to 10^{-6} N. In order to avoid an increase in the force applied, cantilevers with a very low spring constant (that also means longer ones) are the most convenient for these measurements. As epoxy based resist is a very soft material, the use of these probes is interesting if the sample is also very soft. In those cases (e.g. biological samples), there is a high risk to damage the sample by using a typical silicon or silicon nitride probe. In addition, if the substrate is stiff, the wearing of the tip is larger, meaning that the lifetime of the tip would be very short.

In order to test the probes, AFM images of a calibration sample have been acquired (Figure 2.19). This sample contains square structures with 10 µm pitch, 200 nm high and 5 µm wide. In Figure 2.19.a an AFM image of this sample is shown, with a cross section (Figure 2.19.b) showing the depth of the calibration squares.

Figure 2.19

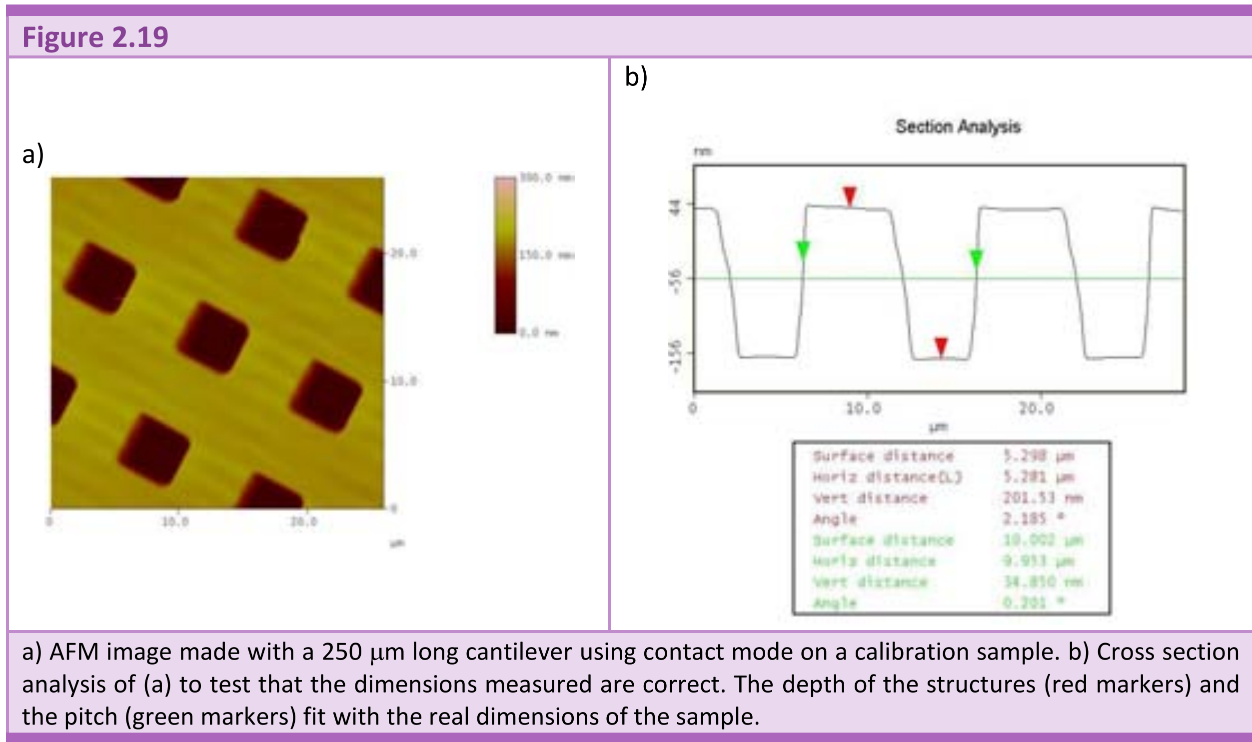

a) AFM image made with a 250 µm long cantilever using contact mode on a calibration sample. b) Cross section analysis of (a) to test that the dimensions measured are correct. The depth of the structures (red markers) and the pitch (green markers) fit with the real dimensions of the sample.

The previous test does not provide any information about the actual resolution of the tip. In order to do that, an aluminum sample was imaged with both a commercial silicon probe and an epoxy based resist probe. The aluminum sample consists in coating a silicon surface with a sputtered aluminum layer of 12 nm thickness. This sample typically results very flat and with small rounded grains of aluminum which can give more information about the aspect ratio of the tip. The comparison can be observed in Figure 2.20. The resolution of the silicon probe (Figure 2.20.b) is much better than that of an epoxy based resist probe (Figure 2.20.a).

Epoxy based resist probes have been improved by growing the sacrificial silicon oxide layer at 950°C as was described section 2.4.1. Resolution of the images has been overcome as it can be observed in Figure 2.21.

Figure 2.20

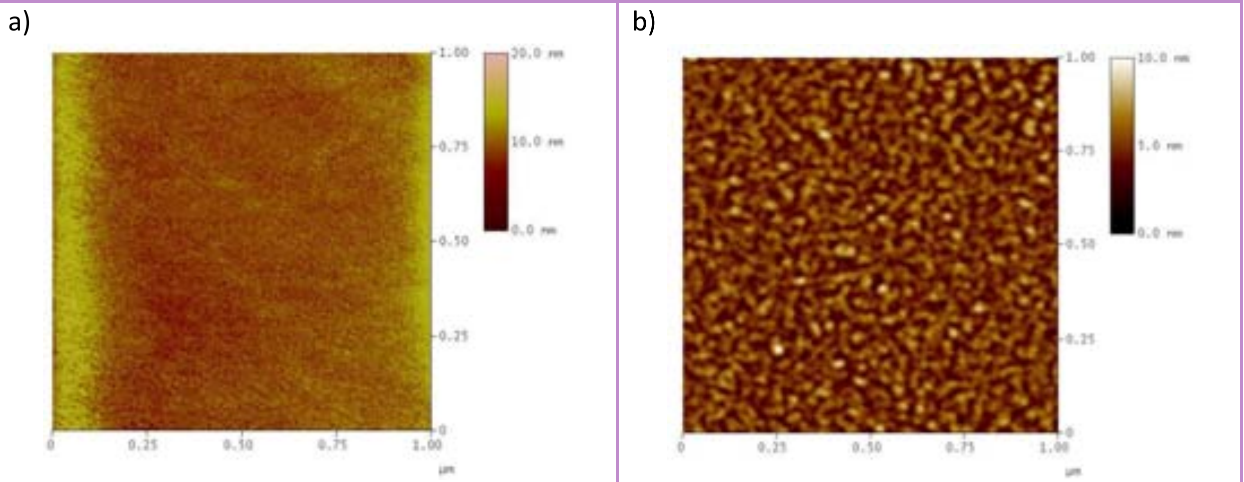

AFM images taken with two different probes, both in contact mode, of the same aluminum sample, (a) was taken using an epoxy based resist probe whereas (b) was taken with a commercial silicon probe. The epoxy based resist probe is further less accurate than the silicon one.

Figure 2.21

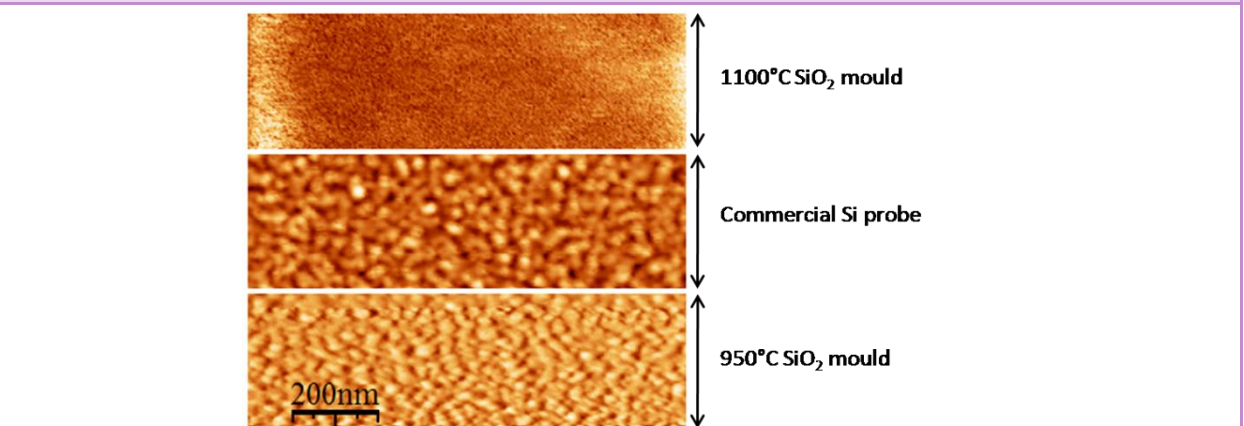

Contact mode AFM measurements on a 12 nm aluminum coated silicon sample. Top part is taken with an epoxy based AFM probe. The silicon oxide sacrificial layer of the mould has been grown at 1100 °C. Middle part is scanned with a commercial silicon probe and for the bottom part an epoxy based AFM probe released from a 950 °C grown silicon oxide layer is used.

Finally, force curves can also be acquired on silicon substrate, coated with 12 nm of aluminum, using epoxy based resist AFM probes, as it can be seen in Figure 2.22.

Figure 2.22

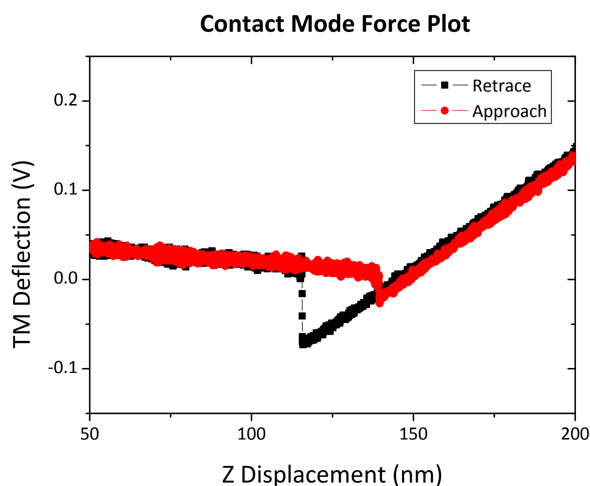

Force-distance curve plot performed with an epoxy based resist AFM probe operating in contact mode on a silicon surface coated with 12 nm of aluminum.

2.5.2 Dynamic mode in air

In dynamic, non-contact mode, the tip is kept in close distance from the sample and it is vibrating at the resonance frequency. Therefore, in this operation mode, both the resonant frequency and the quality factor (dynamic mechanical properties of the cantilevers) have a key role. Having a good peak of resonance is required to achieve good resolution and nice operation in terms of noise and stability. Given that the tip is not in actual contact with the sample, the total force applied is much lower than in contact mode thus the tip is preserved and the epoxy based resist AFM probes can be an excellent option for cheap training probes.

Dynamic measurements in air have been performed in the *Dimension 3100* system and in the *Cervantes* system. The tested probes fit perfectly in both equipments and most of them give enough reflection to the photodiode to allow finding the resonance frequency. This, as it has been commented in previous section, is mainly due to the fact that cantilevers for dynamic mode are shorter, i.e. stiffer, which implies that the deflection is smaller (Figure 2.18).

Experimental measurements of the resonance frequency were very close to the theoretical calculation (Table 2.9). Some deviations can be due to the cantilever size (the exposure time can modify slightly the width and the length) and the homogeneity of the thickness of the SU-8 deposited layer. Several different probes have been tested. The average of the measured quality factors is 30. Even though this value is much smaller than the one for standard silicon

probes, it was possible to acquire AFM images. In Figure 2.23 are represented some resonance frequencies for different cantilever spring constants. As it is expected the quality factor decreases with low spring constants cantilevers.

Epoxy based resist AFM Probe		Theoretical mechanical properties		Experimental mechanical properties	
Type	**Length**	**Spring Constant**	**Resonance Frequency**	**Resonance Frequency**	**Quality factor**
01	100 µm	295 N/m	547 kHz	550 kHz	58
02	175 µm	130 N/m	227 kHz	220 kHz	130
03	200 µm	87 N/m	174 kHz	173 kHz	61
06	350 µm	16 N/m	57 kHz	57 kHz	36
08	425 µm	9 N/m	38 kHz	39 kHz	42
09	450 µm	8 N/m	34 kHz	33 kHz	36
10	500 µm	5 N/m	28 kHz	28 kHz	25
11	525 µm	2 N/m	19 kHz	19 kHz	17
13	850 µm	1 N/m	9 kHz	5 kHz	12

Table 2.9: Summary of the experimental mechanical properties of the fabricated probes in comparison with the analytical calculus. The analytical calculus is adjusted to the probe precedence. Several wafers have been fabricated and the cantilever thicknesses vary.

Figure 2.23

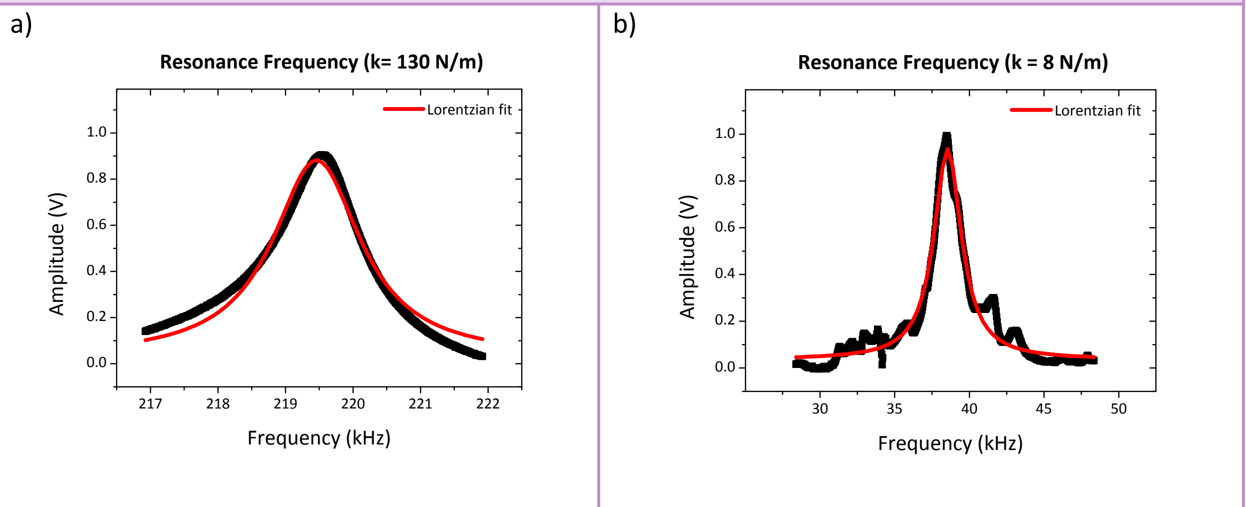

AFM in non-contact/dynamic mode. a) Frequency mechanical response of the cantilever with f = 220 kHz and k = 130 N/m and b) frequency mechanical response of the cantilever with f = 35 kHz and k = 8 N/m.

Frequency spectra for the cantilevers have enough amplitude to allow the AFM system performing measurements in dynamic mode. Figure 2.24 compares a topography image taken with an epoxy based resist AFM probe (a) and the same sample scanned with a commercial

silicon probe (RTESP14 from Veeco). The sample is a silicon wafer coated with 12 nm of sputtered aluminum (same sample used for contact mode measurements). Comparing Figure 2.24 with Figure 2.20, it can be noted that the lifetime of the epoxy based resist tip is much longer in dynamic than in contact mode.

Figure 2.24

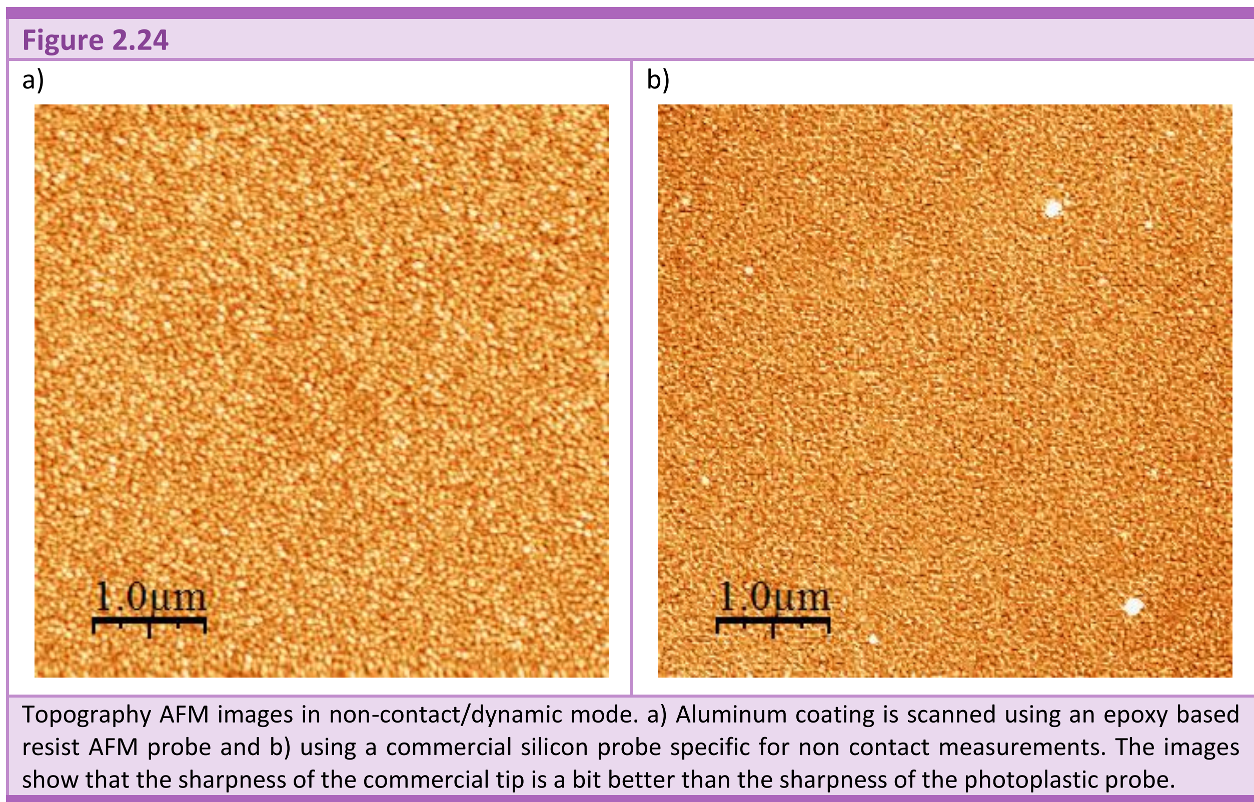

Topography AFM images in non-contact/dynamic mode. a) Aluminum coating is scanned using an epoxy based resist AFM probe and b) using a commercial silicon probe specific for non contact measurements. The images show that the sharpness of the commercial tip is a bit better than the sharpness of the photoplastic probe.

Figure 2.25

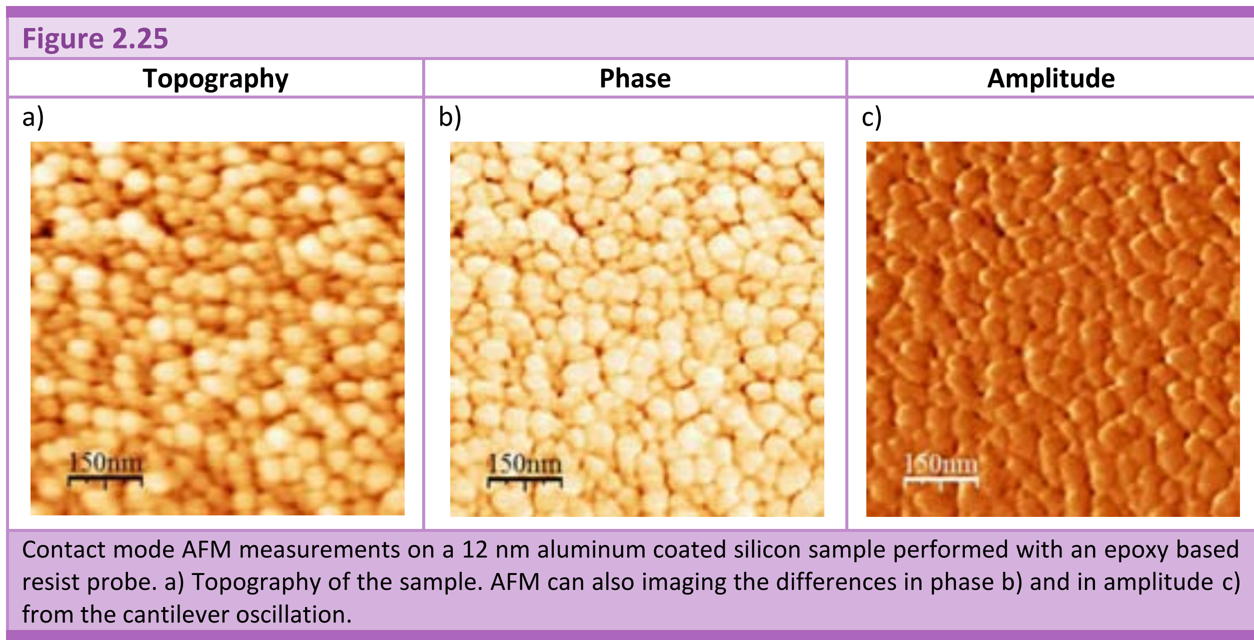

Contact mode AFM measurements on a 12 nm aluminum coated silicon sample performed with an epoxy based resist probe. a) Topography of the sample. AFM can also imaging the differences in phase b) and in amplitude c) from the cantilever oscillation.

Measurement in dynamic mode can bring more than topography information. Figure 2.25 collect phase and amplitude measurement in addition to topography.

An additional advantage of the photoplastic AFM probes is that by adjusting the metallization conditions and thickness of the deposited layer it is possible to obtain probes covered enough to have laser reflection but transparent enough as to look through them to know exactly the tip position while scanning (Figure 2.26).

Figure 2.26

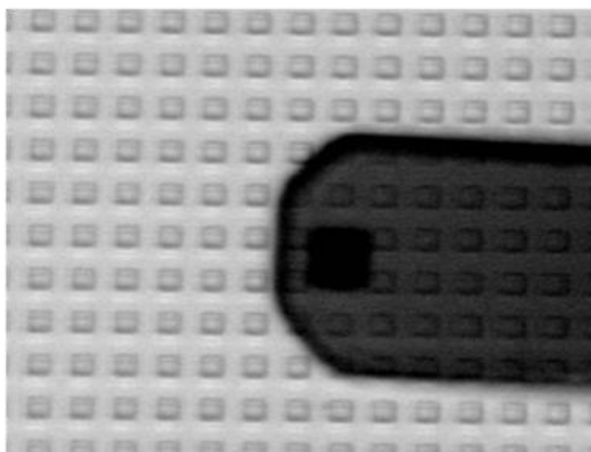

Optical image of standard SU-8 tip while scanning a sample. The coating layer is thick enough to allow enough laser reflection and thin enough to see through it. This is especially interesting for samples like the photographed one, that have many equal structures and it is needed to scan a determined one.

2.5.3 Dynamic mode in liquid

Cantilever type	Spring constant	Air		Liquid	
		Resonance frequency	Q	Resonance frequency	Q
02 (175 µm)	55 N/m	175 kHz	34	33 kHz	38
06 (350 µm)	7 N/m	52 kHz	35	9 kHz	25
07 (400 µm)	5 N/m	48 kHz	44	9 kHz	34
RTESP14 (Veeco) Silicon (rectangular)	50 N/m	285 kHz	500	130 kHz	12
OMCL TR400PSA (Olympus) Silicon Nitride (V-shaped)	0.08 N/m	37 kHz	90	9 kHz	27
ESP7 (Veeco) Silicon (rectangular)	0.2 N/m	12 kHz	35	6 kHz	3

Table 2.10: Resonant frequency and quality factor of different probes

In addition to the measurements performed in air, the probes have also been tested in liquid. When standard silicon (or silicon nitride) probes are used in air, typical values for the resonant frequency are around 300 kHz with a quality factor, Q, of around few hundreds. It is well known that when the probes are immersed in liquid, both the quality factor and the resonant frequency drastically decrease [40, 41].

Figure 2.27

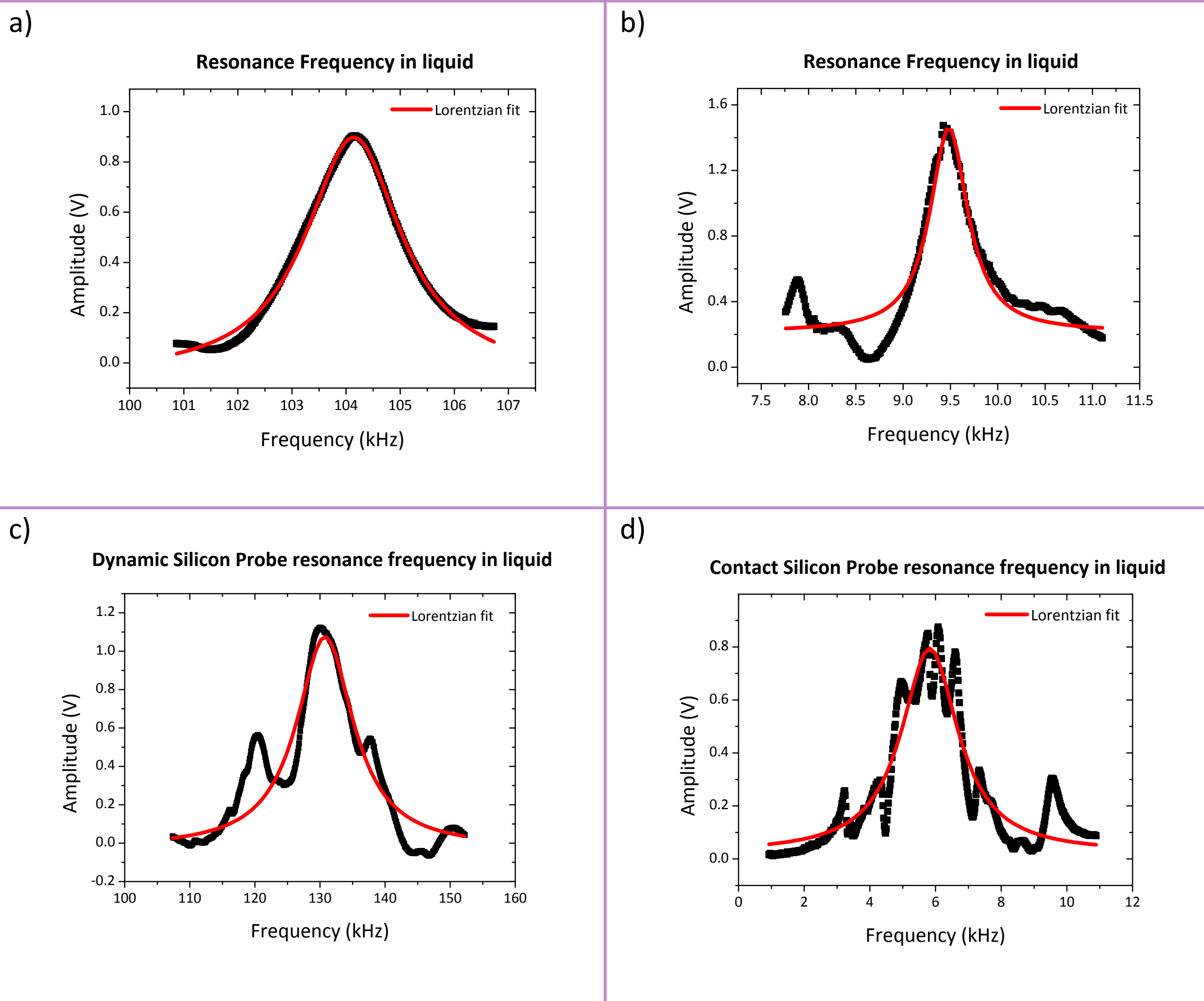

Frequency spectra in liquid. a) Corresponds to an epoxy based resist cantilever with a length of 175 µm, a spring constant of 130 N/m and a resonant frequency in air of 227 kHz. The quality factor in liquid is 48. b) Corresponds to a epoxy based resist cantilever with a length of 400 µm, a spring constant of 11 N/m and a resonant frequency in air of 43 kHz. The quality factor is 20. c) Rectangular silicon probe for dynamic mode in air (RTESP14) with a length around 120 µm, k ≈ 50 N/m and a resonant frequency in air of 285 kHz. Quality factor in liquid is 28. c) Rectangular silicon probe usually used for contact mode in air (SCM-PIC) with a length around 450 µm, k = 0.2 N/m and a resonant frequency in air of 12 kHz. Quality factor in this case is 3.

Figure 2.28

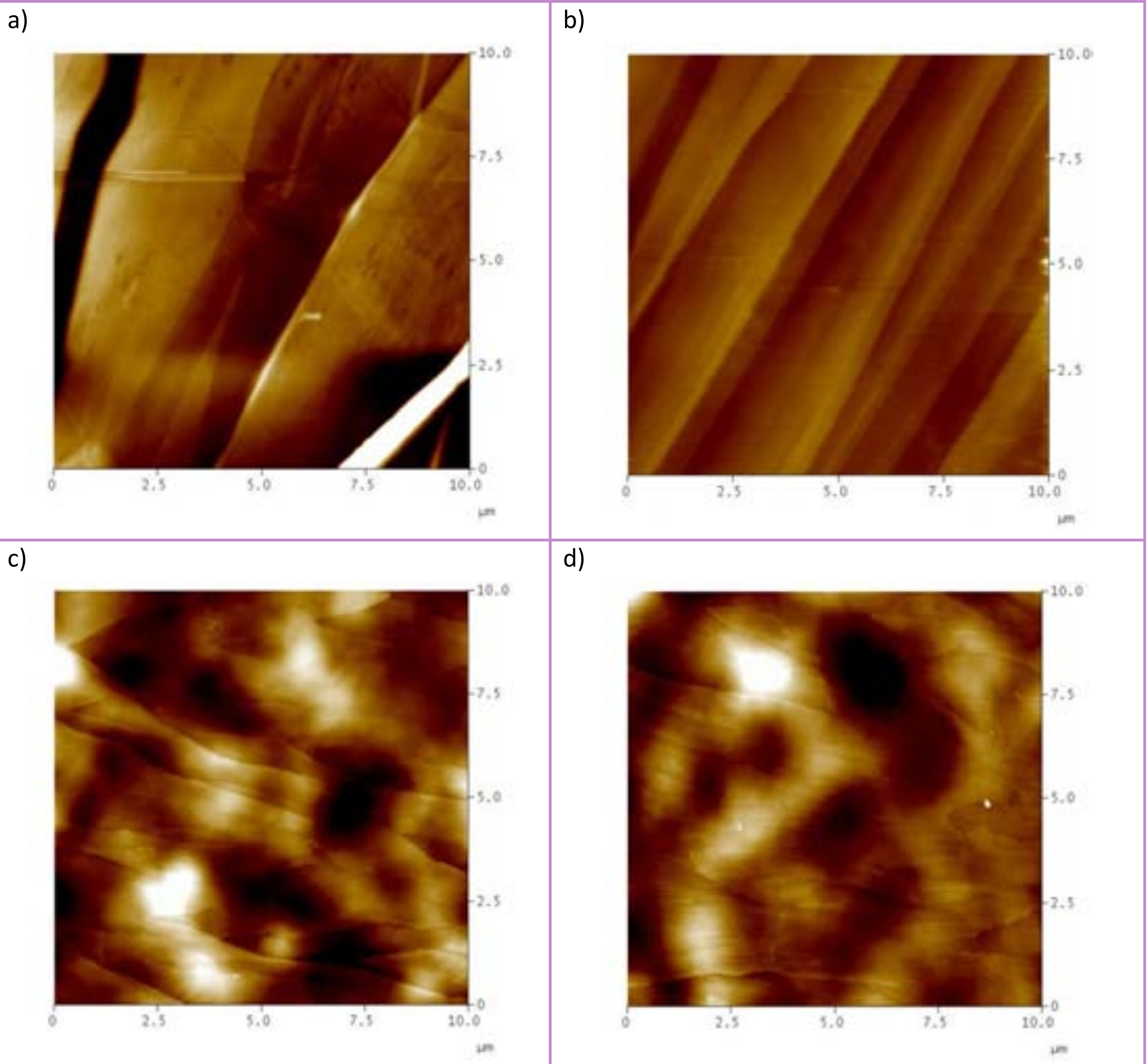

AFM in non-contact/dynamic mode operating in liquid imaging a graphite sample. a) Topography scanned with an epoxy based resist with a k = 40 N/m and a resonant frequency in liquid of 104 kHz. b) Topography scanned with an epoxy based resist with a k = 11 N/m and a resonant frequency in liquid of 9.5 kHz. The repeated steps in the image induce to think that probably the measurement is made with a damaged tip (an effect called double tip). c) Topography scanned with rectangular silicon probe for dynamic mode (RTESP14) with a k = 50 N/m and a resonant frequency in liquid of 130 kHz. c) Image taken with a silicon probe usually used for contact mode in air (SCM-PIC) with a k = 0.2 N/m and a resonant frequency in liquid of 6 kHz. This image is very noisy, which is due to the low quality factor that the probe has. For all the images the Z scale is from 0 to 30 nm. a) and b) images were performed using the same graphite sample, whereas c) and d) were taking a different one, thata is the main reason why the topography looks so different.

Given that epoxy based resist AFM probes have a lower resonant frequency and quality factor than their solid state counterparts (for the same dimensions), it was expected that the change

to liquid did not affect them as much as for silicon or silicon nitride. In fact, nor the quality factor neither the resonant frequency decrease from the air measurements. This causes that the resonance frequency is comparable with the silicon commercial probes in liquid (see Table 2.10 and Figure 2.27). Also the quality of the image is very similar to the commercial silicon probes. In Figure 2.28, an example of operation in liquid using a SU-8 probe is shown.

A good resonance frequency for a cantilever should fit in a Lorentzian curve. As it can be seen in Figure 2.27, the epoxy based resist probes have a very good mechanical oscillation while the silicon probes do not fit as well as the polymeric ones to the Lorentzian curve. Even though, it was possible to take images with all of them. Figure 2.28 shows topography images of graphite.

As it has been explained, the better the resonance peak is, with at least 1 V of amplitude to have enough signal, and the higher the quality factor, the higher resolution and less noisy AFM images can be obtained. From Figure 2.28 it is possible to spot which one of the levers provides a better imaging quality. Figure 2.28.d is very noisy and it shows a lot of bad lines where probably the tip enters in contact with the surface due to the unstable frequency response (Figure 2.27.d). Figure 2.28.b, even though the terraces have a very good resolution is still a little bit noisy. Best image was taken with the highest spring constant cantilever made of epoxy based resist (Figure 2.28.a).

Finally, performing force curves could also be acquired with epoxy based resist probes on the graphite sample in liquid. In Figure 2.29.a no adhesion part or creation of the water meniscus is observed, which is understandable due to the fact that the measurement is performed in liquid.

Figure 2.29

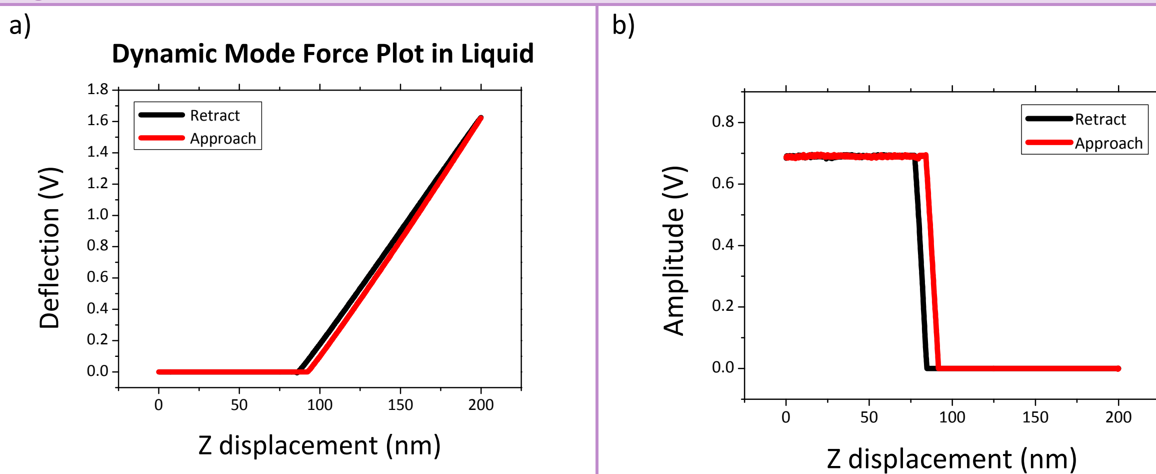

AFM in non-contact/dynamic mode operating in liquid. a) Force plot of an epoxy based resist probe with a spring constant of 80 N/m. b) Amplitude of the oscillation.

2.6 AGING STUDY

Since November 14th 2006 a long term stability study has been carried out and still is in progress. Internal stresses coming from the processing are not the only cause for the initial bending of the cantilever. As it has been reported from other Novopoly partners (Nanoworld, MIC-DTU), epoxy based resists can increase the stress gradient with the past of time. This preliminary result, if confirmed, would represent a huge drawback for an eventual commercialization.

The behavior of the cantilevers as a function of time is very critical for AFM probe companies interested in their commercialization. Companies need to ensure the specifications of the AFM probes that a customer buys. If cantilevers increase its bending with time, there exists the possibility that when the probe is used, no laser reflection can be collected by the photodetector. For that reason, this study must be performed not only under clean room conditions. Environmental conditions and shipping conditions have been also studied in order to see how time, delivery and storage affect the probes quality since their fabrication by the company to the costumer reception. If this aging effect on the deflection angle is confirmed, it would also be interesting to establish a time evolution in order to determine the expiration date of the product.

All different releasing techniques, pre-treatments processes and metal coating have been studied in this aging study. Starting with the initial bending (already presented), periodical measurements have been performed using a confocal microscope.

2.6.1 Study in clean room environment

In first place, the measurements are performed while keeping the probes in the Clean Room at any time. In following pictures, the deflection angle for different levers, corresponding to different release methods, are shown (Figure 2.30-Figure 2.34). As it has been described in section 2.4.2, deflection angle depends on the cantilever length. For that reason, cantilevers with similar lengths have been selected from each of the releasing techniques. The graphs reported in this Thesis resume the behavior observed. In each one is specified the concrete length of the studied cantilever in the graph title.

Figure 2.30

a)

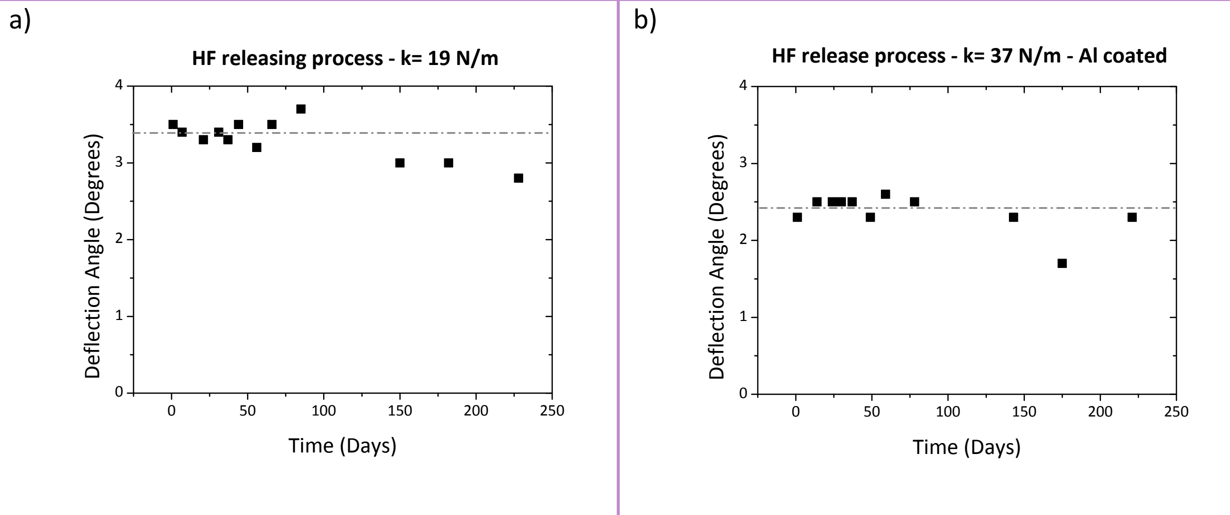

b)

Aging study of two cantilevers released by HF 49% without any hard bake. a) without and b) with metal coating.

Figure 2.31

a)

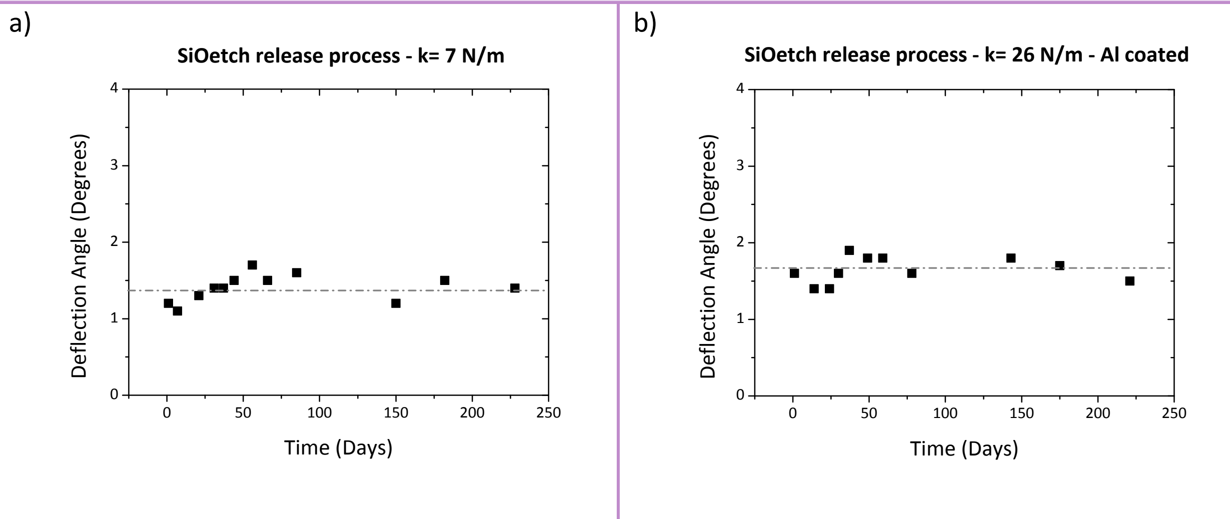

b)

Aging study of two cantilevers released by buffered HF without any hard bake. a) without and b) with metal coating.

As it can be seen, all the cantilevers, no matter which releasing method has been used or treatment processes, are completely stable. The shortest experiment has lasted 150 days (the difference between how long an experiment lasts comes from the fact that the levers were fabricated in different batches). The small fluctuation showed in the graphs, comes from uncertainties present in the measurement technique itself and not from actual fluctuations in the cantilever deflection angle. For that reason in can be concluded that under clean room

conditions the long term stability of the epoxy based resist AFM probes is ensured for all the releasing processes and treatment processes that have been tested. Furthermore, the coating layer does not change this stability.

Figure 2.32

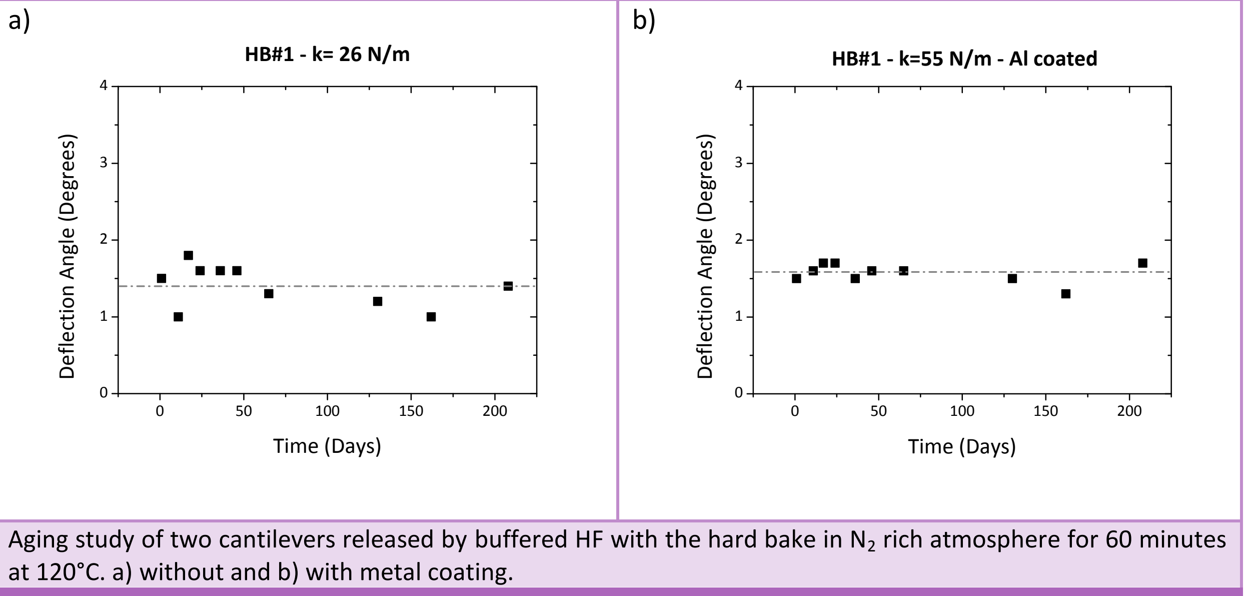

Aging study of two cantilevers released by buffered HF with the hard bake in N_2 rich atmosphere for 60 minutes at 120°C. a) without and b) with metal coating.

Figure 2.33

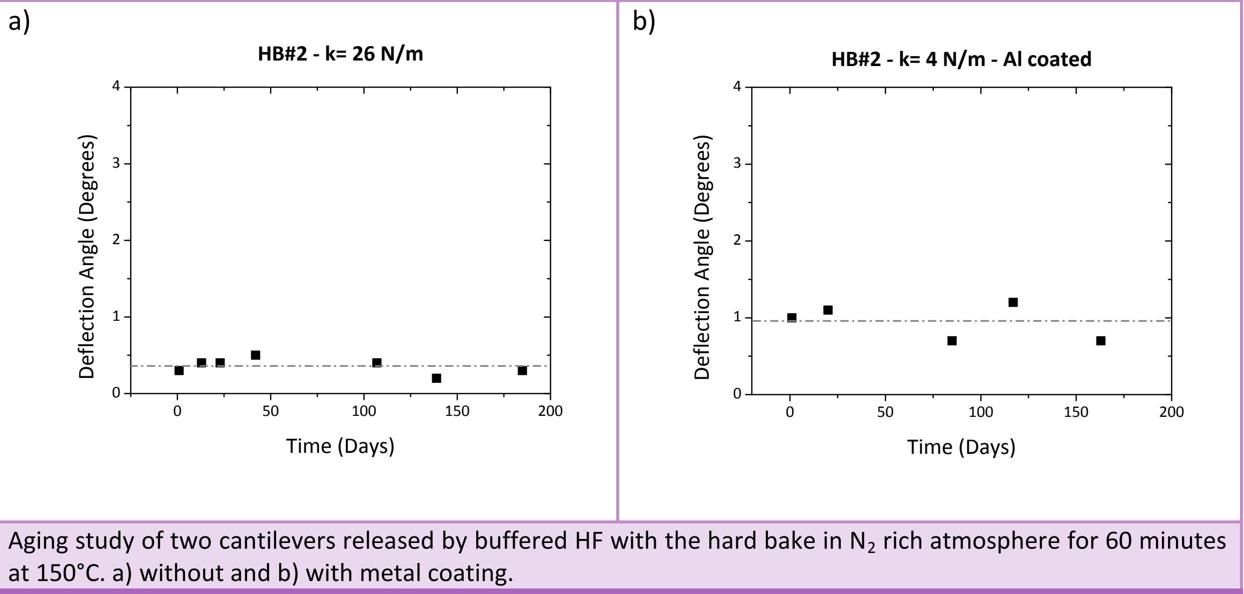

Aging study of two cantilevers released by buffered HF with the hard bake in N_2 rich atmosphere for 60 minutes at 150°C. a) without and b) with metal coating.

Figure 2.34

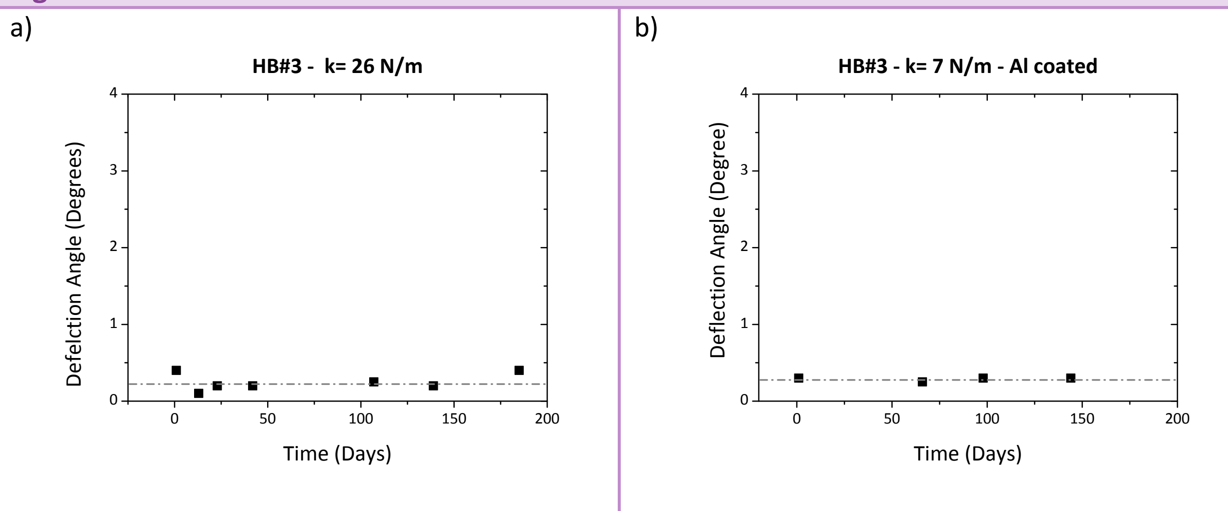

Aging study of two cantilevers released by buffered HF with the hard bake in N_2 rich atmosphere for 120 minutes at 120°C. a) without and b) with metal coating.

2.6.2 Study in non controlled environment

AFM systems can be operated in many environmental conditions, so in most of the cases the microscope will not be placed in a clean room. Even more, in most of the cases there will be no clean and controlled environment to keep the probes in. Therefore, epoxy based resist AFM probes should keep their initial bending constant as a function of time also when stored out of a clean room, in order to be considered as a cheap option for commercialization.

Fabricated probes from all the processes, non-coated and aluminum coated, were stored in room conditions in order to observe if any change in cantilever deflection angle is produced. As a general summary, it must be said that no significant change has been observed as a function of the fabrication processes; therefore just the most relevant treatments, i.e. those which yield probes with deflection angles that allow AFM operation, will be presented here.

Again, cantilevers demonstrate to be very time stable and independent of the differences in the process. The 100 days that this studied lasted were summer days, including the hottest months in Barcelona like July and August where temperatures can easily be above 35 °C. Fluctuation of about 10 °C and the small changes in atmospheric pressure do not affect the deflection angle of epoxy based resist AFM probes.

Figure 2.35

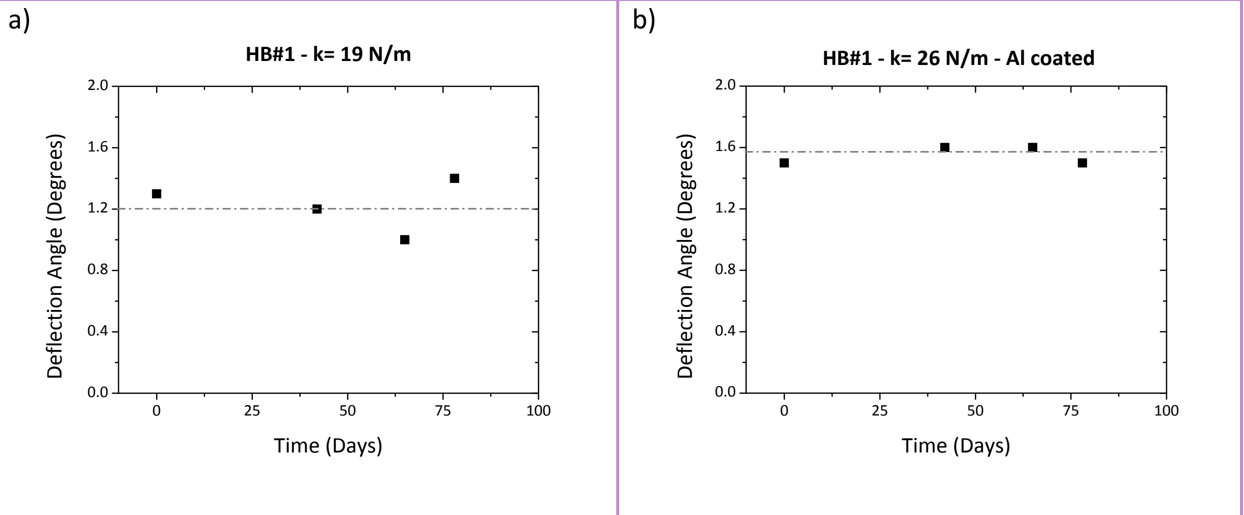

Aging study of two cantilevers released by buffered HF with the hard bake in N_2 rich atmosphere for 60 minutes at 120°C. a) without and b) with metal coating.

Figure 2.36

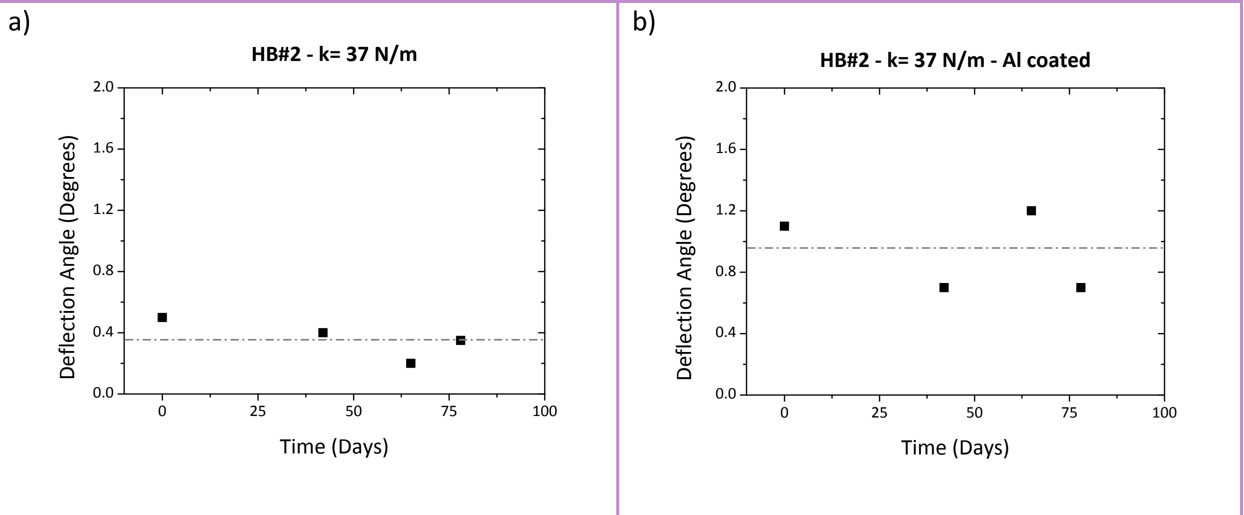

Aging study of two cantilevers released by buffered HF with the hard bake in N_2 rich atmosphere for 60 minutes at 150°C. a) without and b) with metal coating.

Figure 2.37

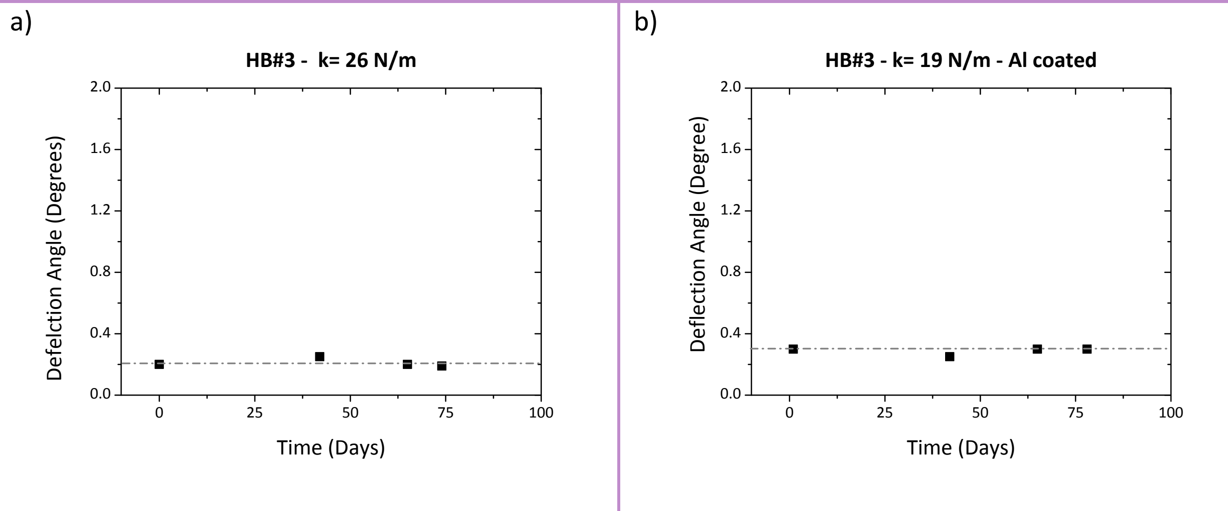

Aging study of two cantilevers released by buffered HF with the hard bake in N_2 rich atmosphere for 120 minutes at 120°C. a) without and b) with metal coating.

2.6.3 Study after delivery

It has been demonstrated that storage of epoxy based resist AFM probes can be done either clean room conditions or room conditions. In both environments it is clear that the fluctuations in temperature and pressure are small enough to not modify the internal stress of the material. From a commercial point of view it is also required to study how standard shipping affects the initial deformation. Although it would be possible to ship the probes in a controlled environment; that would increase the total cost, and that is unwanted one of the major advantages of these probes is their low cost.

To test the probes under the most unfavorable conditions possible, a gel-pax® box was sent in a bubble envelope to MIC-DTU partner, in Copenhagen (Denmark). The probes were handled by a shipping company without any special requirement, which means that air travelling in the aircraft cargo has not controlled pressure and temperature conditions. In addition, in Denmark they were supposed to be under different environmental conditions than in Barcelona (difference in temperatures can be larger than 20 °C from maximum temperature in Barcelona to minimum in Copenhagen). Probes were sent October 29th of 2007 and were received back on November 21st of 2007.

Main results are summarized in the following figures.

Figure 2.38

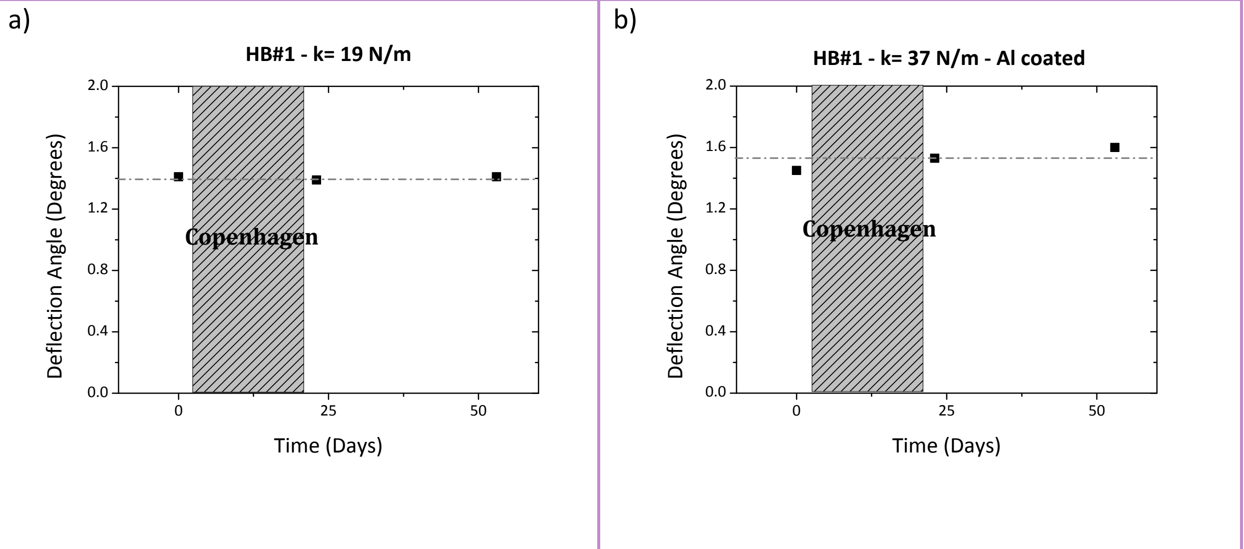

Aging study of two cantilevers released by buffered HF with the hard bake in N_2 rich atmosphere for 60 minutes at 120°C. a) without and b) with metal coating. Dashed grey zone corresponds to the shipping to Copenhagen, stay during 3 weeks and shipping back to Barcelona.

Figure 2.39

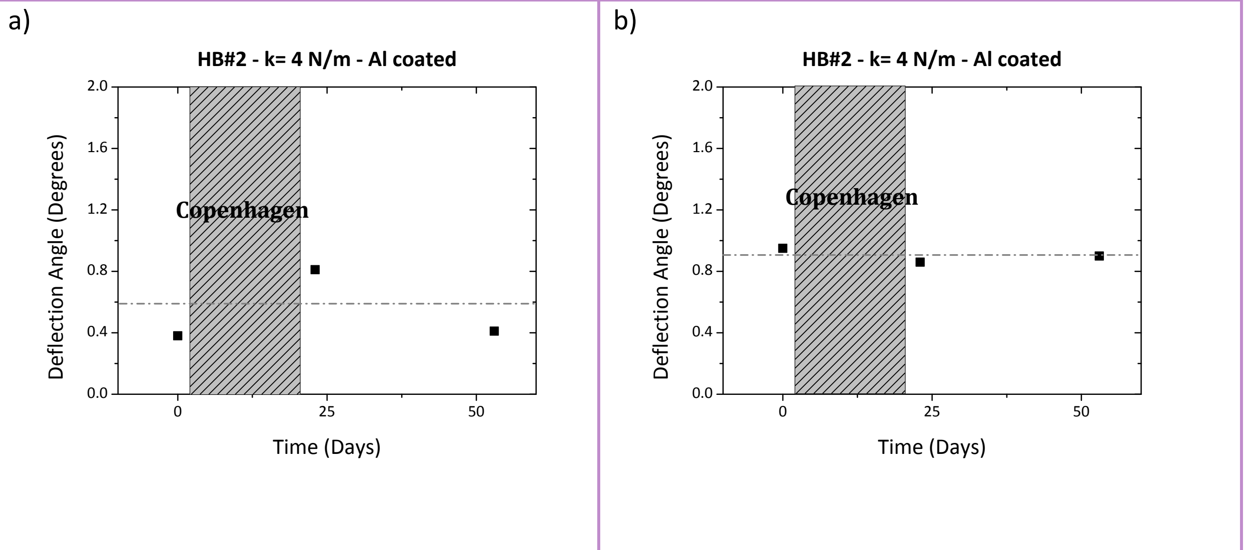

Aging study of two cantilevers released by buffered HF with the hard bake in N_2 rich atmosphere for 60 minutes at 150°C. a) without and b) with metal coating. Dashed grey zone corresponds to the shipping to Copenhagen, stay during 3 weeks and shipping back to Barcelona.

Figure 2.40

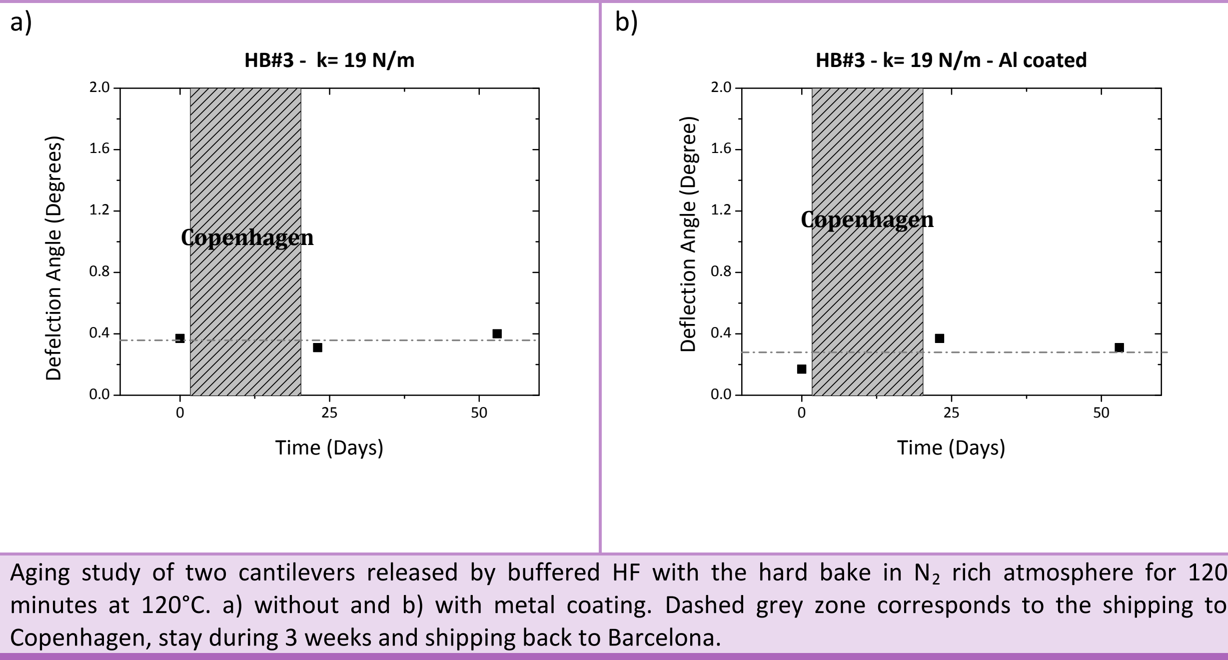

Aging study of two cantilevers released by buffered HF with the hard bake in N_2 rich atmosphere for 120 minutes at 120°C. a) without and b) with metal coating. Dashed grey zone corresponds to the shipping to Copenhagen, stay during 3 weeks and shipping back to Barcelona.

No significant difference in the deflection angle has been observed in the epoxy based resist AFM probes. From this study it is demonstrated that once probes are fabricated, environmental conditions for their storage and shipping procedures do not affect the feasibility of epoxy based resist probes, fabricated with the presented processing techniques, to be used in AFM systems.

2.7 CONCLUSIONS

SU-8 AFM probes have been fabricated and characterized. The fabrication has two main issues to overcome in order to have a proper probe, i.e. tip sharpness and cantilever initial deflection.

In order to achieve a sharp tip, subsequent TMAH etching of an inverted pyramid into the silicon wafer and thermal oxidation at 950°C have been performed, achieving much sharper tips than with higher temperature oxidation, e.g. 1100°C.

Obtaining flat cantilevers in a reproducible way was targeted as one of the basic goals of the project, given that this would be critical for an eventual commercialization of this kind of probes. Several processing steps and release methods were investigated, finding out that the most stable process was to perform a hard bake during 120 minutes at 120°C and then release the structures etching the oxide sacrificial layer using a buffered HF solution.

The fabricated devices were then tested in different commercial AFM equipments. They were proved to be valid for contact and non-contact mode, the latter both in air and liquid. As a general remark, it is possible to assert that the resolution of the tip can be as good as a commercial Si probe.

Finally, a complete aging study has been performed during more than 1 year in some cases in which it has been shown the fact that the probes fabricated by the process flow presented here are stable and neither the shipping nor the storage out of controlled environment affects them.

2.8 REFERENCES

1. G. Genolet, M. Despont, P. Vettiger, D. Anselmetti, and N.F. de Rooij
"All-photoplastic, soft cantilever cassette probe for scanning force microscopy".
Journal of Vacuum Science & Technology B, 2000, **18**(2), 617-620.

2. G. Genolet, J. Brugger, M. Despont, U. Drechsler, P. Vettiger, N.F. de Rooij, and D. Anselmetti
"Soft, entirely photoplastic probes for scanning force microscopy".
Review of Scientific Instruments, 1999, **70**(5), 2398-2401.

3. H. Lorenz, M. Laudon, and P. Renaud
"Mechanical characterization of a new high-aspect-ratio near UV-photoresist".
Microelectronic Engineering, 1998, **42**, 371-374.

4. G. Binnig, C.F. Quate, and C. Gerber
"ATOMIC FORCE MICROSCOPE".
Physical Review Letters, 1986, **56**(9), 930-933.

5. G. Meyer and N.M. Amer
"NOVEL OPTICAL APPROACH TO ATOMIC FORCE MICROSCOPY".
Applied Physics Letters, 1988, **53**(12), 1045-1047.

6. T. Goddenhenrich, H. Lemke, U. Hartmann, and C. Heiden
"FORCE MICROSCOPE WITH CAPACITIVE DISPLACEMENT DETECTION".
Journal of Vacuum Science & Technology a-Vacuum Surfaces and Films, 1990, **8**(1), 383-387.

7. M. Tortonese, R.C. Barrett, and C.F. Quate
"ATOMIC RESOLUTION WITH AN ATOMIC FORCE MICROSCOPE USING PIEZORESISTIVE DETECTION".
Applied Physics Letters, 1993, **62**(8), 834-836.

8. G. Binnig, C. Gerber, E. Stoll, T.R. Albrecht, and C.F. Quate
"ATOMIC RESOLUTION WITH ATOMIC FORCE MICROSCOPE".
Europhysics Letters, 1987, **3**(12), 1281-1286.

9. R. Garcia and R. Perez
"Dynamic atomic force microscopy methods".
Surface Science Reports, 2002, **47**(6-8), 197-301.

10. F.J. Giessibl
"Advances in atomic force microscopy".
Reviews of Modern Physics, 2003, **75**(3), 949-983.

11. O. Wolter, T. Bayer, and J. Greschner
"MICROMACHINED SILICON SENSORS FOR SCANNING FORCE MICROSCOPY".
Journal of Vacuum Science & Technology B, 1991, **9**(2), 1353-1357.

12. M. Despont, J. Brugger, U. Drechsler, U. Durig, W. Haberle, M. Lutwyche, H. Rothuizen, R. Stutz, R. Widmer, G. Binnig, H. Rohrer, and P. Vettiger
"VLSI-NEMS chip for parallel AFM data storage".
Sensors and Actuators A-Physical, 2000, **80**(2), 100-107.

13. P. Vettiger, J. Brugger, M. Despont, U. Drechsler, U. Durig, W. Haberle, M. Lutwyche, H. Rothuizen, R. Stutz, R. Widmer, and G. Binnig
"Ultrahigh density, high-data-rate NEMS-based AFM data storage system".
Microelectronic Engineering, 1999, **46**(1-4), 11-17.

14. M. Lutwyche, C. Andreoli, G. Binnig, J. Brugger, U. Drechsler, W. Haberle, H. Rohrer, H. Rothuizen, P. Vettiger, G. Yaralioglu, and C. Quate
"5X5 2D AFM cantilever arrays a first step towards a Terabit storage device".
Sensors and Actuators A-Physical, 1999, **73**(1-2), 89-94.

15. T.R. Albrecht, S. Akamine, T.E. Carver, and C.F. Quate
"MICROFABRICATION OF CANTILEVER STYLI FOR THE ATOMIC FORCE MICROSCOPE".
Journal of Vacuum Science & Technology a-Vacuum Surfaces and Films, 1990, **8**(4), 3386-3396.

16. O. Tabata, R. Asahi, H. Funabashi, K. Shimaoka, and S. Sugiyama
"ANISOTROPIC ETCHING OF SILICON IN TMAH SOLUTIONS".
Sensors and Actuators a-Physical, 1992, **34**(1), 51-57.

17. R.B. Marcus and T.T. Sheng
"THE OXIDATION OF SHAPED SILICON SURFACES".
Journal of the Electrochemical Society, 1982, **129**(6), 1278-1282.

18. S. Keller, S. Mouaziz, G. Boero, and J. Brugger
"Microscopic four-point probe based on SU-8 cantilevers".
Review of Scientific Instruments, 2005, **76**(12), 125102.

19. R.E. Mahaffy, C.K. Shih, F.C. MacKintosh, and J. Kas
"Scanning probe-based frequency-dependent microrheology of polymer gels and biological cells".
Physical Review Letters, 2000, **85**(4), 880-883.

20. F. Rico, P. Roca-Cusachs, N. Gavara, R. Farre, M. Rotger, and D. Navajas
"Probing mechanical properties of living cells by atomic force microscopy with blunted pyramidal cantilever tips".
Physical Review E, 2005, **72**(2), 021914.

21. A. Boisen, J.P. Rasmussen, O. Hansen, and S. Bouwstra
"Indirect tip fabrication for scanning probe microscopy".
Microelectronic Engineering, 1996, **30**(1-4), 579-582.

22. H. Jansen, M. de Boer, H. Wensink, B. Kloeck, and M. Elwenspoek
"The black silicon method. VIII. A study of the performance of etching silicon using SF6/O-2-based chemistry with cryogenical wafer cooling and a high density ICP source".
Microelectronics Journal, 2001, **32**(9), 769-777.

23. H. Jansen, M. Deboer, R. Legtenberg, and M. Elwenspoek
"The Black Silicon Method - a Universal Method for Determining the Parameter Setting of a Fluorine-Based Reactive Ion Etcher in Deep Silicon Trench Etching with Profile Control".
Journal of Micromechanics and Microengineering, 1995, **5**(2), 115-120.

24. S. Akamine and C.F. Quate
"LOW-TEMPERATURE THERMAL-OXIDATION SHARPENING OF MICROCAST TIPS".
Journal of Vacuum Science & Technology B, 1992, **10**(5), 2307-2310.

25. B.E. Deal
"THERMAL-OXIDATION KINETICS OF SILICON IN PYROGENIC H2O AND 5-PERCENT HCL-H2O MIXTURES".
Journal of the Electrochemical Society, 1978, **125**(4), 576-579.

26. K.E. Petersen
"Silicon as a Mechanical Material".
Proceedings of the IEEE, 1982, **70**(5), 420-457.

27. R.T. Howe and R.S. Muller
"Stress in Polycrystalline and Amorphous-Silicon Thin-Films".
Journal of Applied Physics, 1983, **54**(8), 4674-4675.

28. A. Benitez, J. Bausells, E. Cabruja, J. Esteve, and J. Samitier
"Stress in Low-Pressure Chemical-Vapor-Deposition Polycrystalline Silicon Thin-Films Deposited Below 0.1 Torr".
Sensors and Actuators A-Physical, 1993, **37-8**, 723-726.

29. W. Fang and J.A. Wickert
"Determining mean and gradient residual stresses in thin films using micromachined cantilevers".
Journal of Micromechanics and Microengineering, 1996, **6**(3), 301-309.

30. J.A. Schweitz and F. Ericson
"Evaluation of mechanical materials properties by means of surface micromachined structures".
Sensors and Actuators a-Physical, 1999, **74**(1-3), 126-133.

31. G. Genolet
"New Photoplastic Fabrication Techniques and Devices Based on High Aspect Ratio Photoresist".
Ph.D.Thesis, 2001, École Polytechnique Fédérale de Lausanne.

32. D.J. Monk, D.S. Soane, and R.T. Howe
"A REVIEW OF THE CHEMICAL-REACTION MECHANISM AND KINETICS FOR HYDROFLUORIC-ACID ETCHING OF SILICON DIOXIDE FOR SURFACE MICROMACHING APPLICATIONS".
Thin Solid Films, 1993, **232**(1), 1-12.

33. D. Haefliger, M. Nordstrom, P.A. Rasmussen, and A. Boisen
"Dry release of all-polymer structures".
Microelectronic Engineering, 2005, **78-79**, 88-92.

34. C.K. Chung and Y.Z. Hong
"Surface modification of SU8 photoresist for shrinkage improvement in a monolithic MEMS microstructure".
Journal of Micromechanics and Microengineering, 2007, **17**(2), 207-212.

35. F. Walther, P. Davydovskaya, S. Zucher, M. Kaiser, H. Herberg, A.M. Gigler, and R.W. Stark
"Stability of the hydrophilic behavior of oxygen plasma activated SU-8".
Journal of Micromechanics and Microengineering, 2007, **17**(3), 524-531.

36. G. Hong, A.S. Holmes, and M.E. Heaton
"SU8 resist plasma etching and its optimisation".
Microsystem Technologies-Micro-and Nanosystems-Information Storage and Processing Systems, 2004, **10**(5), 357-359.

37. J. Garra, T. Long, J. Currie, T. Schneider, R. White, and M. Paranjape
"Dry etching of polydimethylsiloxane for microfluidic systems".
Journal of Vacuum Science & Technology a-Vacuum Surfaces and Films, 2002, **20**(3), 975-982.

38. Veeco
"Veeco Instruments".
http://www.veeco.com/, 2008.

39. Nanotec
"Nanotec Electronica".
http://www.nanotec.es/, 2008.

40. J.E. Sader
"Frequency response of cantilever beams immersed in viscous fluids with applications to the atomic force microscope".
Journal of Applied Physics, 1998, **84**(1), 64-76.

41. C.A. Van Eysden and J.E. Sader
"Resonant frequencies of a rectangular cantilever beam immersed in a fluid".
Journal of Applied Physics, 2006, **100**(11), 114916.

Chapter 3. Nanoparticles doped epoxy based resist AFM probes

One of the most important advantages of working with polymers is their capability to be functionalized and modified. Composite materials offer a combination of properties and a diversity of applications which cannot be obtained with metals, ceramics or polymers alone. Taking profit of the added properties, improved AFM probes have been fabricated. Higher quality factors and less stress gradient have been found by the use of a doped material that also increases the Young Modulus of the polymer. In this chapter the composite elaboration process is described, as well as the fabrication, study and characterization of the AFM probes made of the new composite.

3.1 INTRODUCTION

Develop of new functional materials for applications in the area of micro and nano systems is a topic of increasing interest [1]. Recently, many efforts have been directed towards the fabrication of nanocomposite (NC) materials based on an organic component combined with nanometer-sized inorganic nanoparticle [1-6]. The reason lies in the fact that many organic components, such as SU-8 or other epoxy-based resists, do not present any inherent functionality and can only be used to fabricate passive elements. The mixing of organic material with nanoparticles can arise in flexible composites that exhibit advantageous electrical, optical, magnetic or mechanical properties [2, 4].

One of the goals of the Novopoly project [7] is to overcome the limitations of organic materials respect to mechanical, electrical conductivity and high temperature stability properties. One strategy is based on the doping of previously existing photosensitive polymers to add this functionality.

The term “nanoparticle” is a very general one and is often used to cover materials that are better described using other terms. A possible definition for nanoparticles could be: “small clusters of atoms whose dimensions are not larger than 100 nm in any direction” [8-10]. The term “nanocrystals” is generally reserved to structures with well-characterized crystalline interior, while the more general term “nanoparticles” denotes amorphous or inherently multidomain inorganic cores.

The interest in these very small particles originates from their physical properties, which can be vastly different from those of bulk material [8, 9, 11]. Nanoparticles are larger than individual atoms and molecules but are further smaller than bulk solid. For that reason, they obey neither absolute quantum chemistry nor laws of classical physics and have properties that differ from those expected.

There are two major phenomena that are responsible for these different properties, the increase in the surface to volume ratio, and the size of the particle moving into the realm where quantum effects predominate [9].

As the size of a crystal is reduced, the number of atoms at the surface of the crystal compared to the number of atoms in the crystal itself, increases. Properties, which are usually determined by the molecular structure of the bulk lattice, now become increasingly dominated by surface effects. In any material, surface atoms make a distinct contribution to the free energy and they cause the large changes in thermodynamic properties as melting temperature depression or

solid-solid phase transition elevation. This affects both the properties of the particle in isolation and its interaction with other materials or particles. The large surface area of nanoparticles also results in a lot of interactions between the intermixed materials in NCs, leading to special properties such as increased strength and/or increased chemical/heat resistance [4].

The second phenomenon is only noticeable in metals and semiconductors, it is less gradual and basically affects to optical and electrical properties. It is called size quantization and arises because the size of a nanoparticle is comparable to the *de Broglie* wavelength of its charge carriers, i.e. electrons and/or holes. Due to the spatial confinement of the charge carriers, the edge of the valence and conduction bands split into discrete, quantized, electronic levels. These electronic levels are similar to those in atoms and molecules. The spacing between the electronic levels and the band gap increases with decreasing particle size. This is because the electron-hole pairs are now much closer and the Coulomb interaction between them can no longer be neglected giving an overall higher kinetic energy. This increase in band gap can be observed experimentally by the blue-shift in the absorption spectrum or sometimes even visually by the color of the samples [5, 11, 12]. A larger band gap means that more energy is required to excite an electron from the valance band to the conduction band and hence light of a higher frequency and lower wavelength would be absorbed.

Due to the two unique phenomenons which occur in nanoparticles, their properties (electrical, optical, chemical, mechanical, magnetic, etc) can be selectively controlled by engineering the size, morphology, and composition of the particles. These new substances will have enhanced or entirely different properties from their parent materials.

Nanoparticles are currently made out of a very wide variety of materials, e.g. silicates, ceramics, pure metal nanoparticles, carbon nanotubes, fullerenes, etc. There are three main techniques used for producing them, i.e. condensation from vapor, chemical synthesis and solid state processes (such as milling). In addition the particles can be coated with hydrophilic or hydrophobic layers depending on the desired application.

Vapor condensation

This approach is used to make metallic and metal oxide ceramic nanoparticles. It involves evaporation of a solid metal followed by rapid condensation to form nanosized clusters that settle in the form of a powder. Inert gases are used to avoid oxidation when creating metal nanoparticles, whereas a reactive oxygen atmosphere is used to produce metal oxide ceramic nanoparticles. The main advantage of this approach is low contamination levels. Final particle size is controlled by variation of parameters such as temperature, gas environment and evaporation rate.

Chemical synthesis

This technique consists essentially in the growth of nanoparticles in a liquid medium composed of various reactants. Examples are the sol-gel method, the hot-injection method, the precipitation method, solvothermal synthesis, etc. and they are also used to create quantum dots (nanoparticles in which quantum mechanical properties are key to their useful behavior). Chemical techniques are generally better that vapor condensation techniques for controlling the final size of the particles. On the other hand, contamination from the precursor chemicals can be a problem.

Solid state processes

Grinding or milling can be used to create nanoparticles. The milling material, milling time and atmospheric medium affect resultant nanoparticle properties. The approach can be used to produce nanoparticles from materials that do not readily lend themselves to the two previous techniques. Contamination from the milling material can be an issue.

As all the techniques described above require high-tech areas and very expensive equipment, a very important market for nanoparticles is expanding in order to supply them. There is an increasing demand for nanoparticles with well-defined size and shape in high volumes.

Shape of the nanoparticle is also important [13-16]. Nanocrystals assume regular shapes, with the same well defined facets and the same crystal structures as are present in extended solids. This opens up the possibility of manipulating the surface energetic of nanocrystals in a controlled manner. It remains an open question whether it will be possible to prepare nanocrystals with interior bounding geometries that do not occur in the known extended crystal.

Nanoparticle characterization is necessary to establish understanding and control of nanoparticle synthesis and applications. Characterization is done by using a variety of different techniques, mainly drawn from materials science. Common techniques are transmission and scanning electron microscopy (TEM and SEM respectively), atomic force microscopy (AFM), dynamic light scattering (DLS), x-ray photoelectron spectroscopy (XPS), powder x-ray diffraction (XRD), and Fourier transform infrared spectroscopy (FTIR).

Some applications of nanoparticles (if they are successfully incorporated) are to make metals stronger and harder, to give ceramics enhanced ductility, to enable normally insulating materials to conduct heat or electricity, to make protective coatings transparent, etc.

3.1.1 Incorporation of Nanoparticles to polymers

The combination of nanoparticles with polymers to obtain the desirable properties is very recent and it is still in development. The ensuing research revealed a number of key challenges in producing NCs that exhibit the desired behavior. The main issue lies in finding effective methods for controlling the dispersion of the nanoparticles in polymeric hosts, due to the absence of structure-property relationships [1].

The interactions of nanoparticles with polymers are mediated by the ligands attached to the nanoparticles; thus, ligands markedly influence particle behavior and spatial distribution. Therefore, the study of the nanoparticle surface modification and the interactions between these particles and the polymer matrices is so important.

A first step is the functionalization of nanoparticles' surfaces. In functionalization it is possible to attach small molecules and polymers to the nanoparticles by physical adsorption or covalent binding. Synthetic strategies that give polymer-functionalized nanoparticles include performing the particle synthesis directly in the polymer matrix, replacing small molecule ligands inherent to a nanoparticle with functional polymers.

Figure 3.1

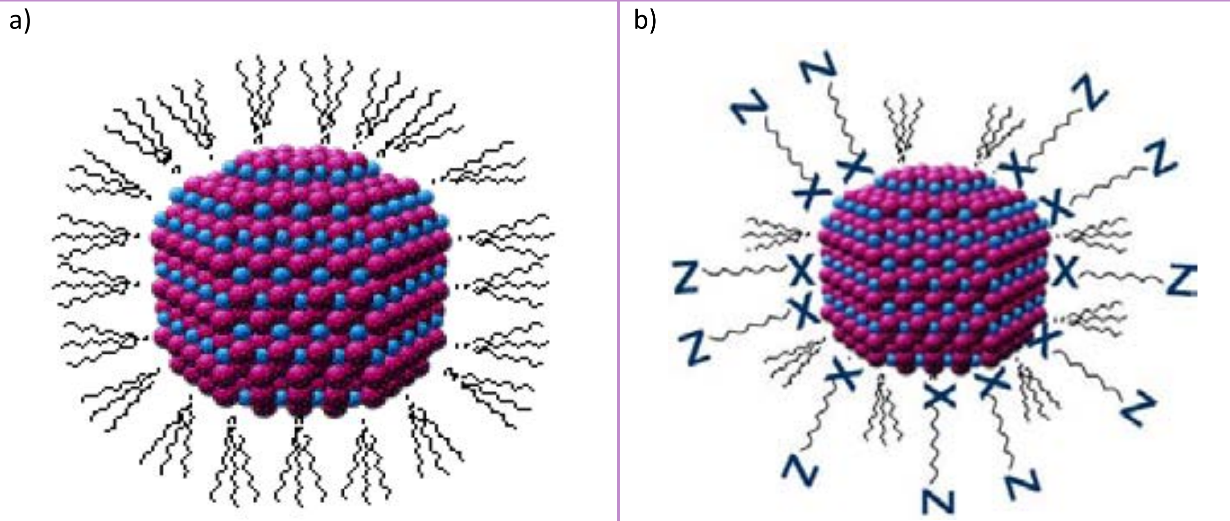

Surface functionalization of nanoparticles to ease their processing and their dispersion in polymers. X represents a chemical function with a high affinity for nanoparticles surface (for example a thiol, an amine or a phosphoric group). Z represents a functional group that allows the solubility of the nanoparticles in different solvent like a polymer, as for example an alkyl chain [17].

Many state of the art of nanoparticle preparations yield in the functionalization of the nanoparticles directly (by chemical synthesis techniques). They are based in the decomposition

of organometallic precursors in a solution environment that leads to surface coverage with small molecules alkane-based ligands. Simply mixing these alkane-covered nanoparticles with most polymers leads to non-uniform particle clustering or aggregation that compromises the properties of the composite. Therefore, replacing of these standard ligands with those that favorably interact with the polymer host is crucial in achieving uniform dispersions. Hence, versatile synthetic strategies are necessary to fine-tune the chemical nature of the ligands.

Summarizing, it seems to be clear that to obtain a good composite it is required to reach, for each nanoparticle, the tailored ligand to be able to attach it to the desired polymer. Then, the distribution, the properties and the behavior can be homogeneous, repeatable and stable.

3.1.2 Composite assembly

In order to add novel functionalities to an epoxy based resist, it has been doped using two different nanoparticles, i.e. γ-Fe_2O_3 and TiO_2. The first one was selected because it has very good magnetic, catalytic and biocompatibility properties; whereas the second one has appealing semiconducting, photocatalytic and optical characteristics [18]. In this section, the synthesis of those nanoparticles and NCs is presented. The elaboration of the doped epoxy based resists has been performed by Dr. Lucia Curri and Dr. Chiara Ingrosso from *Consiglio Nazionale delle Ricerche – Instituto per I Processi Chimico Fisici sezione di Bari* (CNR-IPCF), partners in the Novopoly project.

3.1.2.1 Iron oxide composite (γ-Fe_2O_3)

The protocol used to prepare the composite consists in three steps: first, synthesize the nanoparticles; then its incorporation into the epoxy based resist; and, finally, apply ultrasounds to fully mix the materials.

Colloidal chemistry methods (inside the chemical synthesis technique) are used to prepare the nanoparticles. Colloidal system or solution is a mixture in which one substance is divided into minute particles (called colloidal particles) and dispersed throughout a second substance. There are no strict boundaries on the size of colloidal particles, but they tend to vary between 10^{-9} m and 10^{-6} m in size.

There are two main ways of forming a colloid: reduction of larger particles to colloidal size or condensation of smaller particles, e.g. molecules, into colloidal particles. The latter generally makes use of chemical reactions such as hydrolysis or displacement.

The method chosen to synthesize γ-Fe_2O_3 particles involves thermal decomposition of the precursors in hot coordinating solvents [5]. The emulsion is usually prepared by heating the mixture of solvent with surfactant up to a high temperature (100-300°C) and then the precursor is injected in it as shown in Figure 3.2.

Figure 3.2

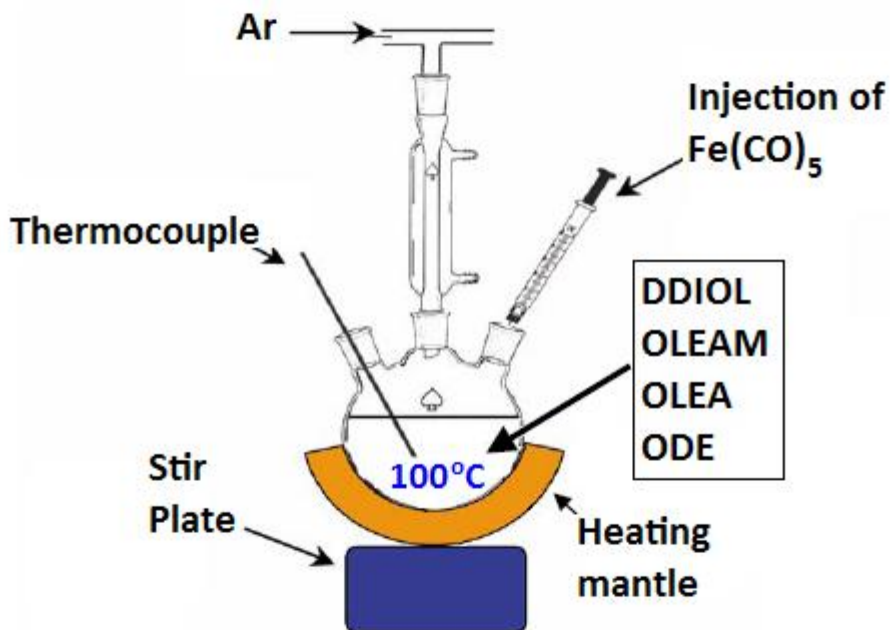

Three-neck flask with the mixture of reactants to obtain nanoparticles with the colloidal technique [17].

The chemicals needed for the synthesis of γ-Fe_2O_3 are: oleic acid ($C_{17}H_{33}CO_2H$ or Olea, 90 %), 1-octadecene ($C_{18}H_{36}$ or ODE, 90 %), oleyl amine ($C_{17}H_{33}CN_2$ or OLEAM, 70 %), iron pentacarbonyl ($Fe(CO)_5$, 98 %), dodecan-1.2-diol ($C_{12}H_{24}(OH)_2$ or DDIOL, 90 %) and 10-undecylenic acid ($C_{10}H_{19}CO_2H$ or 10UDA, 98 %).

2-2.5 mmol of DDIOL, 1.5-3 mmol of OLEAM, 3-6 mmol of OLEA and 20 ml of ODE are loaded in a three-neck flask. The mixture is evacuated during 20 min at 120 °C. After that, it is heated up to the temperature selected for the iron precursor injection (ranging from 240 °C to 300 °C) under N_2 flux. 1 ml of a $Fe(CO)_5$ solution (typically 0.1-2 M in previously degassed ODE) is added in a single portion to the vigorously stirred mixture. This solution is prepared in the glove box (Figure 3.2).

In this synthesis, OLEA and OLEAM are known to act as capping agents while ODE is the solvent. A temporal separation between the nucleation and the growth stages is naturally achieved during iron oxide syntheses. The injection of the $Fe(CO)_5$ is followed by a long incubation time

before a sudden burst of nucleation takes place, that is when a supersaturation threshold is reached. This delayed nucleation is caused by the gradual transformation of $Fe(CO)_5$ into Fe:OLEA or Fe:OLEAM based intermediate species (such as higher nuclearity clusters of carbonyls or metal-surfactant complexes), which then act as the active monomer species during crystal growth [17, 19].

When the threshold is crossed, a sufficiently high concentration of monomers has been accumulated; the subsequent growth of the initially generated nuclei is comparatively much faster. The formation of iron oxide nanoparticles has been typically observed at a minimum reaction temperature of 220 °C. This finding suggests that the active monomer species leading to the production of iron oxide nanoparticles are provided by thermal decomposition of the Fe-surfactant complexes present in the solution.

Thus, under the employed reaction conditions, iron oxide is formed by direct pyrolysis of Fe/O-containing species during the high temperature step under nitrogen, assisted by DDIOL. The subsequent air treatment almost completes the oxidation of the Fe_3O_4 phase into γ-Fe_2O_3. Size and shape control is achieved by adjusting the temperature and/or reactant concentration, according to literature criteria. For instance, the slow heating of all reactant to a target temperature led to spherical nanoparticles, whereas the fast injection of $Fe(CO)_5$ into the already hot surfactant yielded faceted objects, exhibiting a diamond like, hexagonal or triangular shaped profile, depending on the conditions.

Figure 3.3

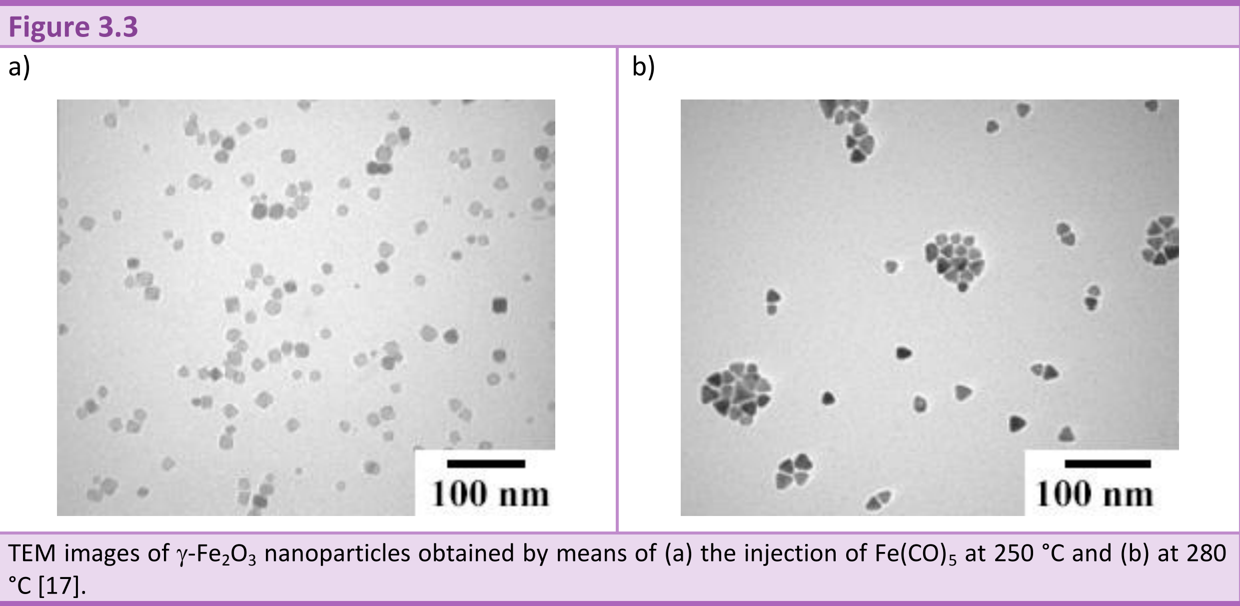

TEM images of γ-Fe_2O_3 nanoparticles obtained by means of (a) the injection of $Fe(CO)_5$ at 250 °C and (b) at 280 °C [17].

After the synthesis, extraction/purification procedure of the iron oxide nanoparticles is performed at room conditions. A 1:1 mixture of acetone and isopropanol is added to the reaction mixture at room temperature and the solution is centrifuged. The precipitate is washed three with a solution of acetone and isopropanol in order to remove the precursor and the surfactant residues. Finally, the obtained nanoparticles can be fully re-dissolved in toluene, chloroform or hexane.

TEM images show different shaped iron oxide nanoparticles (Figure 3.3). The shape as well as the dimension has been typically modulated by the reaction conditions (temperature, concentration of the precursors, type of capping agent and speed of injection). Indeed, diamond and hexagonal shape nanoparticles have been obtained with a direct injection at 250 °C (Figure 3.3.a) while triangular have been prepared at 280 °C (Figure 3.3.b).

The incorporation of the synthesized nanoparticles in the epoxy based resist has been usually done following the ratio of 200 µl of a 0.15 M toluene solution of γ-Fe_2O_3 nanoparticles into 5 grams of resist. As γ-Fe_2O_3 nanoparticles are linked to alkyl chains that enable the solubility in organic media, the dispersion into the polymer is easy. Using the mentioned ratio, a final concentration of nanoparticles in the composite of $6{\cdot}10^{-6}$ mol/g is achieved. To obtain a fully homogeneous composite the mixture is sonicated during 2 hours.

In order to observe a higher magnetic behavior a higher concentration of the nanoparticles has been tried. In this case the mixing ratio was 1 ml of a 0.15 M toluene solution of γ-Fe_2O_3 nanoparticles mixed into 5 grams of resist. This second concentration is 5 times higher than the first one, being $3{\cdot}10^{-4}$ mol/g.

Figure 3.4

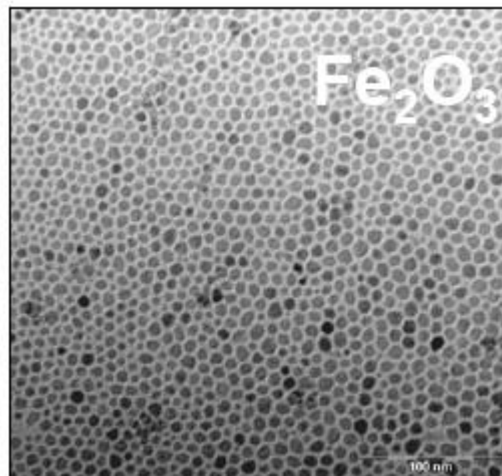

TEM image of γ-Fe_2O_3 NCs highly aggregated [17].

The magnetic behavior of the nanoparticles is demonstrated while the resist is still not cured. In a drop of the higher concentration NC, it is possible to see different states depending on the direction of an external magnetic field.

At first sight, it was observed that both γ-Fe_2O_3 concentrations NC had, apart from the magnetic behavior, a dark color, which of course led to some modifications in the process parameters compared to the standard undoped resist.

3.1.2.2 Titanium Oxide composite (TiO_2)

Elaboration procedure for the titanium dioxide nanoparticles was performed following the methodology described in [20]. There, two methods to synthesize the nanoparticles are presented, the fast and slow hydrolysis. The latter yields almost spherical nanoparticles and needs of more than 48 hours to be completed. On the other hand, the fast one, yields nanoparticles which have an elongate shape and for that reason they are usually named nanorods. The dimensions of the nanorods oscillate between 3-4 nm of diameter and 25-30 nm of length. In this work, only TiO_2 nanorods were produced (fast process).

The chemicals used in this process were: titanium tetraisopropoxide ($Ti(OPri)_4$ or TTIP, 99.999%), trimethylamino-N-oxide dihydrate or anhydrous ($(CH_3)_3NO$ or TMAO, 98%), and oleic acid ($C_{18}H_{33}COOH$ or OLEA, 90%).

In a typical synthesis, 35 g of oleic acid (OLEA) is dried at 120 °C for 1 h under vigorous stirring in a 50 mL three-neck flask, after which it is cooled to 80-100 °C under nitrogen flow. 1-10 mmol of TTIP is then added and allowed to stir for 5 min. The absence of water at this stage prevents the premature hydrolysis of the molecular precursor. A 0.5-5 mL of a 0.1-2 M aqueous base solution (TMAO) is loaded into a 5 mL syringe and then rapidly injected. Upon injection, the temperature drops to about 75-90 °C, after which it is again heated to the initial injection temperature in a few minutes. The solution is maintained in a closed system at 80-100 °C and stirred under mild reflux with water over 6-12 h to promote further hydrolysis and crystallization of the product. The reaction is stopped by removing the heat source.

The TiO_2 nanorods are separated from their growing mixture upon ethanol addition and subsequently subjected to repeated cycles of redissolution in $CHCl_3$ (chloroform) and precipitation with ethanol to wash out surfactant residuals. The obtained nanoparticles have been proved to be stable over months without further addition of phosphoric acid molecules. However, toluene is added to dissolve TiO_2 nanorods because its aromatic structure is more

chemically affine with the polymer and PAG than other solvents typically used, as chloroform [21, 22].

Figure 3.5

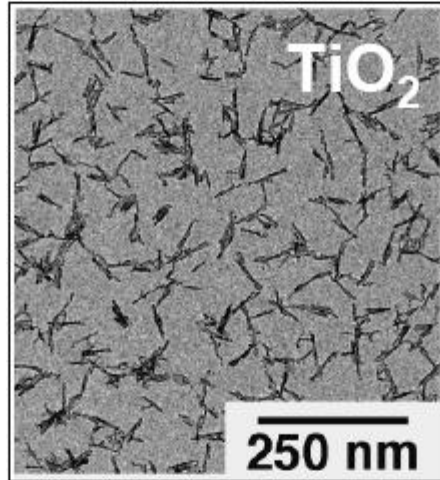

TEM image of the final composite with a concentration of $2 \cdot 10^{-5}$ mol/g [20].

The final concentration of $2 \cdot 10^{-5}$ mol/g is obtained as a result of mixing 200 µl of the 0.5 M toluene solution of TiO_2 nanorods into 5 g of anisole based epoxy based resist. This mixture also requires to be sonicated for 2 hours. The final color of the composite is white.

3.2 PROCESS FLOW

Two different approaches have been carried out to fabricate composite AFM probes. Basically, the process flow is the same that the one explained in the previous chapter using epoxy based resist as structural material but in this case the material for the cantilever changes.

The mould fabrication is exactly the same as the one presented in the previous chapter. In fact, usually several moulds are fabricated at the same time (with a subsequent oxidation at 950°C) and then they are used indistinctly to hold all three possible material for the AFM probes, i.e. epoxy based resist, iron oxide composite and titanium oxide composite.

3.2.1 Single layer cantilever

In the first approach, only the material selected to form the cantilever is modified, together with the parameters of some of the fabrication steps involving the new material.

Figure 3.6

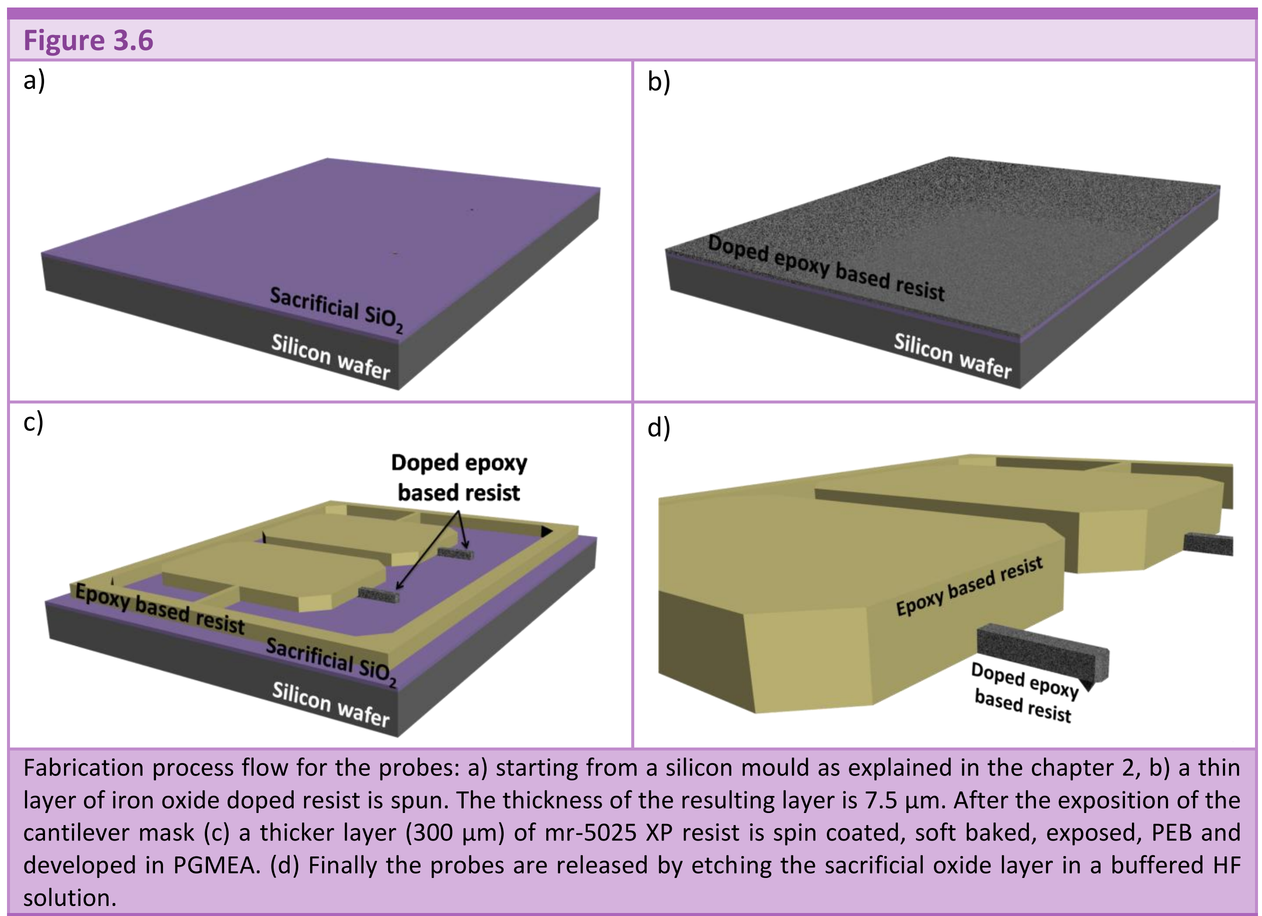

Fabrication process flow for the probes: a) starting from a silicon mould as explained in the chapter 2, b) a thin layer of iron oxide doped resist is spun. The thickness of the resulting layer is 7.5 µm. After the exposition of the cantilever mask (c) a thicker layer (300 µm) of mr-5025 XP resist is spin coated, soft baked, exposed, PEB and developed in PGMEA. (d) Finally the probes are released by etching the sacrificial oxide layer in a buffered HF solution.

After dehydration of the mould (150°C, 30 minutes) in a convection oven (Figure 3.6.a), it is convenient to shake the material to blend the composite because after storage the dispersion of the nanoparticles inside the epoxy based resist is usually not homogeneous. For this process IKA-MS2-minishaker is used at 36.7 Hz during 2 minutes. The composite is then ready to be deposited onto the mould. The spin coating is performed at 1000 rpm during 45 seconds with an acceleration of 400 rpm/s. With these conditions a 7.5 µm thickness layer is obtained for both the iron oxide doped resist and the titanium oxide doped resist (Figure 3.6.b). A relax time of about 10 minutes is recommended to allow the deposited material to be correctly spread on the mould. A short soft bake is performed in a hot plate with a temperature ramp from 65 °C to 95 °C during 15 minutes to cure the resist for the exposition. These resists are not transparent as it is the non doped material, so the exposition dose increases. In the iron oxide case, the dose needed to fully expose the layer is 91 mJ/cm^2 (I-line lamp λ = 365 nm). In the titanium oxide case the dose required is the 182 mJ/cm^2. The sample is relaxed again during 10 minutes before starting the PEB. The PEB takes 20 min in the hot plate in a temperature ramp from 65 °C to 95 °C.

Without any development, a second layer is deposited. This layer corresponds to the body of the probe. To have a homogeneous layer and to ease its curing, the deposition is usually made in two equal steps, which consists in the deposition of 150 µm thickness layer twice that results finally in a total thickness of 300 µm. To deposit 150 µm thickness layer, the mr-5025 XP resist is spin coated at 400 rpm during 45 seconds finalized at 800 rpm during 5 seconds, both with an acceleration of 400 rpm/s. The final increase of the speed is to get rid of the resist close to the border of the wafer. This layer needs to relax for at least 1 hour in a leveled plate and to be soft baked for 2 hours in a hot plate with a temperature ramp from 65 °C to 95 °C. After this layer is cooled it is possible to start to deposit the second one to finally obtain the 300 µm. To expose the whole layer a dose of 1465 mJ/cm^2 is needed. As this dose is quite large, the resist temperature could be increased drastically if exposed in a single step. Hence, the exposition is made in intervals of 20 seconds (8 in total) and it is relaxed after each interval for 40 seconds. In summary, the wafer receives 8 doses of 182 mJ/cm^2 with a cooling time of 40 seconds after each dose. The PEB is performed as in the case of the first layer.

It has been found that it is better to wait 24 hours before the development, leaving the wafers in a leveled plate. All the layers are developed in PGMEA at the same time and the wafer is gently shaken while it takes place (Figure 3.6.c). The development time varies from one time to the other. To finalize the development, immersion in IPA for a couple of minutes is performed.

In the previous chapter was demonstrated that the best post-process for the AFM probes is a hard bake of 2 hours at 120 °C on a hot plate in a N_2 saturated atmosphere. This step is also included in this fabrication process. Finally the probes are released by etching the silicon oxide sacrificial layer (Figure 3.6.d). In Figure 3.7, some fabrication results are shown. From the took SEM images it seems that the resolution of the tip is very good for the iron oxide doped resist but as the titanium oxide concentration is higher, more clusters are formed, increasing the radius of the tip. Even though, as few tips can be imaged using SEM, it is better to wait until imaging is possible to evaluate the quality of the obtained AFM image.

Figure 3.7

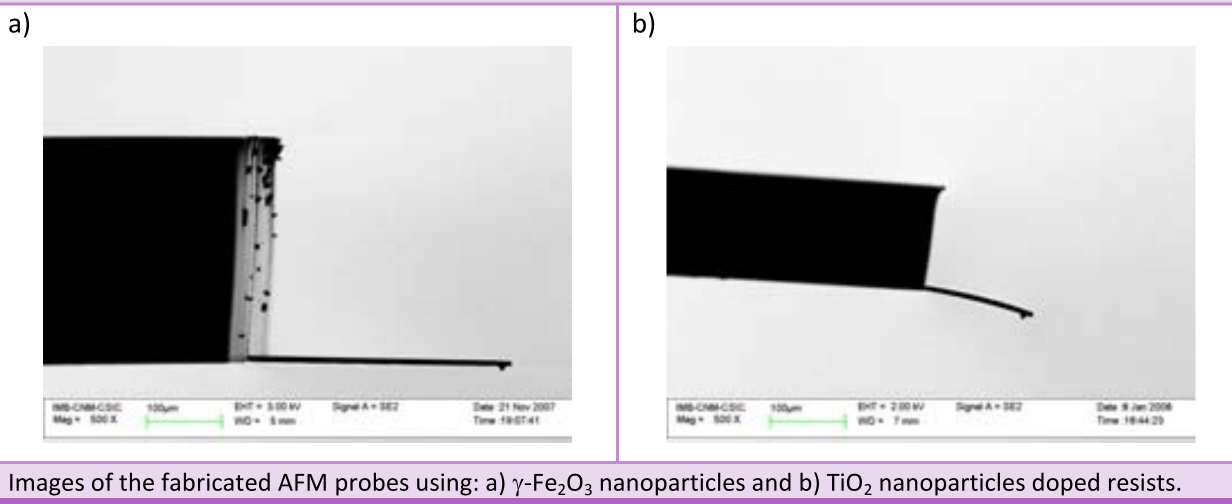

Images of the fabricated AFM probes using: a) γ-Fe_2O_3 nanoparticles and b) TiO_2 nanoparticles doped resists.

3.2.2 Double layer cantilever

The second alternative consists in a double layer cantilever. As the quality of the tips themselves had not been studied in the case of the doped resists, this fabrication process was performed in parallel to the previous one in order to obtain the same tip aspect ratio than for the previous chapter. The first deposited layer is the non doped epoxy based resist which can fully fill the mould. After its exposition, a second layer is spun. This second layer is the iron oxide doped material which can provide the cantilevers with some of the properties of the doped resist without affecting the aspect ratio of the tip by the positioning of any cluster or aggregate of nanoparticles inside the pyramidal mould.

Figure 3.8

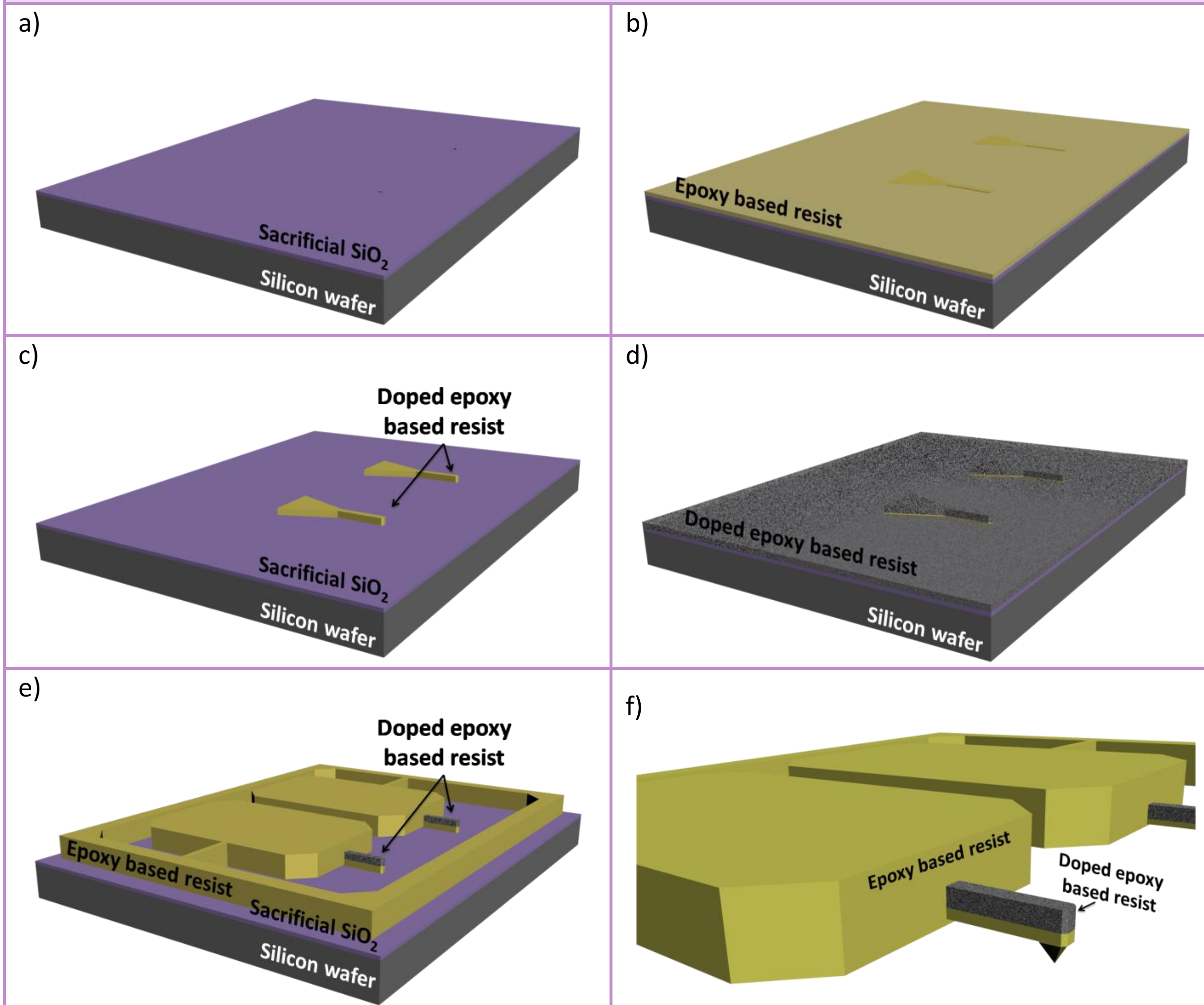

Fabrication process flow for the bilayer cantilever probes: a) starting from a silicon mould, b) a thin layer of 4 µm of mr-L 5005 XP resist is spun. After the exposition of the cantilever mask c) the wafer is developed. To improve the deposition of the second layer the resist is treated with oxygen plasma to turn it less hydrophobic. d) A 3 µm thick doped resist layer is deposited. After its exposition e) a thicker layer (300 µm) of mr-5025 XP resist is spin coated, soft baked, exposed and PEB. Finally the wafer is fully developed in PGMEA. (f) The probes are released by etching the sacrificial oxide layer in a buffered HF solution.

The first deposited layer is the mr-L 5005 XP and it is spun at 3000 rpm during 45 seconds with an acceleration of 400 rpm/s. The resulting thickness is 4 µm. After this layer is soft baked, exposed with a dose of 36.4 mJ/cm^2 (Figure 3.8.b), PEB and developed in PGMEA, the surface is treated with oxygen plasma during 1 min to adequate the resist to the second layer (Figure 3.8.c). The conditions of the plasma are detailed in Table 3.1.

Equipment	Gas Flow	Pressure	Source Power	DC bias	Temperature
Barrel	O_2 – 50 sccm	301 mTorr	71 W	-207 V	20 °C

Table 3.1: Oxygen plasma conditions applied as a release method.

The second deposited layer was the iron oxide doped resist (this fabrication process flow was not performed for the titanium dioxide doped resist). Spin coating at 3000 rpm during 45 seconds with an acceleration of 400 rpm/s results in a 3 µm thickness layer that can be treated as it was explained in the previous section (Figure 3.8.d). The rest of the process flow, the body definition, development (Figure 3.8.e), hard bake and release (Figure 3.8.f) steps are the same that have been described for the single layer cantilever process. Fabrication results of some released probes can be found in Figure 3.9.

Figure 3.9

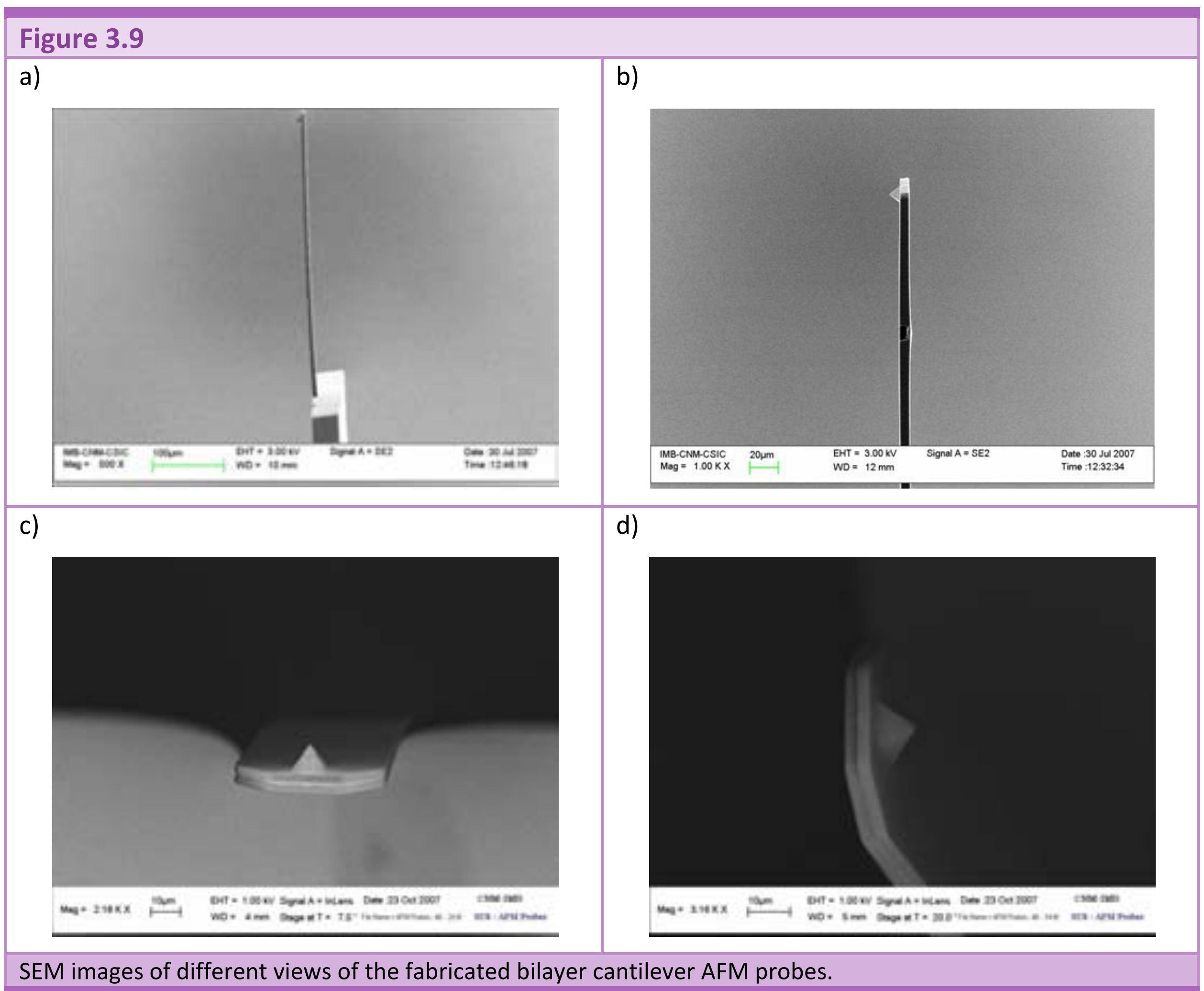

SEM images of different views of the fabricated bilayer cantilever AFM probes.

3.3 STRUCTURAL/FUNCTIONAL CHARACTERIZATION

The obtained AFM probes fabricated with the iron oxide doped resist, using both approaches (simple layer or double layer cantilever) are extremely flat and have a very low stress.

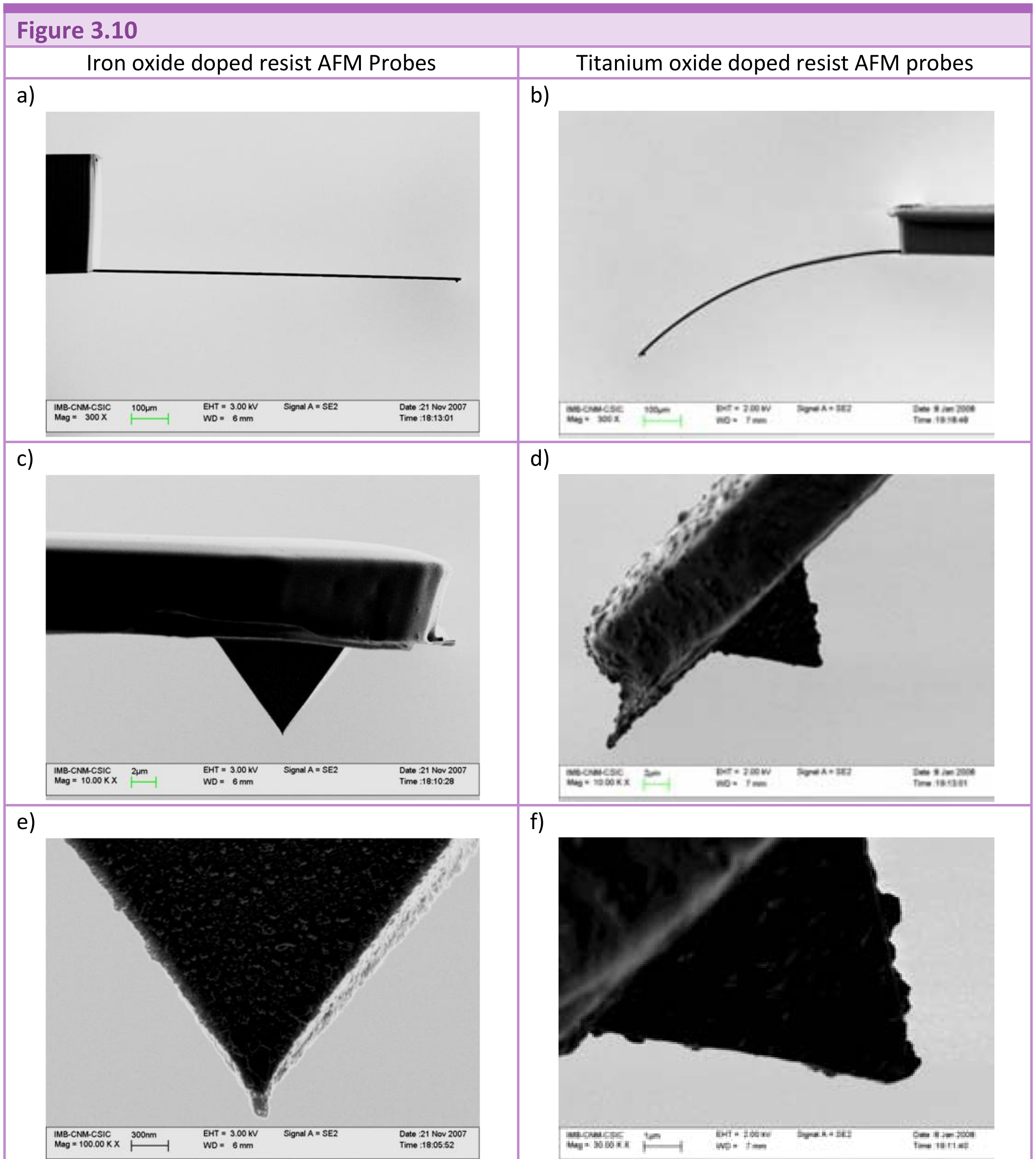

SEM images of the doped resist AFM probes. a) Iron oxide doped resist cantilevers are further more flat than the b) titanium oxide doped resist cantilevers.

On the other hand, cantilevers fabricated using the titanium oxide were so bent that they could not be included in any AFM equipment. The stress gradient causing this deflection is a bit larger than the one for standard (non doped) epoxy based resist, but, in addition, in this case the thickness is much smaller than for the levers presented in previous chapter, so the final deflection is much larger.

In Figure 3.10, the comparison between deflections for single layer cantilevers fabricated with both doped resists can be seen. In addition, it also can be seen that the tips are similar and keep a good aspect ratio.

In order to further explore the quality of the iron oxide doped resist cantilevers, single and double layer levers were compared in terms of deflection and tip aspect ratio, as can be seen in Figure 3.11. As it can be seen, deflection is very similar for both types of cantilevers, that contains iron oxide particles, but extremely different with the deflection of the cantilevers which contains titanium oxide nanoparticles, elucidating that the new properties are directly due to the presence of iron oxide nanoparticles.

Young Modulus of the both composites has been experimentally determined in order to evaluate if the difference in the internal stress of both composites relies in different contribution of the nanoparticles to the elastic modulus.

3.3.1 Preliminary characterization of NCs

As these two novel composites were used to fabricate MEMS in general and AFM probes in particular, the elastic properties of the materials had to be studied. For the mechanical characterization, an *MTS NanoXP indenter* system with a *Berkovich* tip was used. Hardness and modulus were calculated from the load–displacement curves following Oliver and Pharr methodology [23]. The reported data in Table 3.2 were derived from at least 20 individual indentation tests on each sample. All nanoindentation studies were performed in the *Institut de ciència de materials de Barcelona* (ICMAB-CSIC).

Material	Young's modulus	Hardness
Mr-L 5005	4,6 GPa	0,29 GPa
γ-Fe_2O_3	7,54 GPa	0,34 GPa
TiO_2	7,62 GPa	0,32 GPa

Table 3.2: Elastic properties measured by nanoindentation of the standard epoxy based resist and the two NCs. The studied samples had the same processing steps as the AFM probes. A significant increase of the Young's modulus is observed due to the incorporation of the nanoparticles.

Figure 3.11

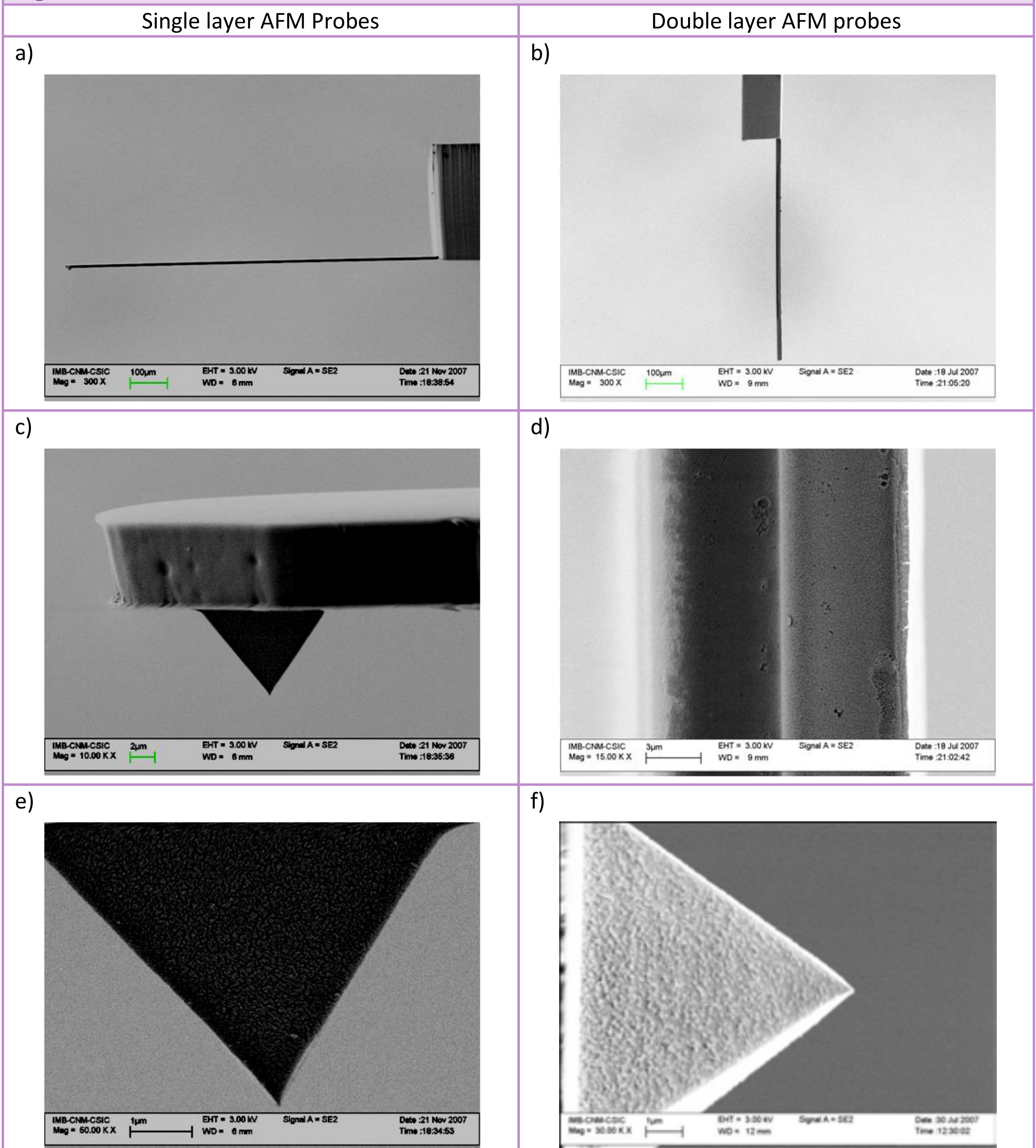

SEM images of fabricated AFM probes using iron oxide doped resist. These cantilevers are very flat and low stressed, even they are a) single or b) double layer. c) Iron oxide doped single layer cantilever is very homogeneous and has a very flat side walls in d) it can be observed the difference between both materials and their good adhesion in the interface. Tip aspect ratio is as good for e) an iron oxide doped resist than f) epoxy based resist, meaning that it is very difficult to find a γ-Fe_2O_3 nanoparticle aggregate in the bottom of the tip.

With the results obtained in Table 3.2 it is not possible to elucidate the fundamental reason for that the stress gradient decrease. It can be due to the shape of the nanoparticles, or to the way they aggregate inside the resist, etc.

In addition, as it can be seen in Figure 3.11.e and Figure 3.11.f, the tip obtained out of doped resist and standard epoxy based resist look the same. Therefore, it is possible to conclude that there is no improvement in making doubled layer cantilever versus single cantilever if both incorporate γ-Fe_2O_3 nanoparticles.

On the other hand, as it has been commented, in the case of the titanium oxide nanorods doped resist, their incorporation had not brought any significant improvement. Cantilevers have a deflection angle above 1° what makes them useless for AFM measurements because the laser reflection cannot be collected by the photodiode.

To fully study the behavior of the iron oxide AFM probes they have been characterized using them to perform AFM topography images. The resonant frequency and quality factor of the cantilevers have been experimentally found and resolution and lifetime of the tip is studied in the following section.

As it was discussed in the previous chapter, epoxy based AFM probes are interesting because they allow measurements with a low spring constant cantilevers but, as the tip is also very soft, it can be damaged when used in contact mode. For that reason, dynamic mode is a more convenient mode for them to be used. Therefore the characterization for the doped AFM probes has been only performed in dynamic mode.

3.3.2 Dynamic mode in air

Fabricated probes have been tested in air using two different equipments in order to see their feasibility. Probes fit in both holders, being ease to focus with the laser and tunned. The measurements showed in this section are taking using a *Dimension 3100* AFM system with a *Nanoscope IV* controller from *Veeco* and a *Cervantes* AFM system with a *Dulcinea* controller from *Nanotec*.

3.3.2.1 Single layer cantilever

Theoretical resonant frequency and elastic constant of the iron oxide composite cantilevers have been calculated (see Table 3.3) taking into account the thickness of the cantilever (7.5 µm) and the increase in the Young's modulus (7.54 GPa). Reducing the thickness of the cantilever, spring constant is decreased $\left(k = \frac{Ewt^3}{4l^3}\right)$, obtaining softener probes. Softener probes are more

susceptible to forces making them more sensitive. Using the original epoxy based resist AFM probes thicker cantilevers have to be fabricated make easier obtaining flat cantilevers.

Probe number	Length (l)	Spring Constant (k)	Frequency (f)
01	100 µm	39.76 N/m	298 kHz
02	175 µm	7.41 N/m	97 kHz
03	200 µm	4.97 N/m	74 kHz
04	225 µm	3.49 N/m	59 kHz
05	250 µm	2.54 N/m	48 kHz
06	350 µm	0.92 N/m	24 kHz
07	400 µm	0.62 N/m	19 kHz
08	425 µm	0.51 N/m	16 kHz
09	450 µm	0.43 N/m	15 kHz
10	500 µm	0.31 N/m	12 kHz
11	525 µm	0.27 N/m	11 kHz
12	800 µm	0.08 N/m	5 kHz
13	850 µm	0.06 N/m	4 kHz
14	1000 µm	0.04 N/m	3 kHz
15	1050 µm	0.03 N/m	2.7 kHz

Table 3.3: Theoretical calculus of the resonant frequency and spring constant of single layer cantilevers for the different lengths fabricated.

As cantilevers are very flat even after coating with gold or aluminium, the interference figure found when focusing the laser is very nice. Moreover, the signal of the reflection of the laser has a high power and also is very stable. A large number of probes with different lengths can be tested, as shown in Table 3.4.

γ-Fe2O3 doped resist AFM Probe		**Theoretical mechanical properties**		**Experimental mechanical properties**	
Type	*Length*	*Spring constant*	*Resonant frequency*	*Resonant frequency*	*Quality factor*
01	100 µm	39.76 N/m	298 kHz	271 kHz	289
02	175 µm	7.41 N/m	97 kHz	81 KHz	267
04	225 µm	3.49 N/m	59 kHz	47 kHz	69
06	350 µm	0.92 N/m	24 kHz	19 kHz	61
07	400 µm	0.62 N/m	19 kHz	14 kHz	87
09	450 µm	0.43 N/m	15 kHz	12 kHz	187
12	800 µm	0.08 N/m	5 kHz	4 kHz	27

Table 3.4: Summary of the mechanical properties of the doped cantilevers.

Compared to the probes described in previous chapter, AFM probes made with iron oxide doped resist are much easier to set up for AFM measurements. Although the quality factor is still far from the commercial silicon AFM probes, laser focusing, photodiode signal and resonant frequency tuning is very similar, making both comparable in terms of speed of preparation for the measurement.

Obtained topographic images of the iron oxide doped resist AFM probes show a high resolution (Figure 3.12.b) when compared to a standard commercial silicon probe. An aluminium coated sample has a roughness of about 2.4 nm and is the same value measured with both probes. This roughness is relatively high, so quantification of the quality of the tip is not possible.

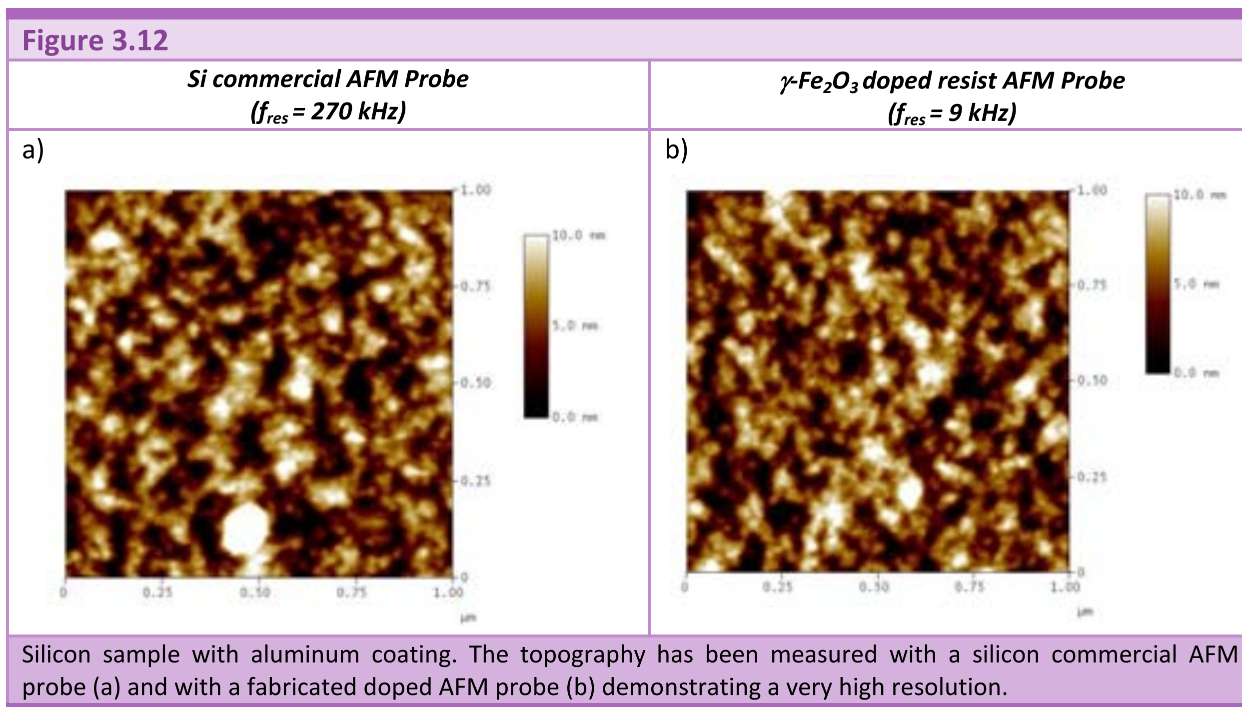

Silicon sample with aluminum coating. The topography has been measured with a silicon commercial AFM probe (a) and with a fabricated doped AFM probe (b) demonstrating a very high resolution.

Therefore, a second sample with very low roughness (0.5 nm) has been prepared specially to quantify the tip radius of the probes. 10 nm diameter (nominative) gold nanospheres have been deposited on a silicon substrate. AFM topography images measured an average diameter of 45 nm with the commercial tip and of 25 nm with the fabricated tip (Figure 3.13).

Figure 3.13

Si commercial AFM Probe ***(f_{res} = 268 kHz)***	***γ-Fe_2O_3 doped resist AFM Probe*** ***(f_{res} = 14 kHz)***
a)	b)

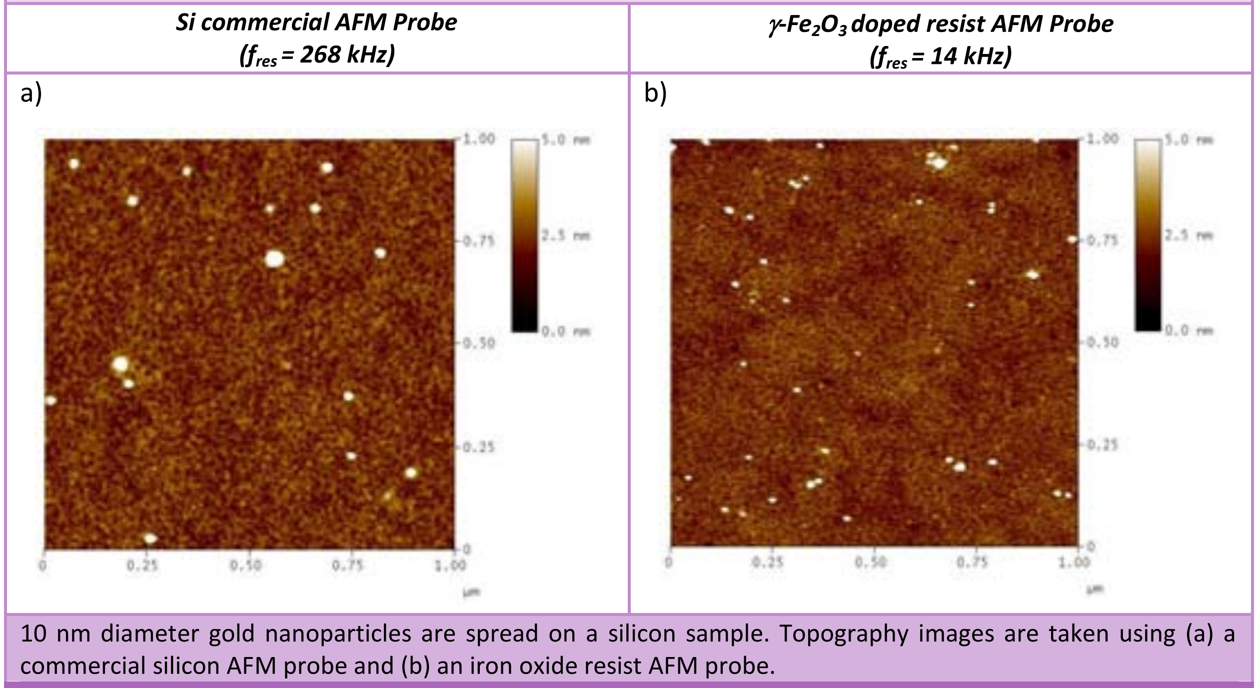

10 nm diameter gold nanoparticles are spread on a silicon sample. Topography images are taken using (a) a commercial silicon AFM probe and (b) an iron oxide resist AFM probe.

3.3.2.2 Double layer cantilever

Theoretical resonant frequency can be calculated taking into account the thicknesses of each layer of the cantilever (4 µm mr-L 5005 XP and 4 µm iron oxide composite), and the two different Young's modulus (4.6 GPa for mr-L 5005 XP and 7.54 GPa for iron oxide composite, Table 3.1). Equations (3.1)-(3.4) are used to find the analytical results, presented in Table 3.5.

$$EI = w \cdot \frac{t_{DR}^4 Y_{DR}^2 + t_{EBR}^4 Y_{EBR}^2 + 2t_{DR}t_{EBR}Y_{DR}Y_{EBR}(2t_{EBR}^2 + 2t_{DR}^2 + 3t_{EBR}t_{DR})}{12(t_{DR}Y_{DR} + t_{EBR}Y_{DR})} \tag{3.1}$$

$$m_a = w(t_{EBR}\rho_{EBR} + t_{DR}\rho_{DR}) = w\rho(t_{EBR} + t_{DR}) = w\rho t \tag{3.2}$$

$$f_{RES} = \frac{\sqrt{12 \cdot 1.03}}{2\pi l^2} \cdot \sqrt{\frac{EI}{m_a}} \tag{3.3}$$

$$k = \frac{3EI}{l^3} \tag{3.4}$$

where, t_{DR} is the thickness of the doped resist layer, t_{EBR} is the thickness of the epoxy based layer; Y_{DR} is the Young's modulus of the doped resist, Y_{EBR} is the Young Modulus of the epoxy based resist; w is the width of the cantilever; ρ_{DR} and ρ_{EBR} are the density of the doped resist

and the epoxy based resist respectively, that can be considered equals due to the low concentration of the doped material. Finally, l is the length of the cantilever.

Probe number	Length (l)	Spring Constant (k)	Frequency (f)
01	100 µm	25.83 N/m	252 kHz
02	175 µm	4.82 N/m	82 kHz
03	200 µm	3.23 N/m	63 kHz
04	225 µm	2.27 N/m	50 kHz
05	250 µm	1.65 N/m	40 kHz
06	350 µm	0.60 N/m	21 kHz
07	400 µm	0.40 N/m	16 kHz
08	425 µm	0.34 N/m	14 kHz
09	450 µm	0.28 N/m	12 kHz
10	500 µm	0.21 N/m	10 kHz
11	525 µm	0.18 N/m	9 kHz
12	800 µm	0.05 N/m	4 kHz
13	850 µm	0.04 N/m	3.5 kHz
14	1000 µm	0.03 N/m	2.5 kHz
15	1050 µm	0.02 N/m	2.3 kHz

Table 3.5: Theoretical calculus of the resonant frequency and spring constant of double layer cantilevers for the different lengths fabricated.

These probes also have very flat cantilevers, so the interference figure founded focusing the laser is as nice as for the single layer ones. In addition, the signal of the reflexion of the laser has also a high power. In Table 3.6 is summarized the mechanical properties characterization of the tested probes.

Double layer cantilever AFM Probe		Theoretical mechanical properties		Experimental mechanical properties	
Type	*Length*	*Spring constant*	*Resonant frequency*	*Resonant frequency*	*Quality factor*
01	100 µm	25.83 N/m	252 kHz	253 kHz	263
02	175 µm	4.82 N/m	82 kHz	67 kHz	184
05	250 µm	1.65 N/m	40 kHz	32 kHz	183
06	350 µm	0.60 N/m	21 kHz	16 kHz	122
07	400 µm	0.40 N/m	16 kHz	11 kHz	81
08	425 µm	0.34 N/m	14 kHz	11 kHz	83
09	450 µm	0.28 N/m	12 kHz	10 kHz	60
10	500 µm	0.21 N/m	10 kHz	7 kHz	23

Table 3.6: Summary of the mechanical properties of the double layer cantilevers.

Again, the quality factor has increased compared to the epoxy based resist cantilevers and it decreases as a function of the cantilever length, as can be expected. Second harmonic have also been found in some cases, giving higher quality factor (also as expected) and allowing the AFM measurement.

3.3.3 Dynamic mode in liquid

Figure 3.14

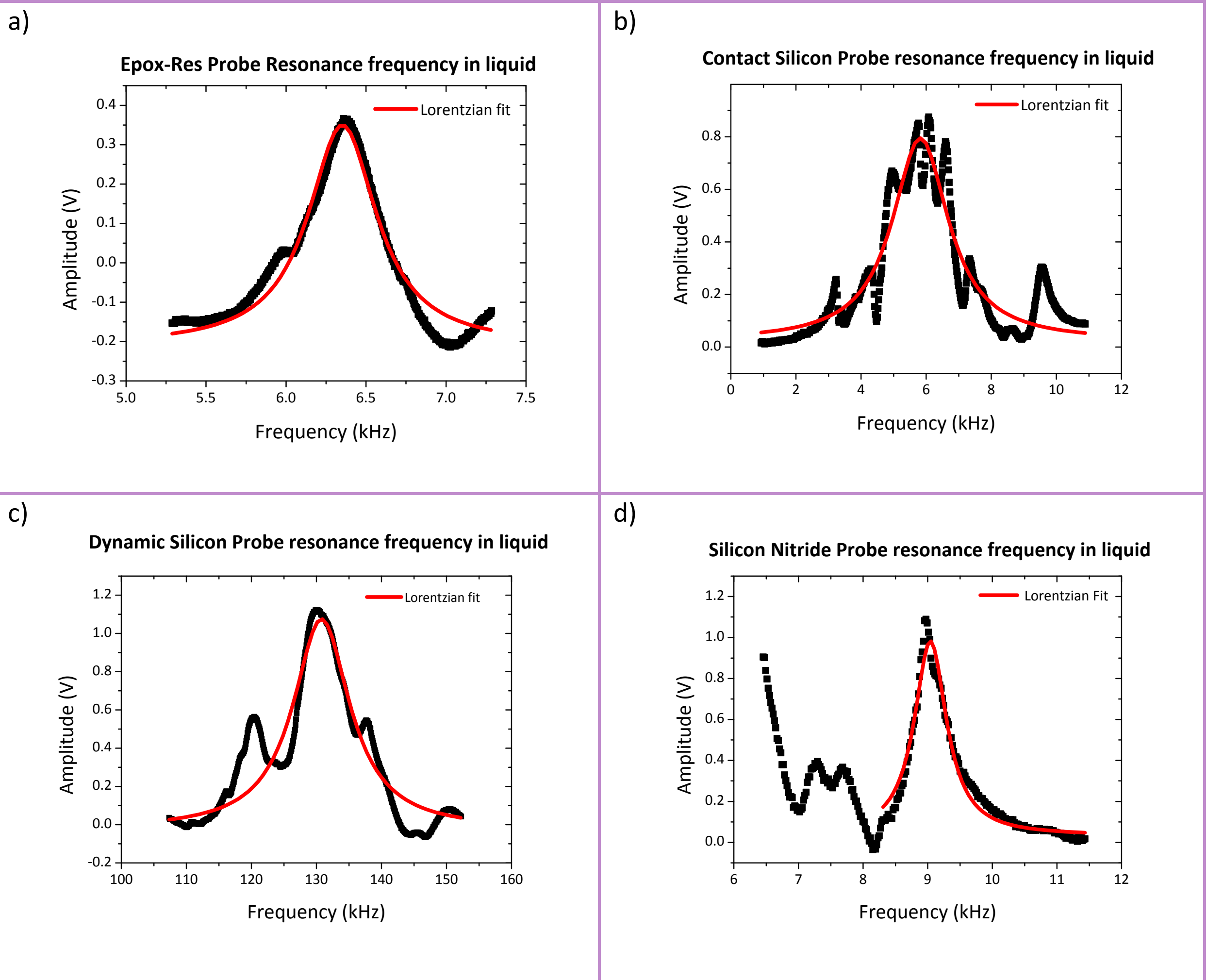

a) Resonant frequency corresponding to an iron oxide doped resist cantilever with 500 µm length, k = 0.4 N/m and a resonant frequency in air of 12 kHz. b) Rectangular silicon probe usually used for contact mode in air (ESP7) with a length around 450 µm, k = 0.2 N/m and a resonant frequency in air of 12 kHz. c) Rectangular silicon probe for dynamic mode in air (RTESP14) with a length around 120 µm, k ≈ 50 N/m and a resonant frequency in air of 285 kHz. d) V-shaped silicon nitride probe either for dynamic or contact modes. Cantilever length is 100 µm and a k = 0.08 N/m. Its resonant frequency in air is 37 kHz. Although the quality factor is around 15 for the iron oxide doped resist lever, the fit is much better than for the commercial rectangular silicon probes (b) and (c).

The single layer doped resist probes have also been tested in liquids. In the previous chapter we have already demonstrated that epoxy based resist AFM probes can perform very good measurements due to the fact that their quality factors do not decrease from air measurements, making their resonant frequency comparable to the silicon commercial probes. In this section it is showed that doped resist AFM probes can also be very useful in this mode of operation. All liquid measurements have been performed using a *Multimode* AFM microscope with a *Nanoscope IVa* or a *Nanoscope IIIa* controller from *Veeco*.

In order to quantify how good are the fabricated iron oxide doped resist AFM cantilevers, their mechanical properties are compared with some of the commercial AFM probes in Table 3.7.

Probe type	**Length**	**Shape**	**Spring constant**	**Mechanical properties in air**		**Mechanical properties in liquid**	
				Resonant frequency	Quality factor	Resonant frequency	Quality factor
RTESP14 (Veeco) Silicon	120 µm	rectangular	50 N/m	285 kHz	500	130 kHz	12
OMCL TR400 PSA (Olympus) Si_3N_4	100 µm	V-shaped	0.08 N/m	37 kHz	90	9 kHz	27
ESP7 (Veeco) Silicon	450 µm	rectangular	0.2 N/m	12 kHz	35	6 kHz	3
Iron oxide	500 µm	rectangular	0.4 N/m	10 kHz	27	7 kHz	34
Iron oxide	400 µm	rectangular	0.6 N/m	14 kHz	61	9 kHz	40

Table 3.7: Mechanical properties of different AFM probes in air and in liquid.

Iron oxide cantilevers can behave as good as the typically commercial probes used for dynamic mode in liquid measurements, the silicon nitride V-shaped probes. V-shaped (or triangular) probes are convenient for liquid measurements because the aperture inside allows the liquid flow while the cantilever oscillates, reducing the damping. Both cantilevers, in addition, have been compared in resolution, obtaining similar results. Figure 3.15 evidences that the iron oxide doped resist tip can imaging with a high resolution and accuracy.

Figure 3.15

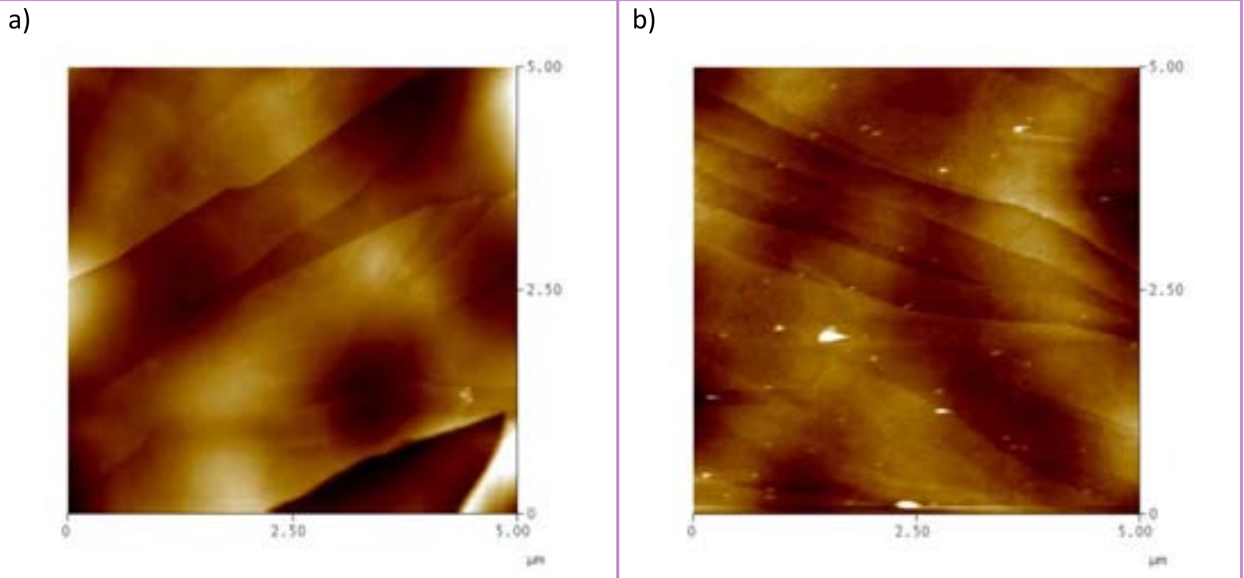

AFM measurements on graphite under deionized water, a) topography image taken with an iron oxide doped resist tip. b) Topography image captured using a commercial silicon nitride tip (OMCL TR400 PSA). Z scale for both images is 30 nm.

Figure 3.16

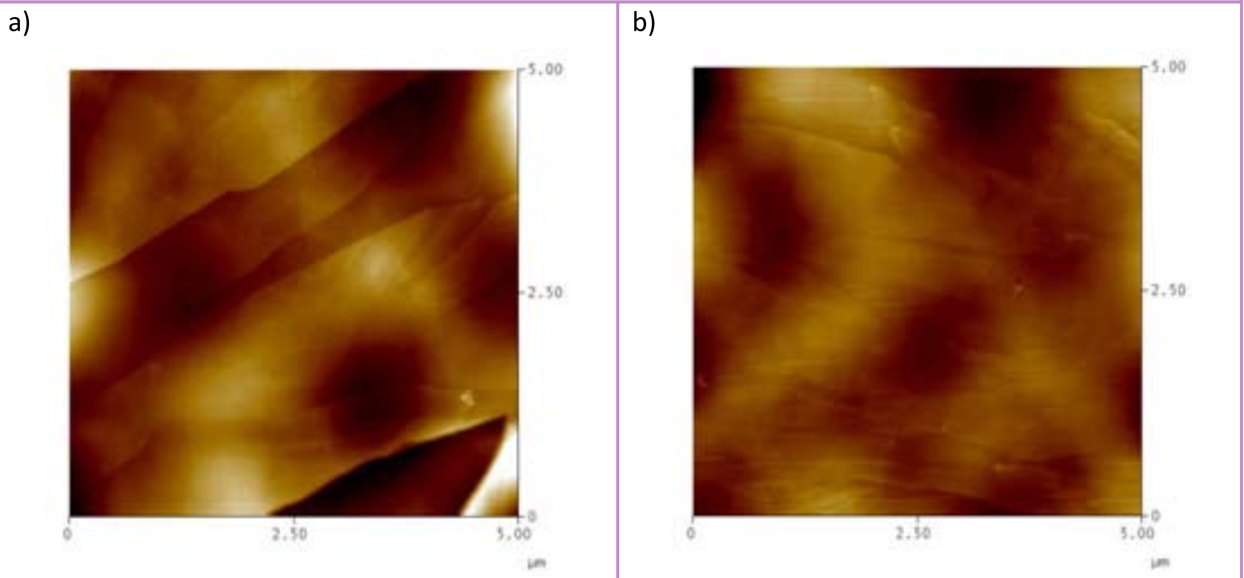

AFM measurements on graphite under liquid. a) Iron oxide doped resist probe image b) Commercial silicon probe (ESP7). Z scale is 30 nm for both images.

On the other hand, if the iron oxide doped probe is compared to a silicon rectangular one, the resolution is much better with the first one than with the latter (Figure 3.16).

3.3.4 Magnetic Actuated Drive mode in air

Dynamic mode actuation can be achieved not only by the standard piezoelectric actuation, but also by magnetic actuation. The Magnetic Actuated Drive (MAD mode) is a mechanism that uses an electromagnet to create a magnetic field to drive magnetic probes. Commercial available probes are coated with a magnetic film (Co or Co/Cr) on the backside (to preserve the tip sharpness). This technique is very useful when performing measurements in liquid, given the fact that the only moving part in the system is the cantilever. Therefore, when operating in liquid, it is easy to identify if a cantilever is working with the magnetic drive, because the spectrum shows only the resonant peak of the probe and not the noise peaks that appear if a piezoelectric actuation is used.

Figure 3.17

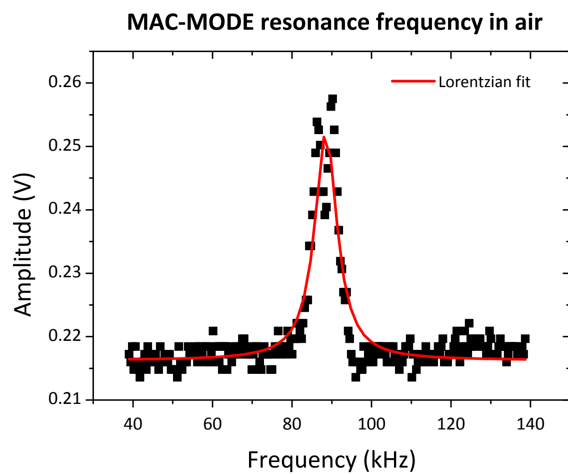

Resonant frequency tuned for a single layer iron oxide doped resist AFM probe in air exited by a magnetic field (MAD mode). The cantilever has a length of 400 µm and a theoretic resonant frequency in air of 89 kHz even the experimental resonant frequency founded by using piezo excitation is 14 kHz. The amplitude of the signal is too low to use it to make AFM measurements.

Using the magnetic properties of the iron oxide nanoparticles, the aim here was to fabricate a probe that could be actuated magnetically without needing additional coatings. In order to achieve that, iron oxide nanoparticles doped resist AFM probes were magnetized during 5 minutes by the effect of a magnet situated below them. The objective was to align the dipoles to the longitudinal axis of the magnet. Then, the cantilever was excited by a coil and if the cantilever was magnetic due to the iron oxide nanoparticles, it had to be found the resonant frequency. MAD mode excitation was performed using a *Multimode* AFM microscope with a *Nanoscope IVa* controller from *Veeco*.

Up to now, just weak signals have been found (Figure 3.17), probably due to the fact that the concentration is too low, and no measurement was made using this actuation technique. The fabrication of levers with a higher concentration of doped particles is intended in a near future to enhance the magnetic response.

3.3.5 Magnetic Force Mode in air

Magnetic force microscopy (MFM) is a special mode of operation of the dynamic mode AFM. This method was introduced shortly after the invention of the AFM [24]. The technique needs a magnetic probe, which is brought close to a sample and interacts with the magnetic stray fields near the surface. The strength of the local magnetic interaction determines the vertical motion of the tip as it scans across the sample.

Single layer and double layer iron oxide doped resist AFM probes were magnetized during 5 minutes by the effect of a magnet situated below them. To perform the MFM measurements, the tip is separated at a certain distance (typically around 100 nm) where Van de Waals forces cannot be detected but where the long distance forces, like magnetic force, can act between a magnetic sample and a magnetic tip.

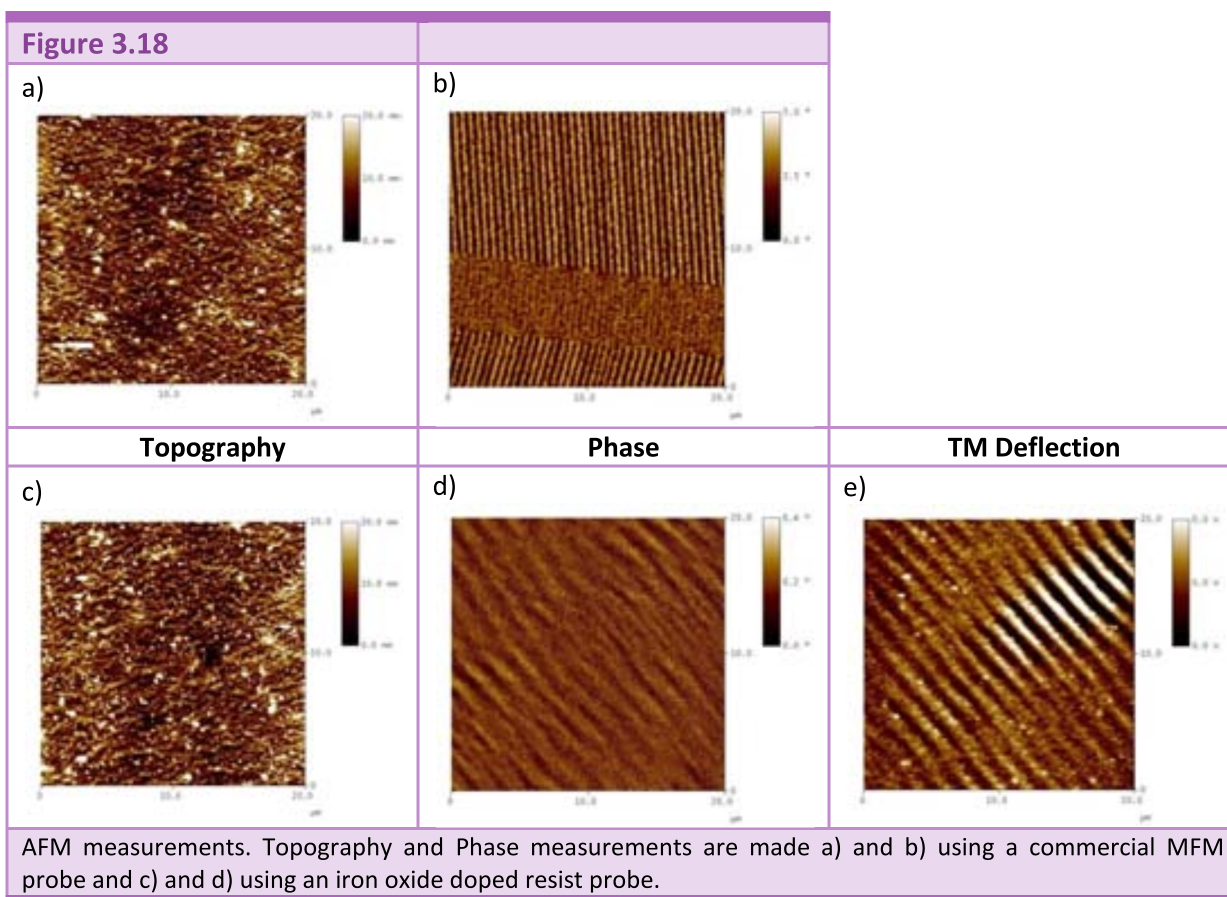

Figure 3.18

AFM measurements. Topography and Phase measurements are made a) and b) using a commercial MFM probe and c) and d) using an iron oxide doped resist probe.

Figure 3.18 shows the differences in the MFM measurements. Although topography images are almost equal for the commercial and the fabricated probes, which reaffirms that the resolution of both probes is very similar, the magnetic response is very different. Commercial cantilever (MADOTR 4 from *Veeco*) clearly detects the magnetic pattern in the magnetic tape scanned at 50 nm over the surface, while the iron oxide doped probe can only detect a very low interference pattern (which does not change the orientation if the sample is moved) in the phase and in the deflection measurements.

No valid magnetic measurement has been recorded with the fabricated tip. The cantilever/tip assembly is the critical element of MFM. The tip shape is important due to the long-range nature of magnetic forces. A lot of effort has been reported on the optimization of the magnetic probes in order to get quantitative information from MFM data [25-27]. Coating conventional probes brings the problem that a pattern of magnetic domains can arrange, which reduces the effective magnetic moment of the tip. The exact domain structure is unknown and can even change during MFM operation.

Therefore, in this case, as in the previous section, it seems that the concentration of the nanoparticles is not high enough to give a magnetic attraction or repulsion or/and as the epoxy based resist involves all the nanodomains, the possible magnetic effects are shielded.

MFM measurements have been performed using a *Dimension 3100* AFM microscope with a *Nanoscope IV* controller from *Veeco*.

3.4 CONCLUSIONS

Structure modification of the polymers by adding nanoparticles has been one of the goals of the Novopoly project. In this chapter the successfully incorporation of nanoparticles has been described. γ-Fe_2O_3 nanospheres and TiO_2 nanorods have been uniformly diluted in anisole based epoxy resist. Both composites increase the Young's modulus of the initial epoxy based resist and change its color, it turns from transparent to black in the iron oxide nanoparticles case, and to white (milky) in the titanium oxide.

Iron oxide composite had also demonstrated the enhancement of the mechanical properties as a structural resist for cantilevers. They are completely flat (below the 0.5° deflection angle) and they have a low intrinsic stress gradient. Furthermore, the frequency spectra is more clear and less noisy than for the initial epoxy based resist cantilevers, being the quality factor at least doubled. Small tip radius can be obtained (in the same range as the tips fabricated out of non doped resist), making this material optimum for the polymeric probes fabrication.

Iron oxide AFM probes can be used either for dynamic mode measurement in air and in liquid, with a very low spring constant if it is desired and giving similar features than commercial ones, especially in liquid.

On the other hand, TiO_2 nanoparticles have not shown to bring any benefit to the doped resist. In fact, initial bending of the levers is larger than in the case of non doped resist, making the cantilevers unable to be used in any commercial AFM equipment.

Finally, even though it was expected that nanoparticles changed other material properties like conductivity or magnetic permeability, none of this effects has been detected.

3.5 References

1. A.C. Balazs, T. Emrick, and T.P. Russell
"Nanoparticle polymer composites: Where two small worlds meet".
Science, 2006, **314**(5802), 1107-1110.

2. S. Jiguet, A. Bertsch, H. Hofmann, and P. Renaud
"SU8-silver photosensitive nanocomposite".
Advanced Engineering Materials, 2004, **6**(9), 719-724.

3. S. Jiguet, A. Bertsch, H. Hofmann, and P. Renaud
"Conductive SU8 photoresist for microfabrication".
Advanced Functional Materials, 2005, **15**(9), 1511-1516.

4. S. Jiguet, A. Bertsch, M. Judelewicz, H. Hofmann, and P. Renaud
"SU-8 nanocomposite photoresist with low stress properties for microfabrication applications".
Microelectronic Engineering, 2006, **83**(10), 1966-1970.

5. C. Ingrosso, V. Fakhfouri, M. Striccoli, A. Agostiano, A. Voigt, G. Gruetzner, M.L. Curri, and J. Brugger
"An epoxy photoresist modified by luminescent nanocrystals for the fabrication of 3D high-aspect-ratio microstructures".
Advanced Functional Materials, 2007, **17**(13), 2009-2017.

6. V.L. Colvin, M.C. Schlamp, and A.P. Alivisatos
"Light-Emitting-Diodes Made from Cadmium Selenide Nanocrystals and a Semiconducting Polymer".
Nature, 1994, **370**(6488), 354-357.

7. C. Martin
"Novopoly Project Webpage".
http://www.cnm.es/projectes/novopoly/, 2007.

8. A.P. Alivisatos
"Semiconductor Nanocrystals".
MRS Bulletin, 1995, **20**(8), 23-32.

9. A.P. Alivisatos
"Perspectives on the physical chemistry of semiconductor nanocrystals".
Journal of Physical Chemistry, 1996, **100**(31), 13226-13239.

10. A.P. Alivisatos
"Semiconductor clusters, nanocrystals, and quantum dots".
Science, 1996, **271**(5251), 933-937.

11. C.C. Chen, A.B. Herhold, C.S. Johnson, and A.P. Alivisatos
"Size dependence of structural metastability in semiconductor nanocrystals".
Science, 1997, **276**(5311), 398-401.

12. M. Bruchez, M. Moronne, P. Gin, S. Weiss, and A.P. Alivisatos
"Semiconductor nanocrystals as fluorescent biological labels".
Science, 1998, **281**(5385), 2013-2016.

13. X.G. Peng, L. Manna, W.D. Yang, J. Wickham, E. Scher, A. Kadavanich, and A.P. Alivisatos
"Shape control of CdSe nanocrystals".
Nature, 2000, **404**(6773), 59-61.

14. L. Manna, E.C. Scher, and A.P. Alivisatos
"Shape control of colloidal semiconductor nanocrystals".
Journal of Cluster Science, 2002, **13**(4), 521-532.

15. E.C. Scher, L. Manna, and A.P. Alivisatos
"Shape control and applications of nanocrystals".
Philosophical Transactions of the Royal Society of London Series A-Mathematical Physical and Engineering Sciences, 2003, **361**(1803), 241-255.

16. V.F. Puntes, K.M. Krishnan, and A.P. Alivisatos
"Colloidal nanocrystal shape and size control: The case of cobalt".
Science, 2001, **291**(5511), 2115-2117.

17. C. Ingrosso
"Hybrid Organic/Inorganic Materials Based on Colloidal Nanocrystals towards Sensing Applications".
Ph.D. Thesis, 2007, University of Bari.

18. A. Petrella, M. Tamborra, M.L. Curri, P. Cosma, M. Striccoli, P.D. Cozzoli, and A. Agostiano
"Colloidal TiO2 nanocrystals/MEH-PPV nanocomposites: Photo(electro)chemical study".
Journal of Physical Chemistry B, 2005, **109**(4), 1554-1562.

19. T. Hyeon, S.S. Lee, J. Park, Y. Chung, and H. Bin Na
"Synthesis of highly crystalline and monodisperse maghemite nanocrystallites without a size-selection process".
Journal of the American Chemical Society, 2001, **123**(51), 12798-12801.

20. P.D. Cozzoli, A. Kornowski, and H. Weller
"Low-temperature synthesis of soluble and processable organic-capped anatase TiO2 nanorods".
Journal of the American Chemical Society, 2003, **125**(47), 14539-14548.

21. R. Buonsanti, V. Grillo, E. Carlino, C. Giannini, M.L. Curri, C. Innocenti, C. Sangregorio, K. Achterhold, F.G. Parak, A. Agostiano, and P.D. Cozzoli
"Seeded growth of asymmetric binary nanocrystals made of a semiconductor TiO2 rodlike section and a magnetic gamma-Fe2O3 spherical domain".
Journal of the American Chemical Society, 2006, **128**(51), 16953-16970.

22. A. Convertino, G. Leo, M. Tamborra, C. Sciancalepore, M. Striccoli, M.L. Curri, and A. Agostiano
"TiO2 colloidal nanocrystals functionalization of PMMA: A tailoring of optical properties and chemical adsorption".
Sensors and Actuators B-Chemical, 2007, **126**(1), 138-143.

23. G.M. Pharr, W.C. Oliver, and F.R. Brotzen
"On the Generality of the Relationship Among Contact Stiffness, Contact Area, and Elastic-Modulus During Indentation".
Journal of Materials Research, 1992, **7**(3), 613-617.

24. Y. Martin and H.K. Wickramasinghe
"Magnetic Imaging by Force Microscopy with 1000-A Resolution".
Applied Physics Letters, 1987, **50**(20), 1455-1457.

25. D. Rugar, H.J. Mamin, P. Guethner, S.E. Lambert, J.E. Stern, I. Mcfadyen, and T. Yogi
"Magnetic Force Microscopy - General-Principles and Application to Longitudinal Recording Media".
Journal of Applied Physics, 1990, **68**(3), 1169-1183.

26. S. Porthun, L. Abelmann, and C. Lodder
"Magnetic force microscopy of thin film media for high density magnetic recording".
Journal of Magnetism and Magnetic Materials, 1998, **182**(1-2), 238-273.

27. U. Hartmann
"Magnetic force microscopy".
Annual Review of Materials Science, 1999, **29**, 53-87.